INSTITUT FOR BÆRENDE KONSTRUKTIONER OG MATERIALER

DTU

Plastic Theory Applied to Shear Walls

Load-Carrying Capacity of Shear Walls

JUNYING LIU

DEPARTMENT OF STRUCTURAL ENGINEERING AND MATERIALS
TECHNICAL UNIVERSITY OF DENMARK Series R No 36 1997

Plastic Theory Applied to Shear Walls

– Load-Carrying Capacity of Shear Walls

Junying Liu

Plastic Theory Applied to Shear Walls
Load-Carrying Capacity of Shear Walls

Tryk:LTT
Danmarks Tekniske Universitet
Lyngby
ISBN 87-7740-227-8
ISSN 1396-2167
Bogbinder:
H. Meyer

PREFACE

This paper has been prepared as the thesis required to obtain the Ph. D. degree at the Technical University of Denmark.

The work was carried out at the Department of Structural Engineering and Materials under the supervision of Professor, dr.techn. M. P. Nielsen.

I wish to express my sincere appreciation to my supervisor for his guidance, encouragement and constant help. Also I wish to thank the entire staff at the department for their help during the time I have been here.

Finally I gratefully acknowledge the financial supports granted by the Chinese National Educational Committee, Daloon Fonden, Knud Højgaards Fond and STVF, the Danish Technical State Research Foundation.

Lyngby, April 1997

Junying Liu

SUMMARY

This paper deals with the ultimate load-carrying capacity of shear walls based on the plastic theory.

A theoretical model which is a strut or a diagonal compression field combined with triangular homogeneous stress fields is derived to predict accurately the ultimate load-carrying capacity of reinforced concrete shear walls. The method developed can be used together with simple standard programs, e.g. optimization programs. This may used for the design of earthquake resistant structures.

The walls with different height-width ratios and with rectangular, barbell and flanged sections subjected to vertical loads as well as lateral loads which may be applied monotonicly, repeatedly or cyclically can be treated by the method developed. The theory is valid for shear walls using normal strength materials and ultra-high strength materials.

The theoretical results found by the method have been compared with test results available in the literature. A satisfactorily good agreement has been found.

RESUME

Denne rapport behandler bestemmelse of bæreevnen af vægge af armeret beton påvirket til forskydning v. h. a. plasticitetsteorien.

En teoretisk model bestående of trykstænger kombineret med trekantede områder med homogene spændingstilstande udvikles med det formål at beregne bæreevnen of væggene.

Metoden kan kombineres med simple standard rutiner udviklet til automatisk databehandling. Teorien vil have stor betydning for beregning of jordskælvspåvirkede konstruktioner.

Vægge med forskellige højde-bredde forhold og med rektangulært tværsnit, søjleforstærket tværsnit og tværsnit med flanger påvirket med lodrette såvel som vandrette belastninger behandles. Belastningen kan være enten monoton, alternerende eller cyklisk.

Teorien dækker både normalstyrkebeton og højstyrkebeton ligesom armeringen kan have såvel lav som meget høj flydespænding.

De teoretiske resultater er sammenlignet med et stort antal forsøg fra litteraturen. Der er fundet en tilfredsstillende overensstemmelse mellem teori og forsøg.

CONTENTS

NOTATIONS

a	:	Height of wall; distance
A	:	Gross area of section
A_{sl}	:	Longitudinal reinforcement area in boundary element
b	:	Width of boundary element of wall
c	:	Cohesion parameter; concrete cover
c_v	:	Coefficient of variation
C	:	Resultant compressive force in boundary element
d	:	Effective width of section in bending calculations
e	:	Parameter determining the position of transverse load on the wall
f_A	:	Seperation resistance of concrete
f_c	:	Uniaxial compressive strength of concrete
f_c^*	:	Plastic compressive strength of concrete, defined as $f_c^* = \nu f_c$
f_{Yl}	:	Yield strength of reinforcement in boundary element
f_{Yx}	:	Yield strength of vertical web reinforcement
f_{Yy}	:	Yield strength of horizontal web reinforcement
h	:	Total width of wall
h_e	:	Effective width of wall in shear calculation, defined as $h_e = h-2c$
h_0	:	Width of web
h'	:	Distance between the centre of the boundary elements of wall
M_p	:	Bending Yield moment
m_p	:	Dimensionless bending yield moment, defined as $M_p = \dfrac{M_p}{td^2 f_c}$
N	:	Normal force
n	:	Normal direction; dimensionless normal force, defined as $n = \dfrac{N}{thf_c}$; number
n*	:	Dimensionless effective normal force, defined as $n^* = \dfrac{N}{th\nu f_c}$

P	:	Transverse load
t	:	Thickness of web
t_f	:	Thickness of boundary element
T	:	Resultant force of tensile reinforcement
T_Y	:	Total yield force of the tensile reinforcement in the longitudinal direction of wall, defined as $T_Y = 2A_{sl}f_{Yl} + \varphi_x f_{Yx} th_0$
v	:	Relative velocity vector
W_E	:	External work
W_I	:	Internal work
x	:	Distance
x_0	:	Height of biaxial compression area corresponding to strut
x_0^*	:	Height of biaxial compression area corresponding to a triangular area
$\overline{x}$	:	Mean value
y_0	:	Height of compression zone in section for bending failure; Width of biaxial compression area corresponding to strut
y_0'	:	Thickness of strut
y_0^*	:	Width of biaxial compression area corresponding to triangular area
α	:	Inclination of relative velocity to y-axis
α^*	:	Inclination of relative velocity to yield line
β	:	Inclination of yield line to x-axis
$\varepsilon_1, \varepsilon_2,$	:	Principal strains
θ, θ_1	:	Inclinations of concrete compression to x-axis
μ	:	Coefficient of friction
ν	:	Concrete effectiveness factor
φ_l	:	Reinforcement ratio in boundary element, defined as $\varphi_l = \dfrac{A_{sl}}{th}$
φ_x	:	Vertical reinforcement ratio in web
φ_y	:	Stirrup reinforcement ratio in web
Φ_l	:	Nominal longitudinal reinforcement degree of wall, defined as $\Phi = 2\Phi_l + \Phi_x + n$ (for upper bound solutions) and

$$\Phi = \Phi_l + \frac{\Phi_x}{2} + \frac{n}{2} \quad \text{(for lower bound solutions)}$$

Φ_l : Longitudinal reinforcement degree in boundary element, defined as $\Phi_l = \dfrac{A_{sl}\, f_{Yl}}{f_c}$

Φ_x : Longitudinal reinforcement degree in web, defined as $\Phi_x = \dfrac{\varphi_x\, f_{Yx}}{f_c}$

Φ^* : Effective nomial longitudinal reinforcement degree of wall, defined as $\Phi^* = \dfrac{\Phi}{\upsilon}$

Φ_l^* : Effective reinforcement degree in boundary element, defined as $\Phi_l^* = \dfrac{\Phi_l}{\upsilon}$

Φ_x^* : Effective longitudinal reinforcement degree in web, defined as $\Phi_x^* = \dfrac{\Phi_x}{\upsilon}$

σ : Normal stress, Standard deviation

σ_s : Normal stress at the bottom of a wall along the edge of the strut

σ_x : Normal stress in concrete at the bottom of a wall along the edge of a triangular area

σ_{sl} : Tensile stress of reinforcement in boundary element

σ_{sx} : Tensile stress of vertical reinforcement in web

σ_{sy} : Tensile stress of stirrup reinforcement in web

τ : Shear stress; Average shear stress

τ_s : Shear stress at the bottom of a wall along the edge of the strut

τ_t : Shear stress along the edge of a triangular area of a wall

ψ : Shear reinforcement degree in web, defined as $\psi = \dfrac{\varphi_y\, f_{Yy}}{f_c}$

ψ^* : Effective shear reinforcement degree in web, defined as $\psi = \dfrac{\Psi}{\upsilon}$

CHAPTER I. INTRODUCTION

1.1 General

Reinforced concrete structural walls have been favored for the design of multistory buildings in seismic zone areas because they provide an efficient bracing system and offer a great potential for lateral load resistance and drift control. Therefore, in the world, there are many research projects regarding reinforced concrete shear walls.

Denmark has a long history for developing failure theories. These are also applicable in seismic design . Generally in structural analysis, it is of great importance to be able to calculate the ultimate load-carrying capacity and the deformations of a structure. The theory of plasticity has been used for concrete structures in Denmark for a long time, and now it is becoming to be accepted in more and more parts of the world. The plastic theory of concrete can lead to a thorough understanding of the failure mechanisms, and can determine the strength of structures in the ultimate limit state in a simple manner by introducing a few experimental parameters.

The stiffness of the structure will decrease when the structure cracks and further when it reaches the stage of plasticity, which makes it very complex and difficult to calculate the load-carrying capacity and the deformations of the structure by common elastic-plastic methods. Therefore, very often implementation of computer methods is not practicable due to the huge amount of CPU-time required.

This paper deals with the theory of the ultimate capacity of shear walls based on the plastic theory. The result of this study proposes a simple method to predict accurately the ultimate load-carrying capacity of shear walls. The method developed can be implemented in simple standard programs, e.g. optimization programs. This will be useful for the design of earthquake resistant structures

The walls dealt with have rectangular, barbell and flanged sections and are subjected to vertical loads as well as lateral loads transmitted by the floors. Shear walls are therefore subjected to axial compression, bending moment and shear force.

The ultimate load-carrying capacity of shear walls may be governed either by bending failure or shear failure. Special attention is given to the shear failure mechanism that results from a combination of a strut action and a diagonal compression field. The theoretical results found on the basis of the plastic theory of concrete have been compared with test results performed in other countries. A satisfactorily good agreement has been found.

1.2 Historical Survey

1.2.1 Overview

The theory of plasticity is a branch of mechanics of materials. This theory deals with materials that can deform plastically under constant load when the load has reached a sufficiently high value. Such materials are called **perfectly plastic** materials, and the theory dealing with the determination of the load-carrying capacity of structures made of such materials is called **limit analysis**. The development of plastic theory of reinforced concrete structures has gone through several stages: First, the yield hinge method for beams and frames was developed; second, the yield line theory for slabs; third, disk and shell theory. During the development a consistent theory containing upper- and lower-bound theorems has been established.

The use of the plastic properties of reinforced concrete structures goes back to the turn of the century. In the Danish code of reinforced concrete of 1908 we find the first traces of a theory of plasticity in the principles given for calculation of continuous beams.

The important development of the plastic theory for reinforced concrete slabs was initiated by Å. Ingerslev [21,1] [23,1]. Ingerslev based the calculation of homogeneously reinforced slabs on the assumption of a constant bending moment along certain lines, called **yield lines**, and he gave several examples of the application of the method.

Later, K. W. Johansen made an essential extension of Ingerslev's method. In his works [31,1] [32,1] [43,1] [62,1] the yield lines, besides the statical, have a **geometrical**

significance as lines along which a plastic rotation is taking place at the collapse load. Hereby it was made possible to estimate yield line patterns by purely geometrical considerations and to calculate upper bounds for the load carrying-capacity by the work equation.

One of the most important improvements in the development of the plastic theory was the establishment of the so-called **upper- and lower-bound theorems**. The general formulation of a complete theory for perfectly plastic materials was given in 1936 by the Russian Gvozdev [38,1] and independently by Drucker, Greenberg, and Prager [52,1] [52,2], and has proved very valuable. These important principles were also stated by Hill [51,1] [52,3].

Historically it is interesting to notice that Johansen proved what is now called the upper bound theorem. The lower bound theorem was considered evident by the early workers of plasticity, so in Johansens mind there was probably nothing new in the works of Gvozdev and Drucker, Greenberg and Prager.

From 1960s there was growing interest in plastic theory for reinforced concrete structures in the world. By the middle 1960s, the slab theory had obtained almost final form and at that time it appeared as a special and useful case of the general theory of perfectly plastic materials. The general theory of perfectly plastic materials for slabs was described by Nielsen [62,2] [64,1], Wood [61,1] as well as Sawczuk and Jaeger [63,1], and Massonnet and Save [63,2].

The theory of disks with a complete set of formulas for orthogonal reinforcement was set up by Nielsen in 1963 [63,3] [64,2] and a complete set of formulas for skew reinforcement in 1969 [69,1].

Within the 1970s, the plastic theory has been applied to a number of nonstandard cases, principally shear in plain and reinforced concrete by Nielsen [78,1], Bræstrup [77,1], at the Technical University of Denmark. Similar research has been carried out at various other institutions. Most of the results obtained during that period were collected in the conference reports [78.2] [79.1] [79.2] and [79.3].

From 1970s, the theory of plasticity began to be widely accepted. In 1982, W. F. Chen published a general description of concrete plasticity in his book [82.1]. Nielsen presented an introduction to applications of plastic theories for the design of concrete structures in the book " **Limit Analysis and Concrete Plasticity**" [84.1]. Particularly useful results have been obtained regarding the strength of slabs, beams and shear walls under shear, torsion, and combined actions [73.1] [74.2] [78.3] [80.1] [85.1] [95.1]. Rational models have been proposed which are adequately accurate and sufficiently simple and general for practical applications. These developments have had a big influence on the formulation of European codes. In North America, similar proposals for shear and torsion design found wide attention mainly from contributions by Vecchio, Collins [78.3][80.3] [81.2] [82.2] [86.2].

During this time, much research work based on the plastic theory has been carried out with the objective of developing an understanding of the behavior of shear walls. Firstly the yield hinge method and elasto-plastic analysis were used to analyze shear walls [68.1] [70.1]. Similarly Paulay has used the plastic hinge method and the conception of ductility to analyze and design shear walls [76.1] [82.3] [92.1].

Later on, plastic theories with slightly different models were developed. The models used in shear wall analysis are mostly extended from beam theory.

1.2.2 Shear Wall Analysis

Shear walls can be defined as vertical cantilevers or squat shear walls (according to the ratio between the height and the width), with various cross sections such as rectangular, I (barbell and flanged), box , and other elevator wall sections. The shear walls support the vertical load, in addition to their function to stiffen the structures by their resistance to lateral loads due to wind, earthquake or blast. Although interior and exterior concrete walls have been used to stiffen structures as long as reinforced concrete itself has been in use, the modern concept of shear walls designed as vertical slender cantilevers were first utilized in 1948 in housing projects in New York City and in Chicago in buildings designed for wind forces, to augment the lateral resistance of the frames [74. 1] .

Analysis for lateral loads on buildings containing shear walls was carried out initially, in the 1950s, by assigning all the lateral loads to the shear walls, since it was felt that the very big difference in stiffness between the shear walls and the frame would cause the shear walls to carry the total lateral loads.

Shear walls can be classified as (a) short shear walls (a/h, less than about 1), and (b) slender shear walls (a/h, more than 2). Short shear walls are mostly governed by their shear strength, while slender shear walls are cantilever beams controlled by

flexure. Another possible classification of shear walls is according to the geometry of the section: rectangular sections, and I-sections (barbell and flanged).
Several models are used in the analysis of shear walls. The most common models used in the analysis of shear walls are the **strut-and-tie model** and the **truss model**.

The strut and tie model is as old as reinforced concrete theory and was normally called a truss model in the old days [22.1] [28.1]. The load in this type of model is carried by concrete bars subjected to compression and tensile bars made up by the reinforcement bars. This model has played an important role when the modern reinforcement theory started to develop [63.1] [63.2] [69.1] and has also been extensively used in practical design for many years [85.1] [86.5] [90.2] [93.1] [93.2]. Figure1.1 illustrates the strut-and-tie model.

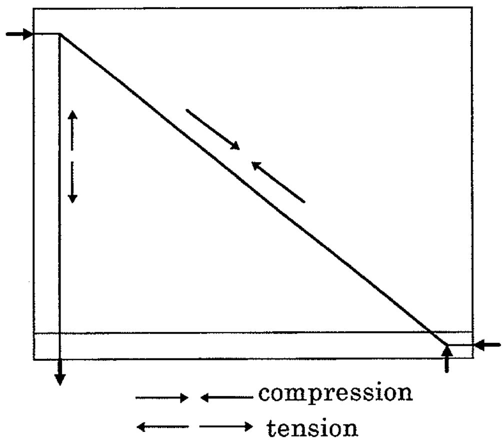

Fig. 1.1 *Strut-and-tie model of a shear wall*

Aoyama and H. Shiohara [86.5] used the strut-and-tie model to calculate the stress field and to predict the ultimate shear load of some perticular shear walls and got good correlation with experimental results. Also by using this model, W.B. Siao found good agreement with test results when predicting the shear capacity of reinforced concrete walls with height-to-width ratios less than or equal to 1 [94.1].

The **truss model** is the most widely used model in shear design and analysis. In its simplest form, a wall acts as a statically determinate truss as illustrated in Fig. 1.2. The concrete between the cracks forms the struts of the truss; the longitudinal reinforcement becomes the longitudinal chords of the truss. Finally the transverse reinforcement makes the tensile ties. Although the truss analogy is a relatively simple model, it is convenient and reasonable for explaining the shear transfer mechanism in a thin web with boundary elements.

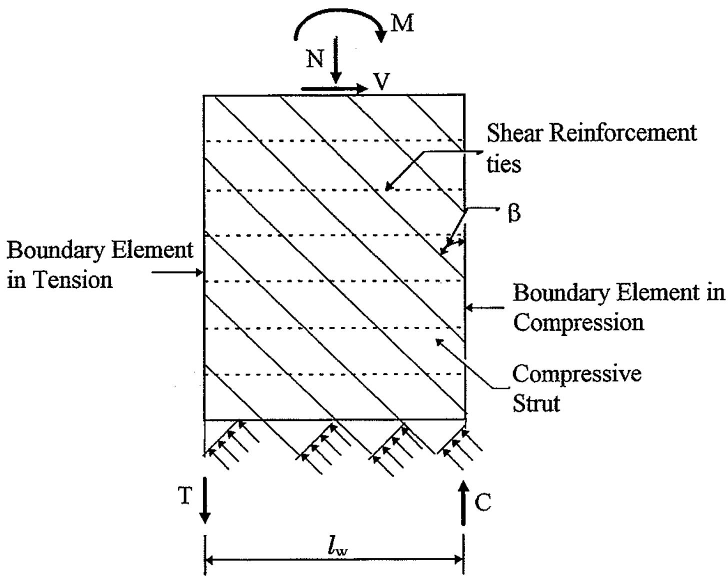

Fig. 1.2 *Truss model for a reinforced concrete wall*

Oesterle et al [84.3] based on his experimentation and study reported that the determination of the shear capacity and the failure criteria may be found using the truss analogy model.

Based on equilibrium and compatibility conditions, as well as a stress-strain relationship for softened concrete which was proposed by Vecchio and Collins [81.2], Hsu and Mo developed a **soften truss model** to predict the strength, behavior, shear design and analysis of low-rise reinforced concrete shear walls [85.2] [86.3] [87.1].

The **modified truss analogy model** is developed from the truss analogy model for reinforced beams and has been used in the ACI building Code. The applicability of this model for low-rise structural walls subjected to earthquake-induced loads has been questioned in discussions around the ACI building Code [83.1] [83.2] [86.1] and was evaluated by Sharon L.Wood [90.1].

The **compressive force and path method** was first developed by Kotsovos [83.3] [84.2] [88.1]. Lefas applied it to structural walls [88.2] (see Figure 1.3). According to this method the wall strength is related to the strength of the concrete in the region of the path in which the compressive forces are transmitted to the wall base. It is believed that the shear force are carried through the wall and can be visualized as a flow of compressive stresses within a path of varying cross-section. Failure is considered to be associated with the development of tensile stresses within a path region. This method generally is used in walls which may be identified with cantilever beams.

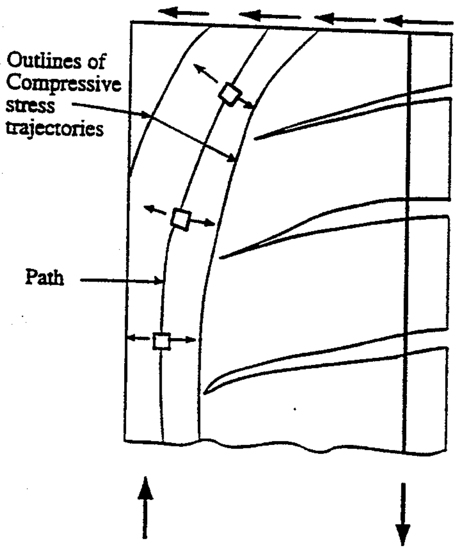

Fig. 1.3 *Compressive force and path method for walls*

In this paper a theoretical model shown in Fig. 1.4 as well as Fig. 1.5 is developed. The model is a strut in combination with triangular homogeneous stress fields which is suitable for squat walls as shown in Fig. 1.4 or a diagonal uniaxial compression field in combination with triangular homogeneous stress fields which is proper for slender walls as shown in Fig.1.5.

The model developed has been inspired by a beam model used by Jensen [81.1].

The triangular areas consist of two diagonal compression fields with different uniaxial compression concrete stresses σ_c^I and σ_c^{II} which are inclined to the vertical axis by angles θ and θ_1, respectively, and one biaxial stress field with concrete compressive stresses f_c and $\sigma_2 \leq f_c$.

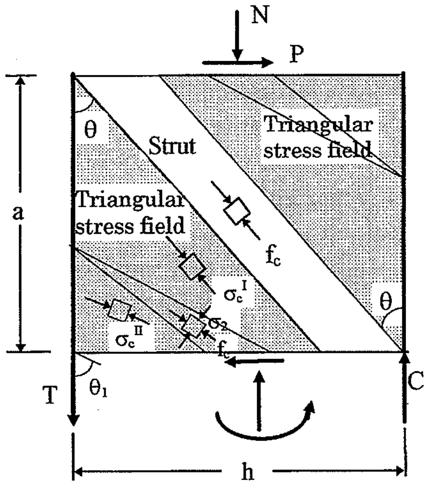

Fig.1.4 *Strut solution combined with triangular stress fields*

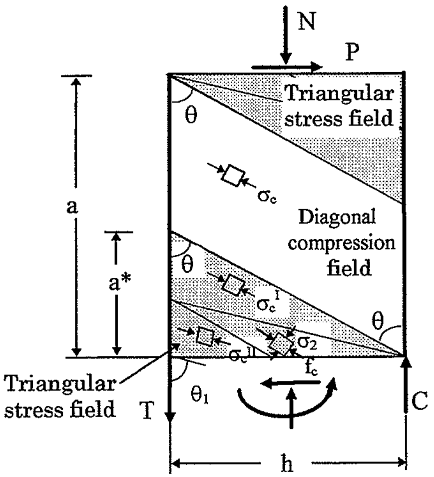

Fig.1.5 *Diagonal compression field combined with triangular stress fields*

In this model, the boundary elements are treated as stringers. The strut and the diagonal stress field carry the uniaxial compression stress f_c and $\sigma_c \le f_c$, respectively. The strut and triangular areas deliver to the top slab and bottom slab shear stresses and compression stresses. The horizontal component of the uniaxial compression stress in the diagonal stress field is eqiulibrated by the stirrups in the web and the vertical one is eqiulibrated by the stringer forces.

If standard computer optimization routines are used, a strut or a diagonal stress field at failure can be determined automatically.

A large number of shear wall tests have been treated using the theory proposed in this paper and the results from theory coincide well with the experimental results.

Chapter II. BASIC THEORY AND ASSUMPTIONS

2.1 Extremum Principles for Rigid-Plastic Materials

A rigid-plastic material is defined as a material in which no deformations occur (at all) for stresses up to a certain limit, the yield point. For stresses at the yield point, arbitrarily large deformations are possible without any change in the stresses. In the uniaxial case, a tensile or compressive rod, this case corresponds to a stress-strain curve as shown in Fig.2.1. The stress, the *yield stress*, for which arbitrarily large strains are possible, is denoted f_Y . In the figure the yield stresses for tensile and compressive actions are assumed equal.

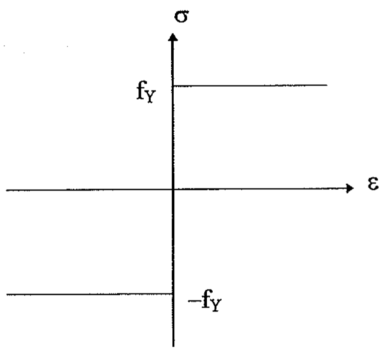

Fig.2.1 Uniaxial stress-strain relation for a rigid-plastic material

As long as the stresses in a body of a rigid-plastic material are below the yield point, no deformations occur. This idealization implies that we cannot determine the stress field in such a body when the stresses are below the yield point. When the loading increases to a point where it can be carried only by stresses at the yield point, unlimited deformations are possible without changing the load, if the strains (determined by the normality condition) correspond to a geometrically possible displacement field. The body is then said to be subjected to collapse by yielding. The corresponding load is called the collapse load or the **load-carrying capacity** of the body. The terms yield load and failure load will also be used. The theory of collapse by yielding is termed **limit analysis**.

For determination of the load-carrying capacity of rigid-plastic bodies the following extremum principles are very useful, see [84.1] for a review.

<u>The Lower-Bound Theorem</u>

Any load corresponding to a safe and satically admissible stress field is smaller than or equal to the yield load of the body.

A safe stress field is defined as a stress field correponding to points within or on the yield surface, which is the surface describing the combination of stresses giving rise to yielding.

A statically admissible stress field satisfies the equilibrium equations including the statical boundary conditions.

<u>The Upper-Bound Theorem</u>

Any load found from the work equation for an arbitrary, geometrically admissible failure mechanism is greater than or equal to the yield load of the body.

To determine the work absorbed by the body a flow rule is needed. In plastic theory the strain increment as a vector is assumed to be perpendicular to the yield surface. This condition is termed the normality condition. In the work equation the work done by the external force is equalised to the work absorbed by the body.

The Uniqueness Theorem

If the lowest upper bound and the highest lower bound coincide, then an exact solution has been found, the coinciding upper and lower bound being the yield load of the body.

2.2 The Solution of Plasticity Problems

Since the displacement and/or the stress field are often discontinuous in plastic solutions, the governing equations are different from those used in the elastic theory [84.1]. The statical discontinuities can be illustrated as follows.

Consider a plane stress field which is devided into two parts I and II by a curve l (see Fig.2.2). According to the law of action and reaction, only the following conditions have to be fulfilled along l:

$$\sigma_n^{I} = \sigma_n^{II}$$

$$\tau_{nt}^{I} = \tau_{nt}^{II}$$

Therefore in a stress field satisfying the equilibrium conditions, there might be a discontinuity in σ_t along l which is called a line of stress discontinuity. This is illustrated in Fig. 2.3.

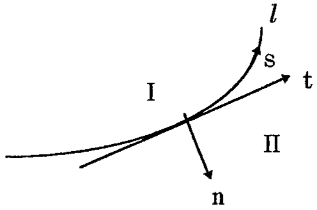

Fig. 2.2 *Coordinate system along a stress discontinuity line in a disk*

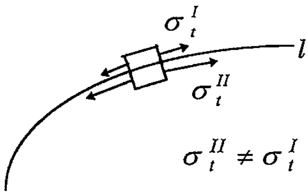

Fig. 2.3 *Example of stress discontinuities in a disk*

In plastic theory no analytical standard method can be used to solve load-carrying capacity problems. Upper and lower bound solutions can be found by the upper and lower bound theorems. An upper bound solution is found by considering a geometrically possible failure mechanism and by solving the work equation. A lower bound solution is found by constructing a statically admissible stress field corresponding to stresses within or on the yield surface.

2.3. Modified Coulomb Material

For a large group of materials it appears that reasonable failure conditions are attended by combining Coulomb's frictional hypothesis with a bound for the maximum tensile stress. The resulting failure criterion makes it natural to distinguish between two failure modes, *sliding failure* and *separation failure*. In both cases the name refers to what we imagine the relative motion between particles on each side of the failure surface to be. At sliding failure there is motion parallel to the failure surface, while motion at the separation failure is perpendicular to the failure surface. By sliding failure in certain materials, motion along the failure surface is combined with motion off the failure surface.

Sliding failure is assumed to occur in a section when the Coulomb frictional hypothesis is fulfilled; that is the shear stress $|\tau|$ in the section exceeds the *sliding resistance*, which, as mentioned, can be determined by two contributions. One contribution is *cohesion*, denoted c. The other contribution terms from a kind of internal friction and equals a certain fraction μ of the normal stress σ in the section. The quantity μ is called the *coefficient of friction*. If σ is a compressive stress, it gives a positive contribution to the sliding resistance; if σ is a tensile stress, it gives a negative contribution.

The condition for sliding failure is therefore

$$|\tau| = c - \mu\sigma \tag{2.1}$$

where c and μ are positive constants and σ is counted positive as a tensile stress. A material complying with this failure condition is called a *Coulomb material*.

Separation failure occurs when the tensile stress σ in a section exceeds the *separation resistance* f_A, that is , when the criterion

$$\sigma = f_A \tag{2.2}$$

is fulfilled.

A material complying with (2.1) and (2.2) is called a ***modified Coulomb material***.

As yield condition (failure criterion) for concrete we adopt the hypothesis called the modified Coulomb failure criterion which is the hypothesis of Coulomb together with a limitation of the tensile strength.

If conditions (2.1) and (2.2) are illustrated in a (σ,τ)-coordinate system, we have the straight lines shown in Fig. 2.4 dividing the plane into two regions.

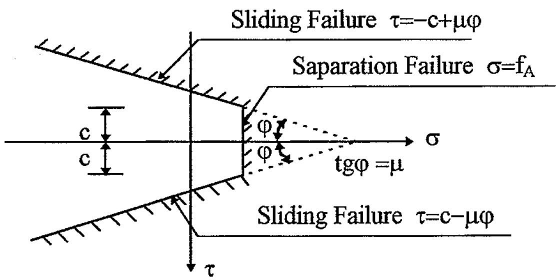

Figure 2.4 *Rupture criterion for a modified Coulomb material.*

2.4 Assumptions

The yield condition for the composite material containing concrete as well as reinforcement bars will be developed using the rigid-plastic theory, and by using the failure criteria for concrete as yield condition for concrete.

Concrete

The concrete is considered to be a rigid-plastic material obeying the modified Coulomb failure criterion with zero tensile cutoff (see Fig.2.5). The compressive strength is $f_c^* = \nu\, f_c$, where f_c is the cylinder strength and ν is an effectiveness factor.

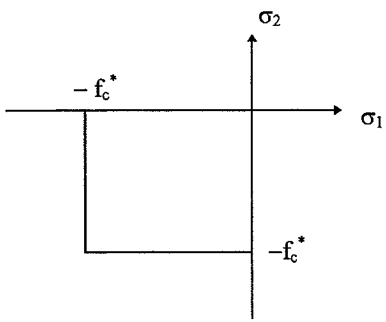

Figure 2.5 *Yield condition for concrete in plane stress, the tensile strength being put to zero.*

Reinforcement

We assume the reinforcement to be capable of carrying longitudinal tensile and compressive stresses only. The material is assumed to be rigid-plastic. In fig.2.6 the stress-strain relation is shown. The yield strength of the reinforcement is denoted f_y. According to this assumption, the reinforcement bars are unable to resist any lateral force, i.e., the dowel effects are neglected.

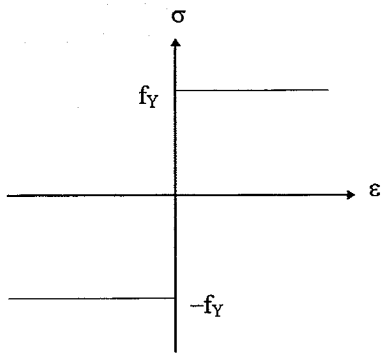

Figure 2.6 *Uniaxial stress-strain relation for a reinforcement bar*

CHAPTER III UPPER BOUND SOLUTIONS FOR SHEAR WALLS

In this chapter we will derive upper bound solutions for shear walls which are subjected to a concentrated transverse load and a vertical load both in the plane of the web.

The behavior of a structural wall within a storey of a multistorey building may be idealized by an isolated wall as shown in figure 3.1. The isolated wall comprises the boundary elements (boundary columns or flanges) and central panel (web). In practice, the central panel of a structural wall is usually provided with uniform reinforcement, i.e. bars of same diameter at equal spacing in both longitudinal and transverse direction. The isolated wall is subjected to vertical and horizontal loads.

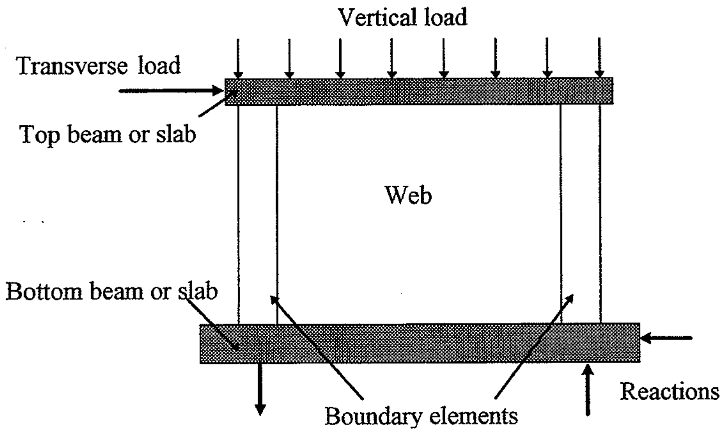

Fig.3.1 *An isolated shear wall*

3. 1 Basic Assumptions

Consider a shear wall as shown in Fig.3.1. The transverse load P is transferred to the wall by means of a top beam or slab and the wall transfers the force to the bottom beam or slab. The top beam or slab might be subjected to normal stresses along the horizontal face, which are statically equivalent to a normal force N.

Besides the assumptions that we have made in section 2.4, we further assume :

1) The wall is in a state of plane stress.

2) The boundary elements are treated as stringers, carrying a force T positive as tension and a force C positive as compression, respectively.

3) The normal stresses on the top beam or slab are assumed to be statically equivalent to a compression force N acting at the middle point of the top slab.

3.2 Upper Bound Solutions

The upper bound solutions of beams, deep beams and corbels without uniformly distributed reinforcement in longitudinal direction were derived by Nielsen, Bræstrup [77.1] , [78.1] and [79.2] and Chen [88.3]. Based on these solutions, the author has derived upper bound solutions of shear walls with uniformly distributed reinforcements in two perpendicular directions and with normal force.

Before starting to derive the formulae, we introduce the term ***reinforcement degree***, defined as being the ratio between the force per unit of length that the reinforcement is able to carry and the force per unit of length that the concrete is capable to carry in pure compression. The reinforcement degree is denoted Φ for longitudinal steel (in vertical direction) and ψ for stirrup steel (horizontal direction). So for the horizontal and vertical directions, respectively, we have

$$\left.\begin{aligned} \Phi_l &= \frac{A_{sl}\, f_{Yl}}{t\,h\,f_c} = \frac{\varphi_l\, f_{Yl}}{f_c} \\ \Phi_x &= \frac{\varphi_x\, f_{Yx}}{f_c} \\ \Psi &= \frac{\varphi_y\, f_{Yy}}{f_c} \end{aligned}\right\} \qquad (3.1)$$

The meaning of the notations is the following:

Φ_l, A_{sl}, f_{Yl}, φ_l : the reinforcement degree, the area, the yield strength and the ratio of the longitudinal reinforcement in the boundary elements, respectively.

Φ_x, f_{Yx}, φ_x	:	the reinforcement degree, the yield strength and the ratio of reinforcement in vertical direction of web, respectively;
ψ, f_{Yy}, φ_y	:	the reinforcement degree, the yield strength and the ratio of reinforcement in horizontal direction of web, respectively;
f_c	:	the uniaxial compression strength of concrete;
t	:	the thickness of the web;
t_f	:	the thickness of the boundary element;
h	:	the total width of the cross section.

A yield line is a kinematical discontinuity line separating the body into two rigid parts. One part is moving relative to the other with the velocity v inclined at the angle α^* to the yield line (Fig.3.2b). The discontinuity is a mathematical idealization of a narrow deforming zone (Fig. 3.2a).

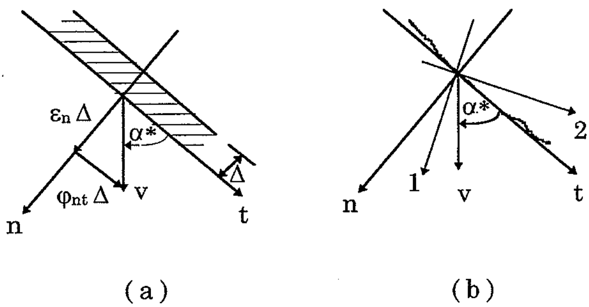

Fig 3. 2 *Yield line in plain concrete*

On the basis of the flow rule of perfectly plastic materials, the normality condition, only the stress state $(\sigma_1, \sigma_2) = (0, -f_c^*)$, corresponding to the lower right corner of the yield locus (Fig.3.3) can produce the strain rate state in the zone.

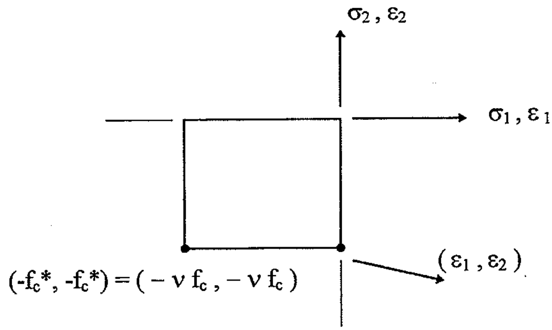

Fig. 3. 3 *Square yield locus for concrete in plane stress.*

Hence the rate of internal work dissipated per unit area of the yield line is given by ([79.2]) :

$$W_I = \frac{1}{2} v f_c^* (1 - \sin\alpha^*) \qquad \text{for } -\pi/2 \le \alpha \le \pi/2 \quad (3.2)$$

Here $f_c^* = \nu f_c$ is the effective concrete compression strength.

The principal directions of stresses and strain rates are indicated on Fig. 3.2b. The first principal axis bisects the angle between the relative velocity vector and the yield line normal.

Fig 3.4 shows a shear wall subjected to the shear force P and the normal force N. It is assumed that the failure mechanism consists of a single yield line inclined at the angle β to the x-axis. The relative velocity is v at an angle α to the y-axis.

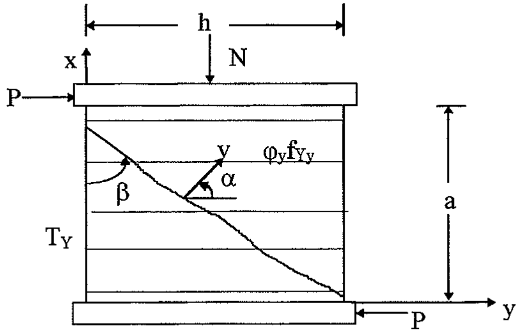

Fig.3.4 *Failure mechanism of a shear wall with horizontal stirrups subjected to transverse loading*

The rate of internal work dissipated in the mechanism is :

$$W_I = \varphi_y\, f_{Yy} \cos\beta \, \frac{th}{\sin\beta}\; v \cos\alpha + \frac{1}{2}\; v\, f_c^* \,[\, 1- \cos(\beta-\alpha)\,]\, \frac{th}{\sin\beta} + $$
$$+T_Y \,\sin\alpha \qquad (3.3)$$

where equation (3.2) has been used.

In (3.3), $T_Y = 2A_{sl}f_{Yl} + \varphi_x f_{Yx}\, th_0$ is the total yield force of the tensile reinforcement in the longitudinal direction.

The ranges of the variables α and β are:

$$\alpha \geq 0 \qquad \text{and} \qquad 0 \leq \cot\beta \leq \lambda \qquad (3.4)$$

where $\lambda = a/h$ is the shear span ratio.

The geometry of the wall imposes the upper limit on cotβ. The lower limit and the bound on α ensure that the stirrups and the longitudinal bars are yielding in tension, respectively.

The rate of external work done by the loading is

$$W_E = v\,P\cos\alpha \tag{3.5}$$

If a normal force N is acting, the external work is

$$W_E = v\,P\cos\alpha - v\,N\sin\alpha \tag{3.6}$$

Then the work equation $W_E = W_I$ yields the upper bound solution:

$$\frac{\tau}{f_c} = \frac{2\psi\cos\alpha\cos\beta + \upsilon\left[1-\cos(\alpha-\beta)\right] + 2\Phi\sin\alpha\sin\beta}{2\sin\beta\cos\alpha} \tag{3.7}$$

Here τ = P/th is the average ultimate shear stress, ν is the concrete effectiveness factor for shear, and we have introduced the shear reinforcement degrees

$$\Psi = \frac{\varphi_y f_{Yy}}{f_c} \tag{3.8}$$

and the nominal longitudinal reinforcement degrees

$$\Phi = \frac{2A_{sl} f_{Yl}}{t\,h\,f_c} + \frac{\varphi_x f_{Yx}}{f_c} + \frac{N}{t\,h\,f_c} \tag{3.9}$$

We may find the lowest upper bound by minimizing equation (3.7) with respect to the variables α and β. The necessary conditions are:

$$\sin\alpha - \frac{\upsilon - 2\Phi}{\upsilon}\sin\beta = 0 \qquad (\partial\tau / \partial\alpha = 0)$$

$$\cos\beta - \frac{\upsilon - 2\Psi}{\upsilon}\cos\alpha = 0 \qquad (\partial\tau / \partial\beta = 0)$$

which were derived by M.W. Bræstrup [79.1].

The lowest upper bound solutions are found to be:

$$\frac{\tau}{\upsilon f_c} = \begin{cases} \frac{1}{2}\left(\sqrt{4\Phi^*(1-\Phi^*)+(\frac{a}{h})^2} - \frac{a}{h}\right) + \Psi^*\frac{a}{h} & \begin{cases}\Psi^* < \Psi_0^* \\ \Phi^* < 0.5\end{cases} \\ \frac{1}{2}\left(\sqrt{1+(\frac{a}{h})^2} - \frac{a}{h}\right) + \Psi^*\frac{a}{h} & \begin{cases}\Psi^* < \Psi_0^* \\ \Phi^* \geq 0.5\end{cases} \\ 2\sqrt{\Phi^*(1-\Phi^*)\Psi^*(1-\Psi^*)} & \begin{cases}\Psi_0^* < \Psi^* < 0.5 \\ \Phi^* < 0.5\end{cases} \\ \sqrt{\Psi^*(1-\Psi^*)} & \begin{cases}\Psi_0^* < \Psi^* < 0.5 \\ \Phi^* \geq 0.5\end{cases} \\ \sqrt{\Phi^*(1-\Phi^*)} & \begin{cases}\Psi^* \geq 0.5 \\ \Phi^* < 0.5\end{cases} \\ \frac{1}{2} & \begin{cases}\Psi^* \geq 0.5 \\ \Phi^* \geq 0.5\end{cases} \end{cases} \qquad (3.10)$$

Here

$$
\begin{aligned}
\Phi^* &= \frac{\Phi}{\upsilon} \\
\Psi^* &= \frac{\Psi}{\upsilon} \qquad\qquad (3.11)\\
\Psi_0^* &= \frac{1}{2}\left(1-\frac{\frac{a}{h}}{\sqrt{4\Phi^*(1-\Phi^*)+(\frac{a}{h})^2}}\right)
\end{aligned}
$$

Since the formulae are based on upper bound solutions the estimates for the ultimate shear stress τ are greater than or equal to the theoretical load-carrying capacity. Corresponding lower bound solutions are determined by the construction of statically admissible stress distributions, see Chapter IV. Only for shear walls with strong main reinforcement or with very low height/width ratio a/h (a/h < 0.5) the lowest upper bound solutions coincide with the highest lower bound solutions.

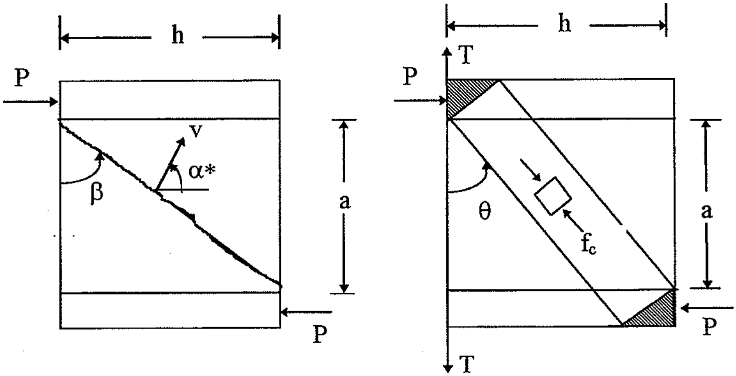

(a) Failure mechanism (b) Stress distribution

Fig. 3.5 *Shear wall without stirrup reinforcement*

For shear walls without web reinforcement ($\psi = 0$) , the upper bound solution is given by $(3.10)_1$ with $\psi = 0$. The failure mechanism is shown in Fig.3.5a and the stress distribution is sketched in Fig. 3.5b, consisting of a single strut between top and bottom plate.

It should be noted that in the analysis the compression stringer is yielding in tension. This means that longitudinal steel in both boundary elements and web have to be taken into account when the nominal longitudinal reinforcement degree Φ is calculated

3.3 The Theoretical Curves of Upper Bound Solutions for Shear Walls

Fig.3.6 shows the upper bound solutions for shear walls subjected to a concentrated transverse loading versus the longitudinal reinforcement degree and the shear reinforcement degree. Here we have set $\nu = 1$.

From Fig. 3.6, we see that the upper bound load-carrying capacity is dependent on the different parameters in the following way:

a. The load-carrying capacity is heavily dependent on the height/width ratio a/h. The smaller the shear span ratio the higher the load-carrying capacity.

b. The load-carrying capacity is much influenced by the longitudinal reinforcement degree Φ when the value of Φ is small (approximately $\Phi < 0.3$). With increasing Φ-value, the influence of Φ on the load-carrying capacity is diminished. A value of Φ higher than 0.5 does not increase the load-carrying capacity.

c. Increasing ψ-values from $\psi = 0$ gives a fast enhancement of the load-carrying capacity. The increasing $\tau/\nu f_c$-value for increasing ψ-value is valid for ψ-values up to 0.5. Higher values of ψ than 0.5 do not increase the load-carrying capacity.

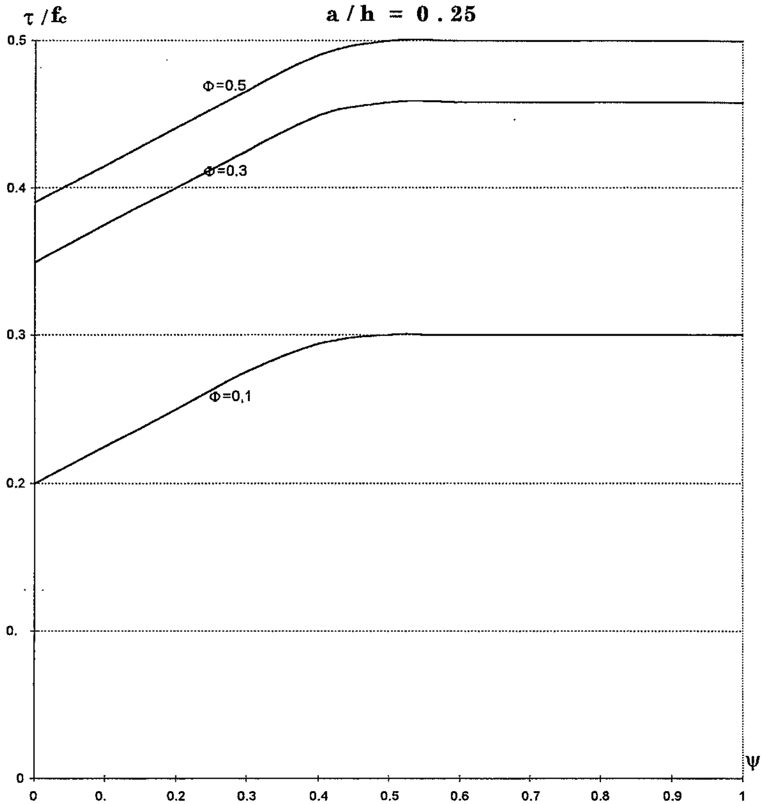

Fig. 3.6 *Upper bound shear capacity of a shear wall loaded by a concentrated transverse force versus the longitudinal reinforcement degree and the shear reinforcement degree*

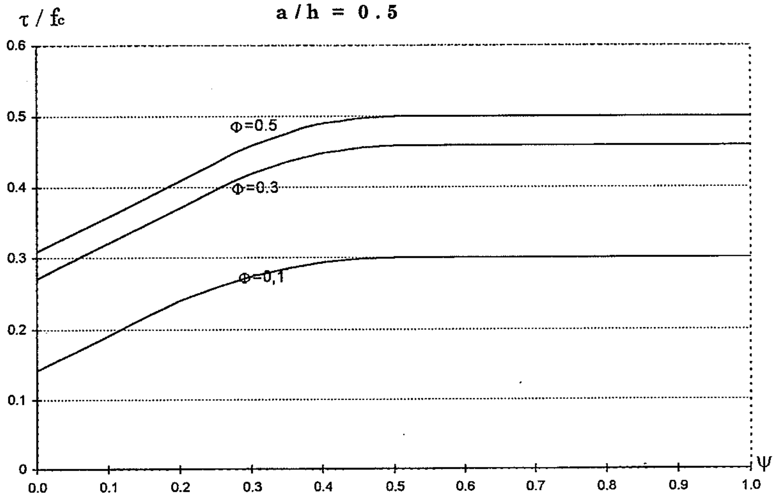

Fig. 3. 6 *(continued)*

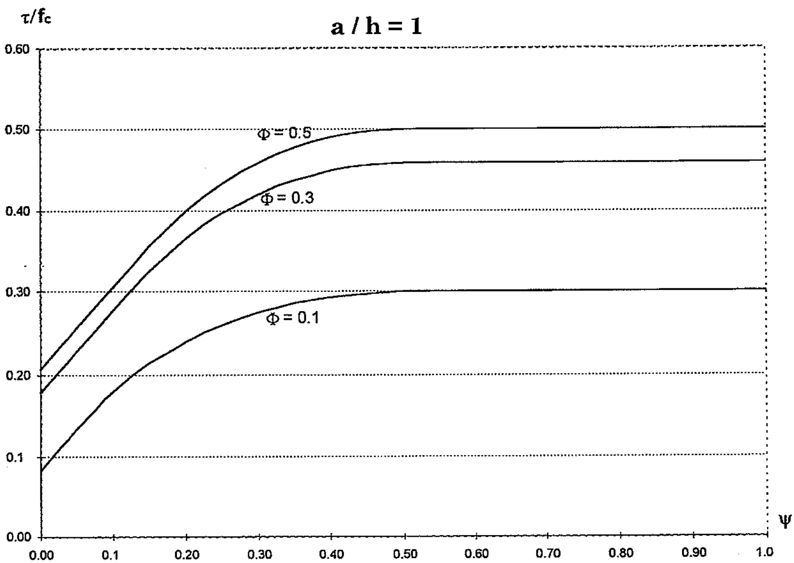

Fig. 3. 6 *(continued)*

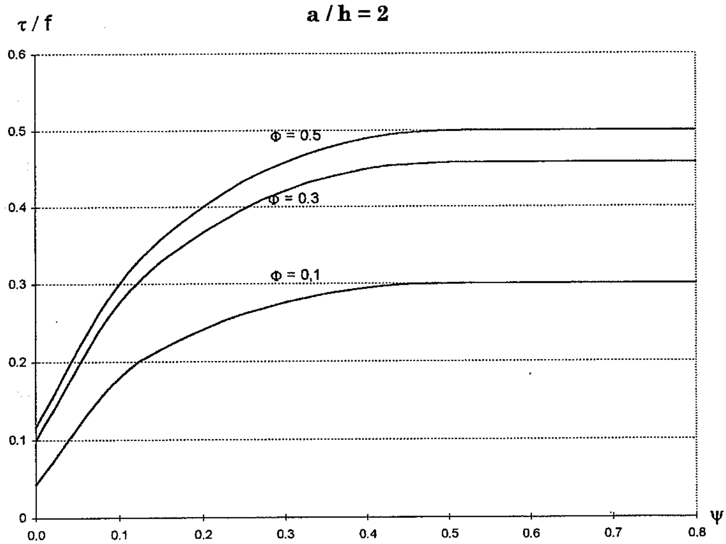

Fig. 3. 6 *(continued)*

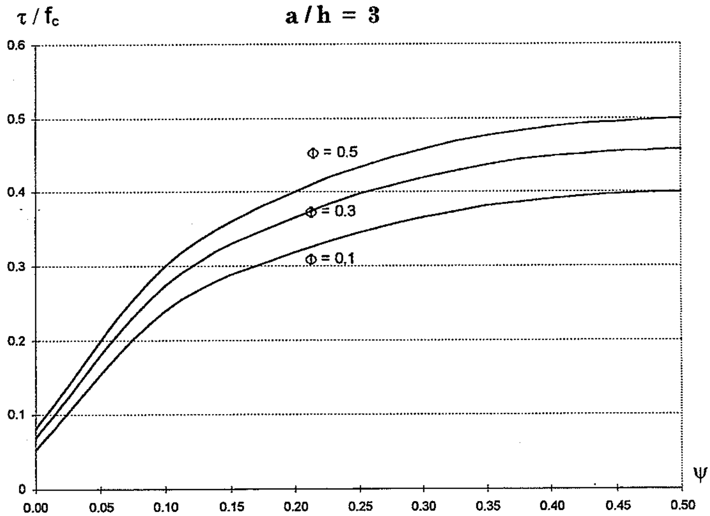

Fig. 3. 6 *(continued)*

CHAPTER IV LOWER BOUND SOLUTIONS FOR SHEAR WALLS

A solution which satisfies the equilibrium conditions and the statical boundary and which is based on a safe stress distribution is a lower bound solution for the load-carrying capacity. In this chapter, lower bound solutions of shear walls will be determined.

4.1 Lower Bound Solution for Shear Walls without Stirrup Reinforcement

In this section we will derive a lower bound solution for shear walls without stirrup reinforcement by using the strut-and-tie model.

The concept of utilizing concrete to resist compression and reinforcement to carry tension gives rise to the **strut-and-tie model**. In this model, a concrete compression strut and a steel tension tie form a truss that is capable of resisting the load.

The strut and tie model will be used in this paper to calculate the load-carrying capacity of shear walls. We will start by treating the single strut.

Consider a wall with reinforced boundary elements on both sides loaded by a transverse force P. Based on the assumptions in section 3.1, the boundary elements can be treated as stringers (see Fig.4.1).

The strut in Fig. 4.1 carries the uniaxial compression strength f_c of concrete [84.1]. The strut is loaded by the shaded area shown in Fig.4.1. This area is in biaxial hydrostatic pressure f_c. The shear span is **a** . The horizontal width of the strut is h.

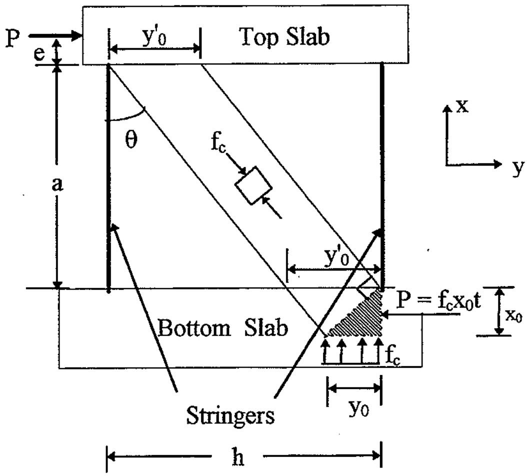

Fig. 4.1 *Strut action in a wall.*

Assuming the strut to be inclined to the vertical axis by the angle θ, we have

$$\tan\theta = \frac{x_0}{y_0} = \frac{h - y_0}{a + x_0} \tag{4.1}$$

If the strut carries the horizontal load P, the shear force along the shear span **a** is

$$P = f_c\, x_0\, t \tag{4.2}$$

t being the thickness of the web.

From formula (4. 2), we get

$$x_0 = \frac{P}{tf_c} \quad \Rightarrow \quad \frac{x_0}{h} = \frac{P}{thf_c} = \frac{\tau}{f_c} \qquad (4.3)$$

Here τ is the average shear stress along the width h.

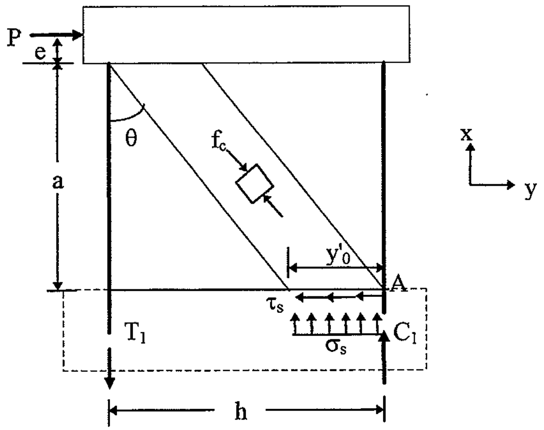

Fig. 4.2 *Stress distribution in a wall without stirrups*

The strut delivers to the top slab and to the bottom slab a shear stress τ_s and a compression stress σ_s both uniformly distributed along y_0' (see Fig. 4.2). These stresses are

$$\tau_s = f_c \cos\theta \sin\theta \qquad (4.4)$$

$$\sigma_s = f_c \cos^2\theta \qquad (4.5)$$

From Fig.4.1, the length y_o' is found to be

$$y_0' = \frac{y_0}{\cos^2\theta} \qquad (4.6)$$

By equilibrium equation of the wall shown in Fig.4.2, the load carried by the wall is

$$P = \tau_s\, y_o'\, t = f_c\, y_o'\, t \sin\theta \cos\theta = f_c\, y_o\, t \tan\theta \qquad (4.7)$$

Then the shear capacity is

$$\frac{\tau}{f_c} = \frac{P}{thf_c} = \frac{y_o}{h}\tan\theta \qquad (4.8)$$

Inserting (4.1) into (4.8) and using (4.3), we get a second degree equation with respect to $\frac{\tau}{f_c}$:

$$\left(\frac{\tau}{f_c}\right)^2 + \frac{a}{h}\frac{\tau}{f_c} - \frac{y_0}{h}\left(1 - \frac{y_0}{h}\right) = 0 \qquad (4.9)$$

Solving equation (4.9), we find that the load carrying capacity of a wall without stirrups is determined by

$$\frac{\tau}{f_c} = \frac{1}{2}\left[\sqrt{4\frac{y_0}{h}\left(1-\frac{y_0}{h}\right)+\left(\frac{a}{h}\right)^2} - \frac{a}{h}\right] \qquad (4.10)$$

The maximum shear capacity of a wall without stirrups may be determined by maximizing (4.10) with respect to $\frac{y_0}{h}$. It appears that the highest lower bound is obtained when $\frac{y_0}{h} = 0.5$, i.e.

$$\frac{\tau}{f_c} = \frac{1}{2}\left[\sqrt{1 + (\frac{a}{h})^2} - \frac{a}{h} \right] \tag{4.11}$$

For a given value of the force or the stress in the tensile stringer we need one more equation to determine the two unknowns, the shear stress τ and y_0.

The force T_l in the tensile stringer may be expressed as

$$T_l = A_{sl}\, \sigma_{sl} = \Phi_l \frac{\sigma_{sl}}{f_{Yl}} th \tag{4.12}$$

where Φ_{sl} is the reinforcement degree, σ_{sl} and f_{Yl} are the tensile stress at the bottom of the stringer and the yield strength of the stringer reinforcement, respectively.

Taking moment about A in the bottom section (see Fig.4.2) :

$$T_l\, h - \frac{1}{2}\sigma_s\, y_0'^2\, t = \quad P(a + e) \tag{4.13}$$

Here the parameter $\boldsymbol{e}$ determines the position of P on the top slab. This moment equation leads to

$$(\frac{\tau}{f_c})^2 + 2\frac{a+e}{h}\frac{\tau}{f_c} + (\frac{y_0}{h})^2 - 2\Phi_l \frac{\sigma_{sl}}{f_{Yl}} = 0 \tag{4.14}$$

if equations (4.4) to (4.6) are used.

Combining equation (4.14) with (4.10), we may get the value of $\frac{y_0}{h}$. Furthermore, the shear capacity of the wall can be determined by the equation (4.10).

If there is a uniform longitudinal reinforcement corresponding to the reinforcement ratio φ_x in the web and a normal force N is acting on the wall as shown in Fig. 4.3, the corresponding subsidiary condition is found to be

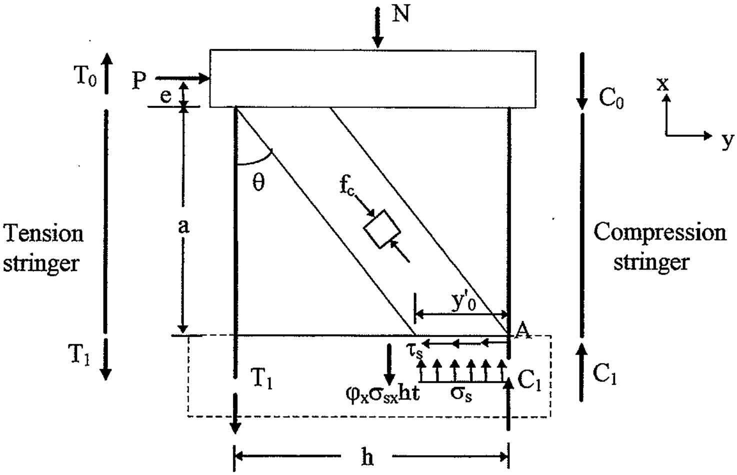

Fig. 4.3 *Shear wall with longitudinal reinforcement in the web loaded by transverse as well as normal forces*

$$\left(\frac{\tau}{f_c}\right)^2 + 2\frac{a+e}{h}\frac{\tau}{f_c} + \left(\frac{y_0}{h}\right)^2 - \left(2\Phi_l \frac{\sigma_{sl}}{f_{sl}} + \Phi_x \frac{\sigma_{sx}}{f_{sx}} + \frac{N}{thf_c}\right) = 0 \qquad (4.15)$$

Here Φ_x is the longitudinal reinforcement degree in the web, σ_{sx} and f_{Yx} are the corresponding stress and yield strength, respectively.

The stringer force C_1 is determined by projection in x-direction in Fig. 4.3 :

$$C_1 = T_1 + \sigma_{sx}\,\varphi_x\; t\,h + N - \sigma_s\, y_0' t$$

$$= (\Phi_l \frac{\sigma_{sl}}{f_{Yl}} + \Phi_x \frac{\sigma_{sx}}{f_{Yx}} + \frac{N}{t h f_c} - \frac{y_0}{h})\, f_c\, h\, t \qquad (4.16)$$

Since there are no stirrups in the wall, the stringer forces are constant :

$$T_0 = T_1 \qquad (4.17)$$

$$C_0 = C_1 \qquad (4.18)$$

If we assume all reinforcement to be yielding in tension, i.e. $\sigma_{sl} = f_{Yl}$ and $\sigma_{sx} = f_{Yx}$, we find the corresponding subsidiary condition :

$$(\frac{\tau}{f_c})^2 + 2\frac{a+e}{h}\frac{\tau}{f_c} + (\frac{y_0}{h})^2 - 2\Phi = 0 \qquad (4.19)$$

Here

$$\Phi = \Phi_l + \frac{\Phi_x}{2} + \frac{n}{2} \qquad (4.20)$$

is the nominal longitudinal reinforcement degree for the lower bound solution and $n = \frac{N}{t\, h\, f_c}$ is the dimensionless normal force. It should be noticed that the value of the nominal longitudinal reinforcement degree Φ for the lower bound solution is only half of that for the upper bound solution (see section 3.2)

If the load P is known, the necessary longitudinal reinforcement degree can be determined by formula (4.19) combined with formula (4.10).

A result, $T > 0$ means a tensile force is in the boundary element and $C > 0$ means a compression force in the boundary element. Since only the stresses in the wall have been dealt with it has been tacitly assumed that the top slab is able to carry the forces acting on it. The solution obtained is also only a true lower bound solution if the stringer force C is not decisive for the load-carrying capacity.

The anchorage of the reinforcement and the whole design of the support regions and the regions around the concentrated forces are extremely important and may be decisive for the load carrying capacity. The problem was described in detail in [81.1] and [84.1].

4.2 Shear Capacity of Shear Walls with Stirrup Reinforcement

In this section we will treat shear walls with horizontal stirrup reinfocement subjected to concentrated transverse loading as well as normal forces .

Generally, a uniform minimum reinforcement in both vertical and horizontal directions should be supplied in a shear wall. The reinforcement in the horizontal direction (see Fig. 4.3) may be taken into account by using a combination of strut action and homogeneous stress fields.

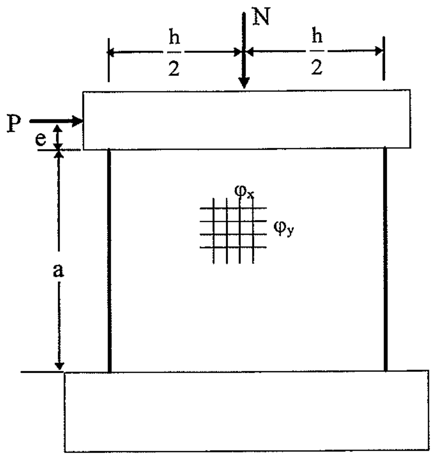

Fig. 4.4 *Shear wall with web reinforcement loaded by transverse as well as normal forces*

4.2.1 Strut Solution Combined with Triangular Stress Fields

When there is a uniform stirrup reinforcement in the web, we suppose that there are two triangular homogeneous stress fields each consisting of three parts in the area outside the strut. The stress distribution in the wall is as shown in Fig. 4.5 (a).

The strut is inclined to the vertical axis by an angle θ matching y_0. In the triangular area DA′D′ there are three different homogeneous stress fields. The area I and the area II are diagonal compression fields with uniaxial concrete stresses σ_c^I and σ_c^{II}, respectively. The stress σ_c^I is inclined to the vertical axis by angle θ and must satisfy the following condition:

$$\sigma_c^I \leq f_c \tag{4.21}$$

The stress σ_c^{II} is inclined to the vertical axis by angle θ_1 which satisfies the condition:

$$\theta_1 \geq \theta \tag{4.22}$$

The area III is a biaxial stress field with principal concrete compression stresses f_c and $\sigma_2 \leq f_c$.

Both the strut and the triangular tress field are loaded by the shaded area which is a biaxial stress field with concrete stresses f_c (see Fig. 4.5 (a)) .

The part BB′D′D as well as the triangular part DA′D′ are shown isolated in Fig.4.5 (b) and (c) .

In Fig.4.5 (b), by projection in the y-direction, we find that

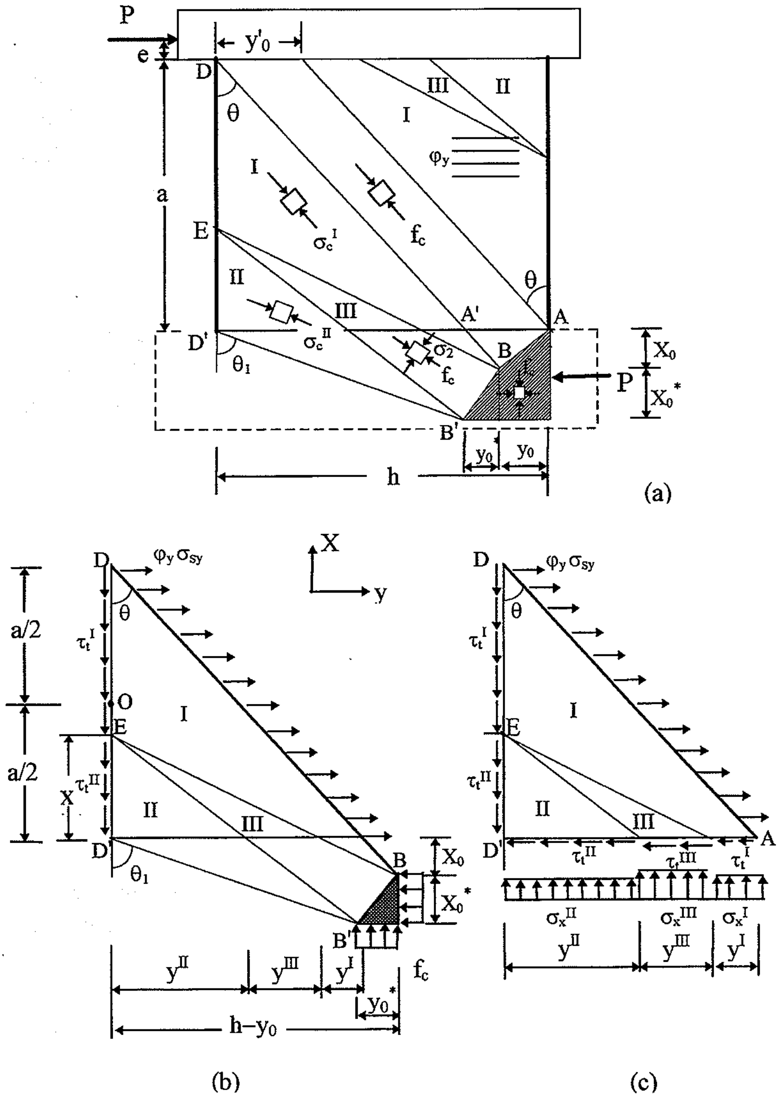

Fig. 4. 5 *Shear wall with strut and homogeneous stress fields in triangular areas*

$$x_0^* f_c = \varphi_y \sigma_{sy} a \quad \Rightarrow$$

$$x_0^* = a \ \psi \frac{\sigma_{sy}}{f_{Yy}} \tag{4.23}$$

Here

$$\psi = \frac{\varphi_y f_{Yy}}{f_c} \tag{4.24}$$

is the reinforcement degree of the stirrups, φ_y , σ_{sy} and f_{Yy} are the reinforcement ratio, the stress and the yield stress of the stirrups, respectively.

Taking moment about the point O , the mid point of DD′, we get

$$y_0^* = h - y_0 - \sqrt{(h-y_o)^2 - a\psi\frac{\sigma_{sy}}{f_{Yy}}\left[a(1+\psi\frac{\sigma_{sy}}{f_{Yy}}) + 2y_0 \tan\theta \right]} \tag{4.25}$$

The concrete stresses in a diagonal compression field with uniaxial concrete stress σ_c, referred to the x,y- system shown in Fig. 4.5, are

$$\left.\begin{aligned} \sigma_x &= -\sigma_c \cos^2\theta = -\tau_t \cot\theta \\ \sigma_y &= -\sigma_c \sin^2\theta = -\tau_t \tan\theta \\ \tau_t &= \left|\tau_{xy}\right| = \sigma_c \sin\theta \cos\theta \end{aligned}\right\} \tag{4.26}$$

Using the boundary conditions along D-D′

$$\sigma_y + \varphi_y \sigma_{sy} = 0 \tag{4.27}$$

and inserting it into (4.26), we obtain

$$\left.\begin{aligned} \tau_t^{I} &= \varphi_y \sigma_{sy} \cot\theta \\ \tau_t^{II} &= \varphi_y \sigma_{sy} \cot\theta_1 \end{aligned}\right\} \tag{4.28}$$

$$\left.\begin{aligned} \sigma_c^{I} &= \frac{\varphi_y \sigma_{sy}}{\sin^2\theta} = \varphi_y \sigma_{sy}(1+\cot^2\theta) \\ \sigma_c^{II} &= \frac{\varphi_y \sigma_{sy}}{\sin^2\theta_1} = \varphi_y \sigma_{sy}(1+\cot^2\theta_1) \end{aligned}\right\} \tag{4.29}$$

The angle θ_1 may be determined by the following equation:

$$\tan\theta_1 = \frac{h - y_0 - y_0^*}{x_0 + x_0^*} \tag{4.30}$$

or

$$\tan\theta_1 = \frac{h - y_0 - y_0^*}{y_0 \tan\theta + a\psi \dfrac{\sigma_{sy}}{f_{Yy}}} \tag{4.31}$$

Since $\theta_1 > \theta$, it is obvious that $\sigma_c^{II} \leq \sigma_c^{I}$.

By an equilibrium condition in the x-direction in Fig. 4.5 (b)

$$\tau_t^{I}(a-x) + \tau_t^{II} x = y_0^* f_c \tag{4.32}$$

we find

$$x = \frac{a\psi \frac{\sigma_{sy}}{f_{Yy}} \cot\theta - y_0^*}{\psi(\cot\theta - \cot\theta_1)\frac{\sigma_{sy}}{f_{Yy}}} \tag{4.33}$$

Here the equation (4.28) has been used.

The following geometrical relations may be found from Fig.4.5 (b) :

$$\left.\begin{aligned} y^{II} &= x \frac{h - y_0 - y_0^*}{x + y_0 \tan\theta + \psi a \frac{\sigma_{sy}}{f_{Yy}}} \\ y^{III} &= \frac{x(h - y_0)}{x + y_0 \tan\theta} - y^{II} \\ y^{I} &= h - \frac{y_0}{\cos^2\theta} - y^{II} - y^{III} \end{aligned}\right\} \tag{4.34}$$

By projection in the y-direction in Fig.4.5 (c), we have :

$$\tau_t^I y^I + \tau_t^{II} y^{II} + \tau_t^{III} y^{III} = \varphi_y \sigma_{sy} a \tag{4.35}$$

Thus the load carried by the wall is found by combining the strut with the triangular homogeneous stress fields as shown in Fig. 4.6 :

$$P = f_c t y_0' \sin\theta\cos\theta + t \sum_{i=I,III} \tau_t^i y^i = t y_0 f_c \tan\theta + \varphi_y \sigma_{sy} a t \tag{4.36}$$

Here the equations (4.7) and (4.35) have been used.

By means of equation (4.36) and using equation (4.10), the shear capacity of the wall with stirrups may be determined by the following equation :

$$\frac{\tau}{f_c} = \left[\sqrt{4\frac{y_0}{h}\left(1-\frac{y_0}{h}\right)+\left(\frac{a}{h}\right)^2} - \frac{a}{h} \right] + \psi \frac{a}{h}\frac{\sigma_{sy}}{f_{Yy}} \qquad (4.37)$$

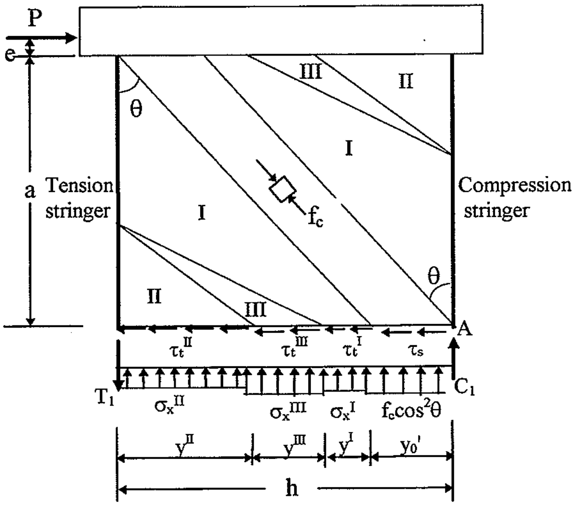

Fig. 4.6 *Stress distribution on the wall with stirrups*

In equation (4.37), the first term on the right hand side is the contribution from the strut and the second one is the contribution from the triangular homogeneous stress fields. The stresses delivered to the bottom slab from the left triangular area is shown in Fig. 4.5 (c) .

Next we look for the subsidiary conditions for this case. Using equations (4.26) and (4.29), it is easy to find that :

$$\left.\begin{aligned} \sigma_x^{I} &= \varphi_y \sigma_{sy} \cot^2\theta \\ \sigma_x^{II} &= \varphi_y \sigma_{sy} \cot^2\theta_1 \end{aligned}\right\} \qquad (4.38)$$

By projection in x-direction in Fig.4.5 (c), we get

$$\sigma_x^{III} = \frac{f_c y_0^* - \varphi_y \sigma_{sy}(y^{I}\cot^2\theta + y^{II}\cot^2\theta_1)}{y^{III}} \qquad (4.39)$$

Here (4.32) has been used.

Similarly, taking moment about point A in Fig. 4.6, we get

$$A_{sl}\sigma_{sl}h - \sigma_x^{II} t y^{II}(h - \frac{y^{II}}{2}) - \sigma_x^{III} t y^{III}(h - y^{II} - \frac{y^{III}}{2}) -$$

$$\sigma_x^{I} t y^{I}(\frac{y^{I}}{2} + \frac{y_0}{\cos^2\theta}) - y_0 t f_c \frac{y_0}{2\cos^2\theta} = P(a+e) \qquad (4.40)$$

Inserting equations (4.38) and (4.39) into (4.40), the following subsidiary condition may be found :

$$\frac{\tau}{f_c}(\frac{a}{h}+\frac{e}{h}) - \Phi_1\frac{\sigma_{sl}}{f_{Yl}} + \frac{\psi}{2}\frac{\sigma_{sy}}{f_{Yy}}\left[\cot^2\theta_1\frac{y^{II}}{h}(\frac{y^{II}}{h}+\frac{y^{III}}{h}) - \cot^2\theta\frac{y^{I}}{h}(\frac{y^{I}}{h}+\frac{y^{III}}{h})\right] +$$

$$\frac{y_0^*}{h}(1-\frac{y^{II}}{h}-\frac{y^{III}}{2h}) + \frac{1}{2}(\frac{y_0}{h\cos\theta})^2 = 0 \qquad (4.41)$$

For the case where there is a uniform longitudinal reinforcement with reinforcement ratio φ_x in the web and where a normal force N is acting on the wall as shown in Fig. 4.7, the subsidiary condition is found to be:

$$\frac{\tau}{f_c}\left(\frac{a}{h}+\frac{e}{h}\right)-\Phi_l\frac{\sigma_{sl}}{f_{Yl}}-\frac{1}{2}\Phi_x\frac{\sigma_{sx}}{f_{Yx}}-\frac{1}{2}\frac{N}{t h f_c}+\frac{\psi}{2}\frac{\sigma_{sy}}{f_{Yy}}\left[\cot^2\theta_1\frac{y^{II}}{h}\left(\frac{y^{II}}{h}+\frac{y^{III}}{h}\right)\right.$$

$$\left.-\cot^2\theta\frac{y^{I}}{h}\left(\frac{y^{I}}{h}+\frac{y^{III}}{h}\right)\right]+\frac{y_0^{*}}{h}\left(1-\frac{y^{II}}{h}-\frac{y^{III}}{2h}\right)+\frac{1}{2}\left(\frac{y_0}{h\cos\theta}\right)^2=0 \qquad (4.42)$$

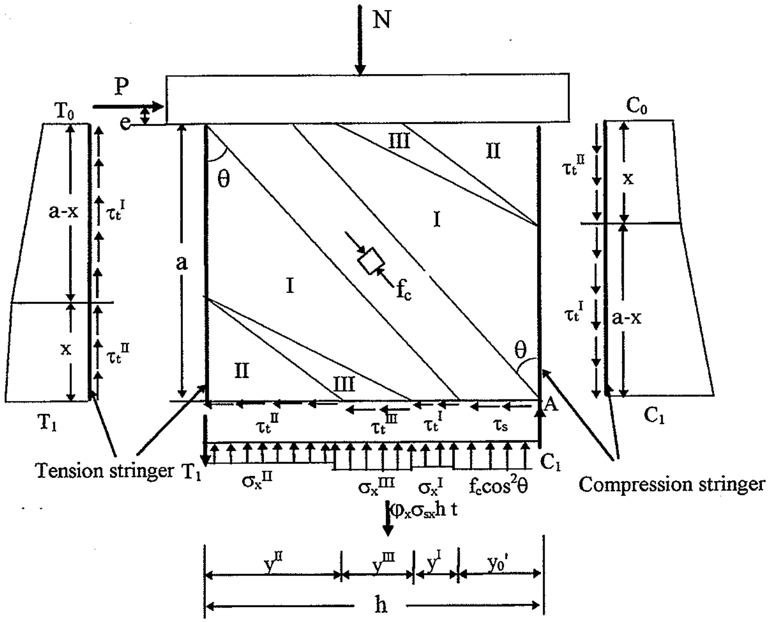

Fig. 4.7 *Shear wall with uniform reinforcement in both vertical and horizontal direction in the web loaded by transverse as well as normal forces*

Having constant shear stress along each particular length, the stringer forces vary linearly (see Fig. 4.7). The stringer forces are as follows :

$$\left.\begin{aligned}
T_1 &= A_{s1}\sigma_{s1} = \Phi_1 \frac{\sigma_{s1}}{f_{Y1}} f_c\, h t \\
C_1 &= T_1 + \varphi_x \sigma_{sx}\, t h + N - \sigma_s y_0' t - (\sigma_x^{I} y^{I} + \sigma_x^{II} y^{II} + \sigma_x^{III} y^{III})t \\
&= [\, \Phi_1 \frac{\sigma_{s1}}{f_{Y1}} + \Phi_x \frac{\sigma_{sx}}{f_{Yx}} + n - (\frac{y_0}{h} + \frac{y_0^*}{h})\,] f_c\, h t \\
T_0 &= T_1 - \tau_t^{I}(a-x)t - \tau_t^{II} x t \\
&= (\Phi_1 \frac{\sigma_{s1}}{f_{Y1}} - \frac{y_0^*}{h}) f_c\, h t \\
C_0 &= C_1 - \tau_t^{I}(a-x)t - \tau_t^{II} x t \\
&= [\, \Phi_1 \frac{\sigma_{s1}}{f_{Y1}} + \Phi_x \frac{\sigma_{sx}}{f_{Yx}} + n - (\frac{y_0}{h} + \frac{2y_0^*}{h})\,] f_c\, h t
\end{aligned}\right\} \qquad (4.43)$$

Here $\frac{y_0^*}{h}$ is determined by equation (4.25)

When $\sigma_{sl} = f_{Yl}$, $\sigma_{sx} = f_{Yx}$ and $\sigma_{sy} = f_{Yy}$, we obtain the following shear capacity of the wall with stirrups :

$$\frac{\tau}{f_c} = \frac{1}{2}\left[\sqrt{4\,\frac{y_0}{h}(1-\frac{y_0}{h}) + (\frac{a}{h})^2} - \frac{a}{h}\right] + \psi\,\frac{a}{h} \qquad (4.44)$$

Correspondingly, the subsidiary condition may be written :

$$\frac{\tau}{f_c}\left(\frac{a}{h}+\frac{e}{h}\right)-\Phi+\frac{y}{2}\left[\cot^2\theta_1\frac{y^{II}}{h}\left(\frac{y^{II}}{h}+\frac{y^{III}}{h}\right)-\cot^2\theta\frac{y^{I}}{h}\left(\frac{y^{I}}{h}+\frac{y^{III}}{h}\right)\right]$$

$$+\frac{y_0^*}{h}\left(1-\frac{y^{II}}{h}-\frac{y^{III}}{2h}\right)+\frac{1}{2}\left(\frac{y_0}{h\cos\theta}\right)^2=0 \qquad (4.45)$$

Here Φ is the nominal longitudinal reinforcement degree (see section 4.1) and

$$y_0^*=h-y_0-\sqrt{(h-y_o)^2-a\psi\left[a(1+\psi)+2y_0\tan\theta\right]} \qquad (4.46)$$

If (4.44) is maximized with respect to $\frac{y_0}{h}$, we may get the maximum average shear stress, which can be carried by the shear wall with strut and triangular homogeneous stress fields corresponding to $y_0/h = 0.5$,

$$\frac{\tau}{f_c}=\frac{1}{2}\left[\sqrt{1+\left(\frac{a}{h}\right)^2}-\frac{a}{h}\right]+\psi\,\frac{a}{h} \qquad (4.47)$$

For this case, the stringer forces are :

$$\left.\begin{aligned}
T_1 &= \Phi_l\, f_c\, h\, t\\
C_1 &= f_c\, h\, t\left[\,\Phi_l+\Phi_x+n-\left(\frac{y_0}{h}+\frac{y_0^*}{h}\right)\right]\\
T_0 &= f_c\, h\, t\left(\Phi_l-\frac{y_0^*}{h}\right)\\
C_0 &= f_c\, h\, t\left[\,\Phi_l+\Phi_x+n-\left(\frac{y_0}{h}+2\frac{y_0^*}{h}\right)\right]
\end{aligned}\right\} \qquad (4.48)$$

Formulas (4.44) through (4.48) may be used to design a shear wall.

4.2.2 The Uniaxial Diagonal Compression Field Combined with Triangular Stress Fields

In this section we consider the case where there is no strut in the wall. When the angle, by which the strut is inclined to the vertical axis,

$$\theta \geq \text{Arctan}\left(\frac{h}{a}\right)$$

the strut does not exist in the wall. In this case there is a diagonal unaxial compression field between the two triangular stress fields.

Consider a homogeneous stress field in the wall consisting of a uniaxial compressive stress σ_c in the concrete [84.1] as shown in Fig.4.8. This diagonal compression stress forms an angle θ with the vertical x-axis. The stress field referred to the (x,y)-system may be found by the equation (4.26).

For the areas connecting the top as well as the bottom slab, we suppose there are homogeneous stress fields in each triangular area, which are the same as those described in section 4.2.1.

The height a* of the triangular area has the following relation with the width h of the triangular area :

$$a^* = h \cot\theta \tag{4.49}$$

The procedure in section 4.2.1 is used to find all the parameters, stresses, forces and shear capacity of the wall. Thus they will be given without derivation in details.

For the wall with a diagonal compression field, we have :

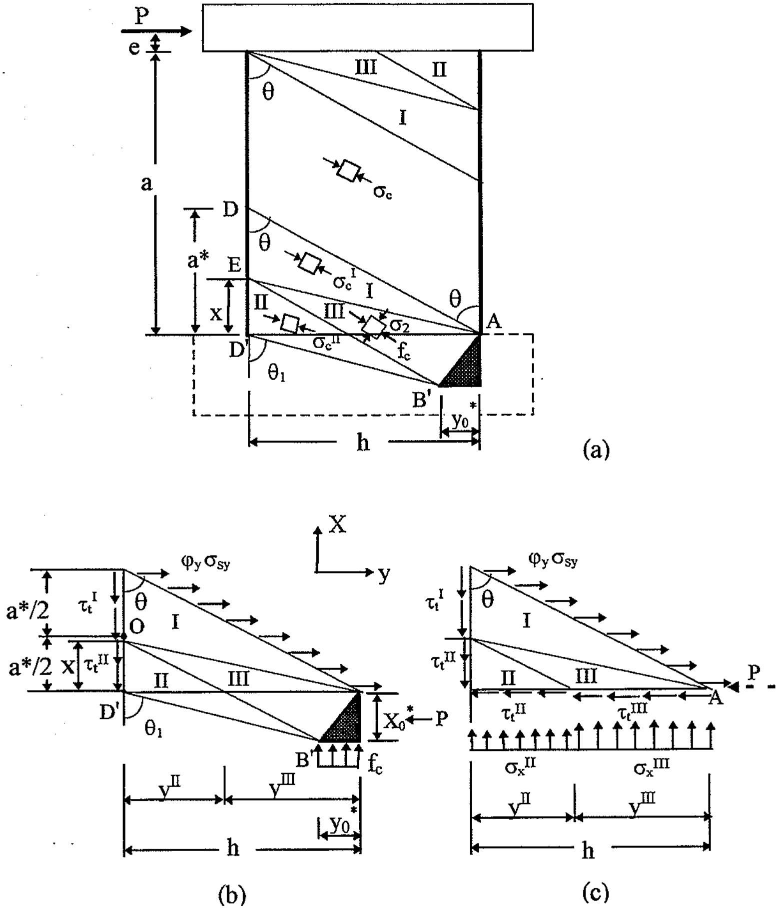

Fig. 4.8 *Shear wall with diagonal compression field*

$$x_0^* = a^* \ \psi \frac{\sigma_{sy}}{f_{Yy}} = h \ \psi \ \cot\theta \ \frac{\sigma_{sy}}{f_{Yy}} \tag{4.50}$$

$$y_0^* \ = \ h - \sqrt{h^2 - h^2 \psi \cot^2 \theta \frac{\sigma_{sy}}{f_{Yy}} \left(1 + \psi \frac{\sigma_{sy}}{f_{Yy}}\right)} \tag{4.51}$$

or

$$\frac{y_0^*}{h} = 1-\sqrt{1-\cot^2\theta\,\psi\frac{\sigma_{sy}}{f_{Yy}}\left(1+\psi\frac{\sigma_{sy}}{f_{Yy}}\right)} \tag{4.52}$$

$$\tan\theta_1 = \frac{h - y_0^*}{x_0^*} \tag{4.53}$$

or

$$\tan\theta_1 = \frac{1 - \dfrac{y_0^*}{h}}{\psi\,\dfrac{\sigma_{sy}}{f_{Yy}}\cot\theta} \tag{4.54}$$

$$\tau_t^I\,(a^* - x) + \tau_t^{II} x = y_0^*\, f_c \tag{4.55}$$

$$x = \frac{a^*\,\psi\,\dfrac{\sigma_{sy}}{f_{Yy}}\cot\theta - y_0^*}{\psi\,(\cot\theta - \cot\theta_1)\dfrac{\sigma_{sy}}{f_{Yy}}} \tag{4.56}$$

$$\left.\begin{aligned} y^{II} &= x\,\frac{h - y_0^*}{x + \psi\, a^*\,\dfrac{\sigma_{sy}}{f_{Yy}}} \\ y^{III} &= h - y^{II} = h - x\,\frac{h - y_0^*}{x + \psi\, a^*\,\dfrac{\sigma_{sy}}{f_{Yy}}} \end{aligned}\right\} \tag{4.57}$$

$$\left.\begin{aligned} \sigma_x^{II} &= \varphi_y\,\sigma_{sy}\cot^2\theta_1 \\ \sigma_x^{III} &= \frac{f_c\, y_0^* - \varphi_y\,\sigma_{sy}\cot^2\theta_1\, y^{II}}{y^{III}} \end{aligned}\right\} \tag{4.58}$$

The load carried by the wall is found to be (see Fig.4.8 (c))

$$P = \tau_x^{II} y^{II} + \tau_x^{III} y^{III} = \varphi_y \sigma_{sy} a^* t \tag{4.59}$$

The shear capacity of the wall is found from (4.59) :

$$\frac{\tau}{f_c} = \psi \frac{\sigma_{sy}}{f_{Yy}} cot\,\theta \tag{4.60}$$

The subsidiary condition is

$$\frac{\tau}{f_c}\left(\frac{a}{h}+\frac{e}{h}\right)-\Phi_1\frac{\sigma_{sl}}{f_{Yy}}+\frac{y\,\sigma_{sy}}{2\,f_{sy}}\frac{y^{II}}{h}\cot^2\theta_1+\frac{1}{2}\frac{y_0^*}{h}\frac{y^{III}}{h}=0 \tag{4.61}$$

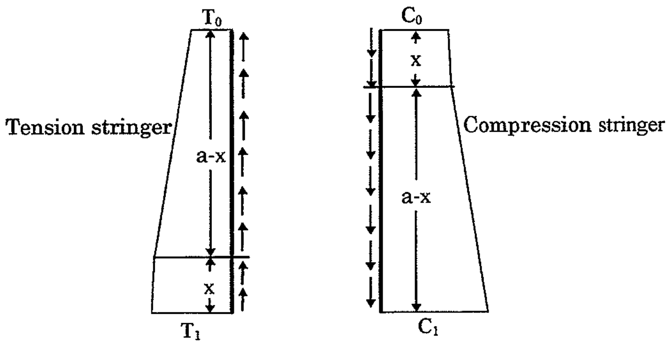

Fig. 4. 9 *Forces in flanges*

For the case where there is a uniform longitudinal reinforcement with reinforcement ratio φ_x in the web and a normal force N is acting on the wall, the subsidiary condition is

$$\frac{\tau}{f_c}\left(\frac{a}{h}+\frac{e}{h}\right)-\Phi_1\frac{\sigma_{sl}}{f_{Yy}}-\frac{1}{2}\Phi_x\frac{\sigma_{sx}}{f_{Yx}}-\frac{1}{2}\frac{N}{thf_c}+\frac{\psi\,\sigma_{sy}}{2\,f_{sy}}\frac{y^{II}}{h}\cot^2\theta_1+\frac{1}{2}\frac{y_0^*}{h}\frac{y^{III}}{h}=0 \tag{4.62}$$

The stringer forces are as follows (see Fig.4.9)

$$\left.\begin{aligned}
T_1 &= A_{s1}\,\sigma_{s1} = \Phi_1 \frac{\sigma_{s1}}{f_{Y1}} f_c\, ht \\
C_1 &= T_1 + \varphi_x\,\sigma_{sx}\, ht + N - (\sigma_x^{II} y^{II} + \sigma_x^{III} y^{III})t \\
&= [\, \Phi_1 \frac{\sigma_{s1}}{f_{Y1}} + \Phi_x \frac{\sigma_{sx}}{f_{Yx}} + \frac{N}{thf_c} - \frac{y_0^*}{h}] f_c\, ht \\
T_0 &= T_1 - \tau_t^{I}(a-x)t - \tau_t^{II} xt \\
&= [\, \Phi_1 \frac{\sigma_{s1}}{f_{Y1}} - \psi \frac{\sigma_{sy}}{f_{Yy}} \cot\theta (\frac{a}{h} - \cot\theta) - \frac{y_0^*}{h}] f_c\, ht \\
C_0 &= C_1 - \tau_t^{I}(a-x)t - \tau_t^{II} xt \\
&= [\, \Phi_1 \frac{\sigma_{s1}}{f_{Y1}} + \Phi_x \frac{\sigma_{sx}}{f_{Yx}} + \frac{N}{thf_c} - \psi \frac{\sigma_{sy}}{f_{Yy}} \cot\theta (\frac{a}{h} - \cot\theta) - \frac{2y_0^*}{h}] f_c\, ht
\end{aligned}\right\} \quad (4.63)$$

Assuming all the reinforcement to be yielding, the shear capacity of the wall is determined by (4.60) :

$$\frac{\tau}{f_c} = \psi \cot\theta \tag{4.64}$$

Setting

$$\sigma_c = \varphi_y\, f_{Yy}\, (1+\cot^2\theta) = f_c \tag{4.65}$$

the web crushing criterion, we get by solving the above two equations for τ and θ

$$\frac{\tau}{f_c} = \sqrt{\psi\,(1-\psi)} \tag{4.66}$$

$$\tan\theta = \sqrt{\frac{\psi}{1-\psi}} \tag{4.67}$$

Obviously, when $\psi = 0.5$ the shear capacity is at the maximum value $\tau = 0.5 f_c$. It is easily verified that the conditions $\sigma_s = f_Y$ and $\sigma_c = f_c$ give the highest lower bound. Further it is clear that for $\psi > 0.5$ the stirrup reinforcement does not yield and the shear capacity will be constant at

$$\frac{\tau}{f_c} = 0.5 \tag{4.68}$$

and the θ-value is constant at 45^0.

This means that when the tensile reinforcement and the compression stringer are sufficiently strong, i.e. the subsidiary condition

$$\frac{\tau}{f_c}\left(\frac{a}{h}+\frac{e}{h}\right)-\Phi+\frac{\psi}{2}\frac{y^{II}}{h}\cot^2\theta_I+\frac{1}{2}\frac{y_0^*}{h}\frac{y^{III}}{h} = 0 \tag{4.69}$$

is satisfied, the shear capacity of a shear wall as a function of ψ is determined by (4.66) and the formula for the maximum shear capacity (4.68) .

In equation (4.69)

$$\frac{y_0^*}{h} = 1-\sqrt{1-\cot^2\theta\,\psi\,(1+\psi)} \tag{4.70}$$

of course, it must be assumed that the top and bottom slabs are able to carry the forces acting on them.

Correspondingly, the stringer forces are as follows :

$$\left.\begin{aligned}
T_1 &= \Phi_1 f_c h t \\
C_1 &= (\Phi_1 + \Phi_x + n - \frac{y_0^*}{h}) f_c h t \\
T_0 &= [\Phi_1 - \psi \cot\theta(\frac{a}{h} - \cot\theta) - \frac{y_0^*}{h}] f_c h t \\
C_0 &= [\Phi_1 + \Phi_x + n - \psi \cot\theta(\frac{a}{h} - \cot\theta) - \frac{2y_0^*}{h}] f_c h t
\end{aligned}\right\} \quad (4.71)$$

Formulae (4.66) through (4.71) are available for the design of shear walls.

4.3 The Effectiveness Factor for Shear

A fair accordance between theory and test results is obtained only if the theory is modified by the introduction of an effective compressive strength of the concrete. This means that in applications f_c is replaced by $f_c^* = \nu f_c$. At the present stage of the development it is impossible to give more than a qualitative explanation of the strength reduction in reinforced concrete. We must rely on empirical formulas derived from tests.

The value of the effectiveness factor is not known very well in the case of shear walls with both longitudinal and transverse web reinforcement. For pure shear in disks with normal strength concrete, i.e., f_c < 50 MPa, it seems that the simple formula for the effectiveness factor

$$\nu = 0.7 - \frac{f_c}{200} \qquad (f_c \text{ in MPa}) \qquad (4.72)$$

gives reasonable agreement with tests. The formula was originally suggested for shear in beams, but it has turned out to be more generally applicable [84.1].

The ν–formula (4.72) is not very accurate for high strength concrete. According to Japanese tests, the following formula was suggested by Japanese researchers [91.1],

$$\nu = \frac{1.9}{f_c^{0.34}} \leq 1 \qquad (f_c \text{ in MPa}) \qquad (4.73)$$

The theory developed in this thesis has been compared with a large number of tests, cf. Chapter 6. The comparison shows that the following simple formulas may be used:

$$
\nu = \begin{cases} 0.8 - \dfrac{f_c}{200} + 0.725\dfrac{N}{A\,f_c} & f_c < 70\text{MPa} \\ \\ \dfrac{1.9}{f_c^{0.34}} + 0.725\dfrac{N}{A\,f_c} & f_c \geq 70\text{MPa} \end{cases} \tag{4.74}
$$

The second term on the right hand side of the formula (4.74) is added to take into account the enhancement of ν due to compressive normal stresses induced by the normal force N. A is the total area of the cross section of the wall. From (4.74), it is can be seen that f_c = 70 MPa has been chosen as the transitional point between normal strength concrete and high strength concrete instead of the usual value f_c = 50 MPa. The coefficient of variation is improved a little in this way.

The test cover height/width ratios up to 2.4. The formula (4.74) is remarkable because it has not been found necessary to include a dependence on the height/width ratio as has been the case for beams [78.1] [88.3].

According to the present understanding the dependence on the height/width ratio is due to sliding in initial cracks. Thus we may conclude that the shear walls in the tests have not developed a crack system giving rise to sliding in cracks. It is believed that this is due partly to the presence of a uniform reinforcement in the web. In the case of shear walls with boundary elements, crack sliding may have been prevented by the strong stringers.

4.4 The Theoretical Curves for Lower Bound Solutions of Shear Walls

The theoretical curves for the lower bound solution of shear walls obtained by the theory developed are depicted in Fig. 4.10. They have been found by standard computer optimization routines, see Chapter 6.

The curves are valid in the case where there is no normal force N and no vertical web reinforcement φ_x. Further the parameter e=0.

From Fig.4.10, we can see that the lower bound solution is very different from the upper bound solution for a/h > 0.5. The load-carrying capacity corresponding to the lower bound solution is much lower than that of the upper bound solution for this case.

The curves in Fig. 4.10 illustrate that:

a. The load carrying capacity is heavily dependent on the depth/width ratio a/h, which is as same as we found for the upper bound solution.

b. For $a/h \leq 0.5$, the higher longitudinal reinforcement degrees,i.e. $\Phi > 0.5$, do not lead to higher load carrying capacity than obtained for $\Phi = 0.5$.

C. The influence of the ψ-value on the load carrying capacity is diminished with increasing depth/width ratio a/h and decreasing Φ–value. Especially when $a/h > 0.3$ as well as $\Phi \leq 0.1$, there is almost no contribution from the horizontal reinforcement to the load-carrying capacity of the walls.

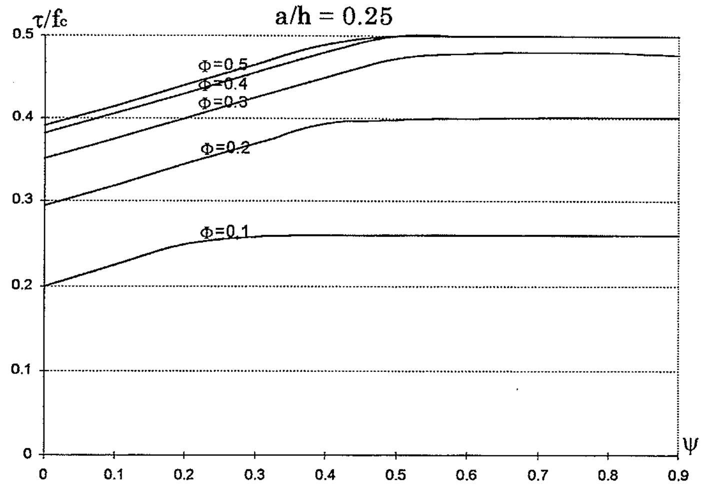

Fig. 4.10 *The shear capacity of shear walls loaded by a concentrated transverse force versus longitudinal reinforcement degree and shear reinforcement degree.*

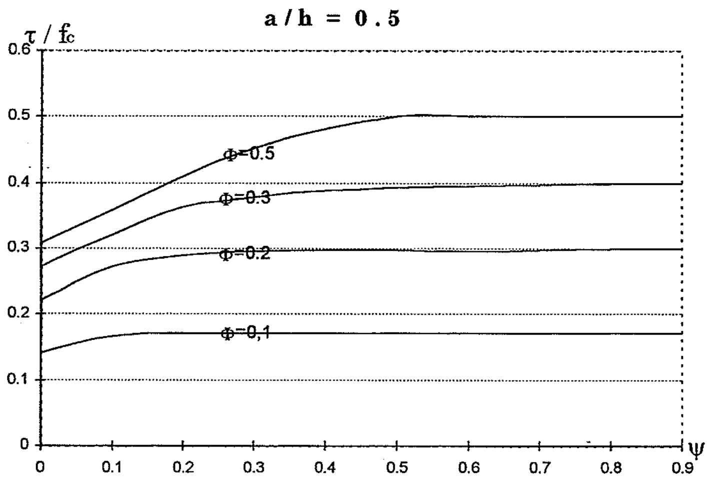

Fig. 4.10 *(Continued)*

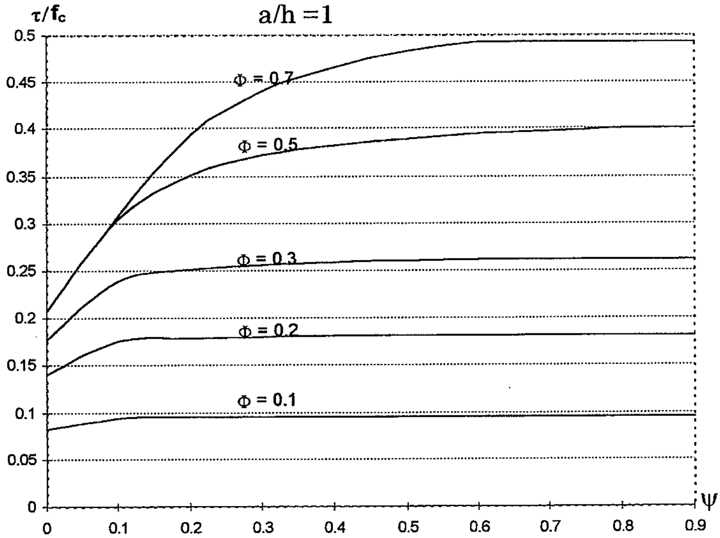

Fig. 4.10 *(Continued)*

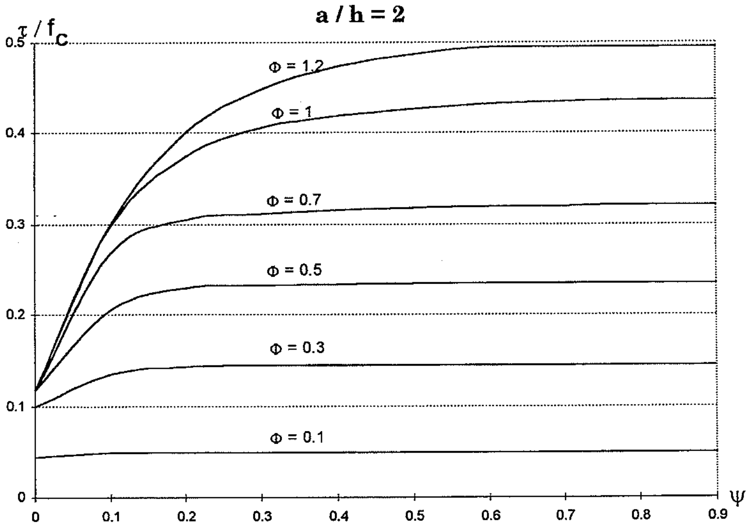

Fig. 4.10 *(Continued)*

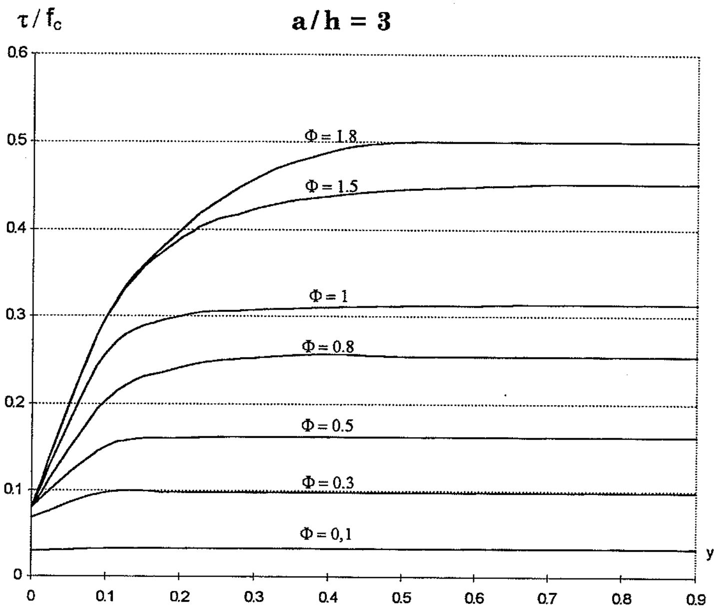

Fig. 4.10 *(Continued)*

CHAPTER V. BENDING CAPACITY OF SHEAR WALLS

This chapter deals briefly with the bending capacity of reinforced concrete shear walls. Since it has been shown that the determination of the bending capacity of reinforced concrete beams can be solved by the plastic theory, see [84.1] and [84.4] , it is natural to extend this method to determine the bending capacity of reinforced concrete shear walls.

This chapter gives an analytical model to predict the strength of an isolated structural wall with or without boundary elements failing in bending.

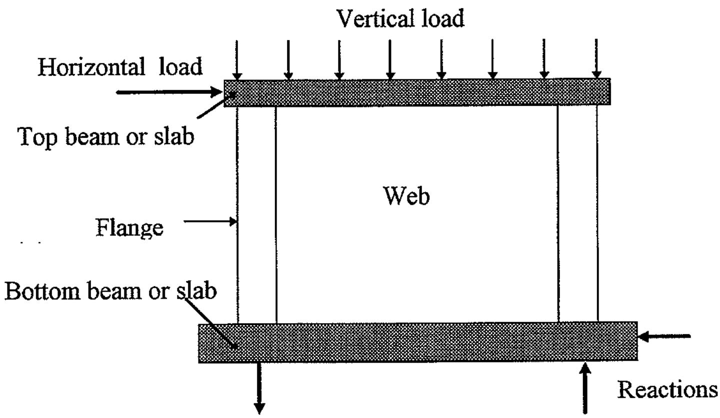

Fig.5.1 *An isolated wall*

5.1 Pure Bending

The shear walls treated in this section are assumed to be loaded in pure bending.

The vertical reinforcement and the horizontal reinforcement with the same tensile and compressive yield strength f_{Yx} and f_{Yy} respectively are assumed to be uniformly distributed in the web.

Because the horizontal reinforcement gives no contribution to the bending capacity of the wall, we will only discuss the influence of the vertical reinforcement .

The concrete is assumed to be perfectly plastic with the compressive strength $f_c^* = \nu_b f_c$. Here ν_b is an effectiveness factor for bending and f_c is the compressive cylinder strength of concrete.

5.1.1 Shear Walls with Rectangular Section

A shear wall with rectangular section (without boundary elements) subjected to a horizontal force is shown in Fig. 5.1. Only uniform reinforcement is assumed, i.e. there is no concentrated reinforcement at both ends of the section.

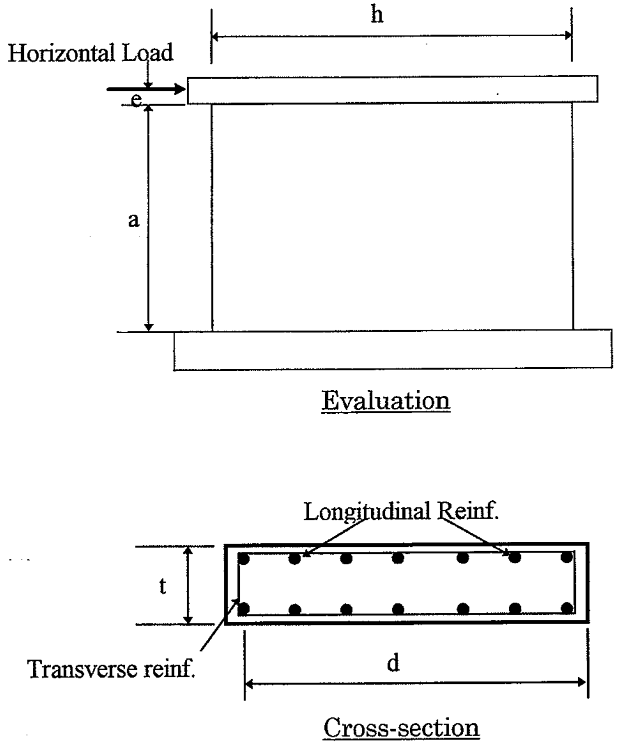

Fig. 5.1 *Wall with rectangular section*

When a flexural failure occurs, the stress distribution in the cross section will be as shown in fig. 5.2.

Projection gives

$$\frac{y_0}{d} = \frac{\Phi_x}{\nu_b + 2\Phi_x} \tag{5.1}$$

Here ν_b is the effectiveness factor for bending and d is the distance from the center of the first row reinforcement on one side to the face of the other one (see Fig. 5.1).

The yield moment of the section is found to be

$$M_p = \Phi_x \, t \, f_c \, (d - y_0) \, \frac{d}{2} \tag{5.2}$$

or by using equation (5.1)

$$M_p = \frac{t d^2}{2} \, f_c \, \Phi_x \, (\nu_b + \Phi_x) /(\nu_b + 2 \, \Phi_x) \tag{5.3}$$

In (5.2), y_0 is the depth of the compression zone in the section.

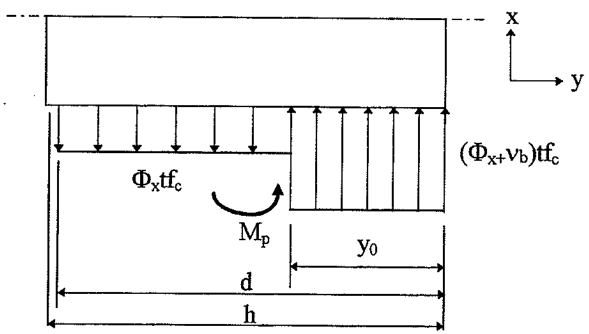

Fig.5.2 *The stress distribution in the section*

Then we can obtain the dimensionless yield moment m_p as follows

$$m_p = \frac{1}{2}(\nu_b + \Phi_x)/(\nu_b + 2\Phi_x) \qquad (5.4)$$

Here the dimensionless yield moment m_p is defined by

$$m_p = \frac{M_p}{t\, d^2 f_c}$$

5.1.2 Shear Walls with Boundary Elements

A shear wall with boundary elements is shown in Fig. 5.3.

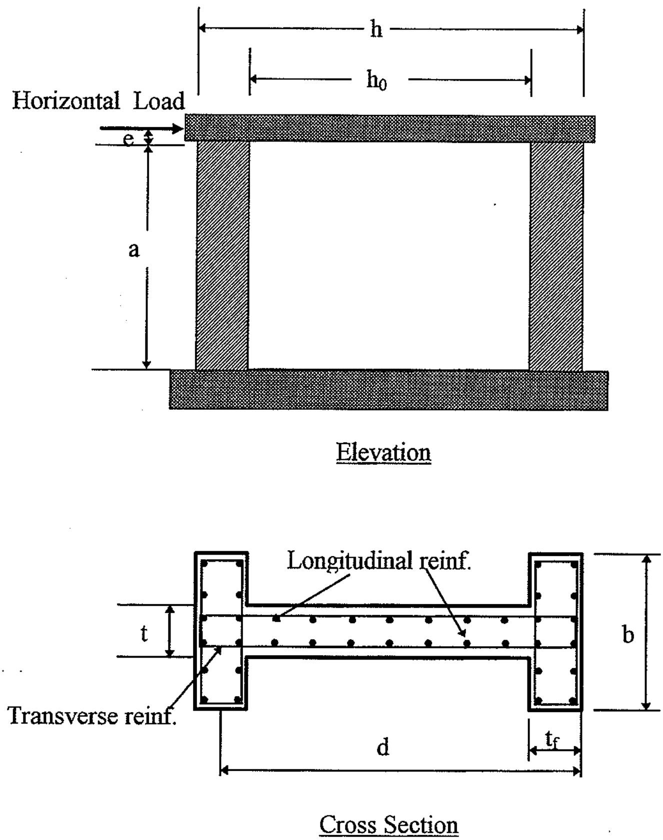

Fig. 5.3 *A wall with boundary elements*

The reinforcement with the same tensile and compressive yield strength f_{yl} and the areas A_{sl} in both boundary elements is assumed to be concentrated in a stringer at a distance d from the other end of the cross section as shown in Fig. 5.3. All data and assumptions are as same as those mentioned before.

The stress distribution of the section is shown in Fig. 5.4. The same procedure as in section 5.1.1 is used to derive the yield moment formulas. Thus the complete solution will be given without derivation. The dimensionless yield moment is found to be

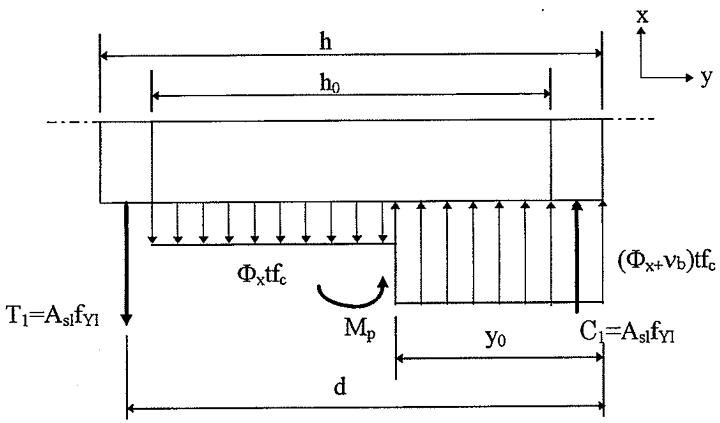

Fig. 5.4 *Stress distribution on the section*

$$
m_p = \begin{cases}
\alpha_1^2\Phi_l + \dfrac{\alpha_1\alpha_2}{2}\Phi_x - \dfrac{\alpha_3}{2\upsilon_b}(2\alpha_1\Phi_l + \alpha_2\Phi_x)^2 \\
\qquad \text{for } \dfrac{2\alpha_3}{\alpha_4}(2\alpha_1\Phi_l + \alpha_2\Phi_x) < \upsilon_b \\[2ex]
\dfrac{\alpha_1}{2}(\alpha_1 - \alpha_4)(2\Phi_l + \dfrac{\alpha_2}{\alpha_1}\Phi_x) + \dfrac{1}{8}\dfrac{\alpha_4^2}{\alpha_3}\upsilon_b \\
\qquad \text{for } \dfrac{2\alpha_2\alpha_3}{\alpha_4}\Phi_x \le \upsilon_b \le \dfrac{2\alpha_3}{\alpha_4}(2\alpha_1\Phi_l + \alpha_2\Phi_x) \\[2ex]
\dfrac{\alpha_1}{2}[\ 2(\alpha_1 - \alpha_4)\Phi_l + \alpha_2\Phi_x\ ] - \dfrac{1}{2\upsilon_b}\alpha_2^2\alpha_3\Phi_x^2 \\
\qquad \text{for } \dfrac{\alpha_1\alpha_3}{\alpha_4}\Phi_x < \upsilon_b < \dfrac{2\alpha_2\alpha_3}{\alpha_4}\Phi_x \\[2ex]
\alpha_1(\alpha_1 - \alpha_4)\Phi_l + \dfrac{1}{2}(\alpha_1^2 - 2\alpha_1\alpha_4 + 2\alpha_4^2)\Phi_x + \dfrac{\alpha_4^2}{2}(1 - \dfrac{1}{\alpha_3})\upsilon_b \\
\quad - \dfrac{1}{2}\cdot\dfrac{1}{2\Phi_x + \upsilon_b}\left[\alpha_1\Phi_x + \alpha_4(1 - \dfrac{1}{\alpha_3})\upsilon_b\ \right]^2 \\
\qquad \text{for } \dfrac{\alpha_2\alpha_3}{\alpha_4}\Phi_x > \upsilon_b
\end{cases} \tag{5.5}
$$

Here

$\alpha_1 = \dfrac{h}{d}$; $\alpha_2 = \dfrac{h_0}{d}$; $\alpha_3 = \dfrac{t}{b}$; $\alpha_4 = \dfrac{t_f}{d}$;

$d = h - \frac{1}{2}t_f$: the distance from the center of one boundary element to the face of the other one ;

h_0 : the width of the web ;

$m_p = \dfrac{M_p}{t\ d^2\ f_c}$: the dimensionless yield moment .

Since the wall is symmetrically reinforced, the reinforcement degrees are same in the two flanges.

5.2 Bending with Normal Force

The bending moment and the normal force, positive as compression, will be referred to the middle point of the section as shown in fig. 5.5. All the data and assumptions are in agreement with those mentioned in section 5.1 .

As in section 5.1.2 , the derivation of the formulas will not be given, because the procedure is the same as before. Here, only the case of bending moments and positive normal force will be considered.

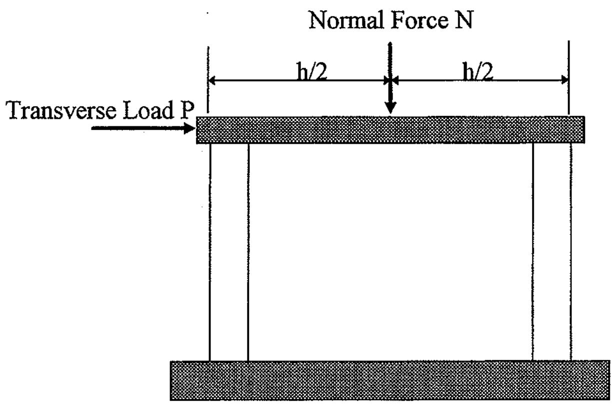

Fig. 5.5 *Shear wall with normal force*

5.2.1 Shear Walls with Rectangular Section

The stress distribution in the section is shown in Fig. 5.6. Introducing the dimensionless normal force by n = $\frac{N}{t\,h\,f_c}$, the following expression are found for the dimensionless yield moment as a function of the normal force:

$$m_p = \frac{n+\Phi_x}{2} \cdot \frac{\Phi_x + \upsilon_b - n}{2\Phi_x + \upsilon_b} \tag{5.6}$$

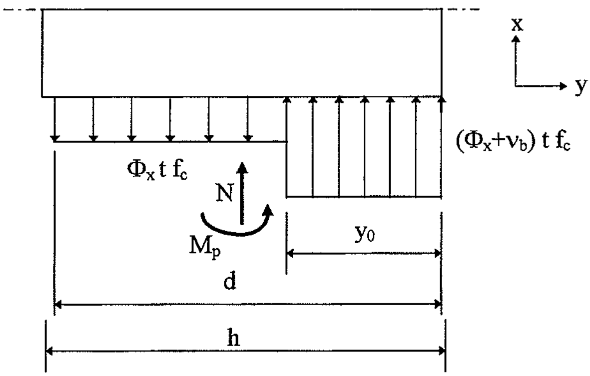

Fig. 5.6 *The stress distribution in the section*

5.2.2 Shear Walls with Boundary Elements

The stress distribution in the section is shown in Fig. 5.7.

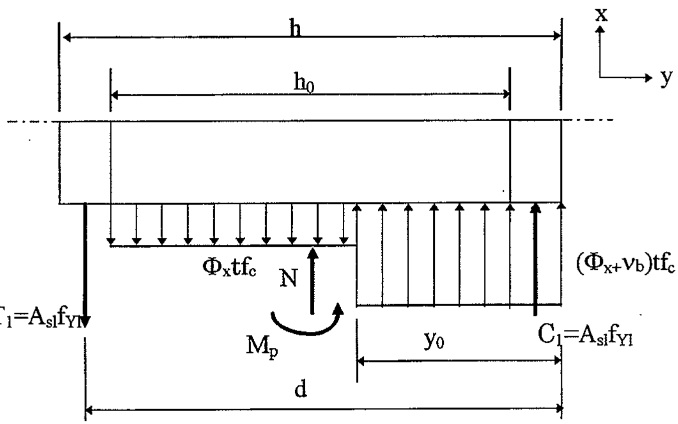

Fig. 5.7 *The stress distribution in the section*

The complete solution for the bending moment for shear walls with boundary elements is given by

$$
m_p = \begin{cases}
\frac{\alpha_1}{2}[\ \alpha_1(2\Phi_l+n)+\alpha_2\Phi_x\ ]-\frac{\alpha_3}{2\upsilon_b}[\ \alpha_1(2\Phi_l+n)+\alpha_2\Phi_x\ ]^2 \\
\qquad for\ \ n<\frac{\alpha_4}{2\alpha_1\alpha_3}\upsilon_b-2\Phi_l-\frac{\alpha_2}{\alpha_1}\Phi_x \\
\\
\frac{\alpha_1}{2}(\alpha_1-\alpha_4)(2\Phi_l+n+\frac{\alpha_2}{\alpha_1}\Phi_x)+\frac{1}{8}\frac{\alpha_4^2}{\alpha_3}\upsilon_b \\
\qquad for\ \ \frac{1}{\alpha_1}(\frac{\alpha_4}{2\alpha_2}\upsilon-2\alpha_1\Phi_l-\alpha_2\Phi_x)\le n \\
\qquad\qquad n\le\frac{1}{\alpha_1}(\frac{\alpha_4}{2\alpha_3}\upsilon-\alpha_2\Phi_x) \\
\\
\frac{\alpha_1}{2}[\ 2(\alpha_1-\alpha_4)\Phi_l+\alpha_1 n+\alpha_2\Phi_x\ ]-\frac{\alpha_3}{2\upsilon}[\ \alpha_1 n+\alpha_2\Phi_x\ ]^2 \\
\qquad for\ \ \frac{1}{\alpha_1}(\frac{\alpha_4}{2\alpha_3}\upsilon_b-\alpha_2\Phi_x)<n<\frac{1}{\alpha_1}(\frac{\alpha_4}{\alpha_3}\upsilon-\alpha_2\Phi_x) \\
\\
\alpha_1(\alpha_1-\alpha_4)\Phi_l+\frac{1}{2}(\alpha_1\alpha_2+2\alpha_4^2)\Phi_x+\frac{\alpha_4^2}{2}(1-\frac{1}{\alpha_3})\upsilon_b+\frac{\alpha_1^2}{2}n- \\
-\frac{1}{2}\cdot\frac{1}{2\Phi_x+\upsilon_b}[\ \alpha_1(\Phi_x+n)+\alpha_4(1-\frac{1}{\alpha_3})\upsilon_b\ ]^2 \\
\\
\qquad for\ \ \frac{1}{\alpha_1}(\frac{\alpha_4}{\alpha_3}\upsilon_b-\alpha_2\Phi_x)<n \\
\qquad\qquad n<\frac{1}{\alpha_1}[\ \alpha_2\Phi_x+(\alpha_2+\frac{\alpha_4}{\alpha_3})\upsilon_b\ ] \\
\\
\alpha_1(\alpha_1-\alpha_4)\Phi_l+\frac{\alpha_2}{2}(\alpha_1 n-\alpha_2\Phi_x)+[\ (\alpha_1-\alpha_4)\frac{\alpha_4}{\alpha_3}+\frac{\alpha_2^2}{2}(\frac{1}{\alpha_3}-1)\ ]\upsilon_b- \\
-\frac{\alpha_3}{2\upsilon_b}\ \alpha_1 n-\alpha_2\Phi_x+\alpha_2(\frac{1}{\alpha_3}-1)\upsilon_b\ ]^2 \\
\\
\qquad for\ \ \frac{1}{\alpha_1}[\ (\frac{\alpha_4}{\alpha_3}+\alpha_2)\upsilon_b+\alpha_2\Phi_x\ ]\le n \\
\qquad\qquad n<\frac{1}{\alpha_1}[\ (\frac{3}{2}\cdot\frac{\alpha_4}{\alpha_3}+\alpha_2)\upsilon_b+\alpha_2\Phi_x\ ]
\end{cases}
\qquad (5.7)_1
$$

$$m_p = \begin{cases} \frac{\alpha_1}{2}(\alpha_1 - \alpha_2)(2\Phi_l - n + \frac{\alpha_2}{\alpha_1}\Phi_x) + \frac{\upsilon_b}{2\alpha_3}[\ (\alpha_1 - \alpha_4)\ (1 + \alpha_2\alpha_3) + \\ \quad + \alpha_2\ (2\alpha_1 + \frac{1}{2}\alpha_4) - 2\alpha_4^2 - 1\ ] \\ \\ \quad for\ \ \frac{1}{\alpha_1}[\ \alpha_2\Phi_x + \frac{1}{\alpha_2\alpha_3}(\alpha_3 - 2\alpha_2 + \alpha_2\alpha_3)\,\upsilon_b\ ] \le n < 2\Phi_l + \frac{\alpha_2}{\alpha_1}\Phi_x \\ \quad\quad + \frac{\upsilon_b}{\alpha_1(\alpha_1 - \alpha_2)\,\alpha_3}[\ (\alpha_1 - \alpha_4)(1 + \alpha_2\alpha_3) + \alpha_2(2\alpha_1 + \frac{1}{2}\alpha_4) - 2\alpha_4^2 - 1\ ] \end{cases} \qquad (5.7)_2$$

Here $m_p = \dfrac{M_p}{t\ d^2\ f_c}$ is the dimensionless yield moment .

5.3 The Effectiveness Factor for Bending

For pure bending of a rectangular section with tensile reinforcement only, the effectiveness factor ν_b has been analytically determined by Exner [79.3], using stress-strain curves measured by P.T. Wang et al. [78.4]. It turns out that ν_b is a function of the unaxial compressive strength f_c, the yield stress of the reinforcement f_Y and the reinforcement ratio φ_{sl}.

For practical purposes, ν_b can be calculated approximately by the simple empirical formula

$$\upsilon_b = 0.97 - \frac{f_Y}{5000} - \frac{f_c}{300} \qquad for \begin{cases} f_Y < 900\,MPa \\ f_c < 60\,MPa \end{cases} \qquad (5.8)$$

For most practical cases f_Y will be less than 600 MPa, and conservatively we get

$$\upsilon_b = 0.85 - \frac{f_c}{300} \qquad for \begin{cases} f_Y < 600\,MPa \\ f_c < 60\,MPa \end{cases} \qquad (5.9)$$

The effectiveness factor for rectangular sections with compressive reinforcement and normal force can also be calculated by the equations (5.8) and (5.9), see [84.1].

For shear walls, the ν_b–formula (5.9) can be used without the limitations of f_c and f_Y. Thus we have generally

$$\upsilon_b = 0.85 - \frac{f_c}{300} \qquad (5.10)$$

Comparison between the theory using the ν_b- formula (5.10) and tests shows very good agreement, see Fig. 5.8.

5.4 Experimental Verification

Comparison between 45 shear wall tests from different test series and the formulas derived using the v_b-formula (5.10), can be found in Fig. 5.8. The dimensions, material properties and measured ultimate loads are listed in Appendix A. The statistical values for the ratios of test to theory by using (5.4) through (5.7) and the v_b-value of (5.10) are shown in table 5.1.

Table 5.1

item	number n	mean $\bar{x}$	standard deviation σ	coeff. of variation c_v
statistical values	46	0.954	0.113	0.118

The agreement is thus very good which may also be seen in Fig. 5.8. In this figure the measured ultimate loads are compared with the theoretical ones.

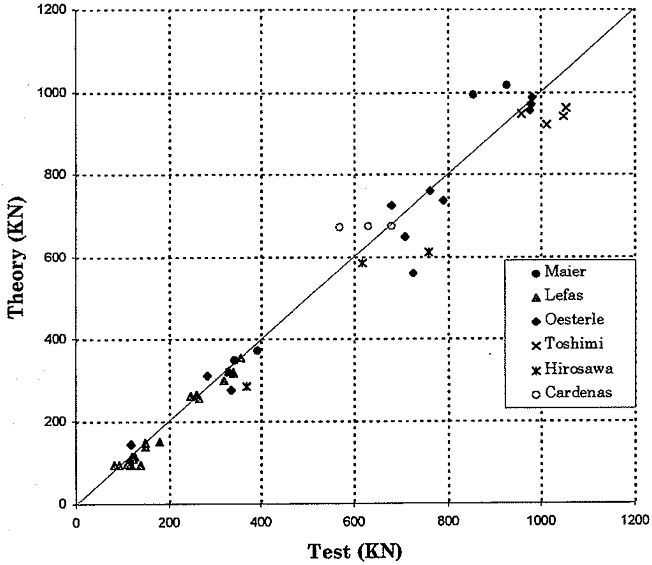

Fig. 5.8 *Theoretical bending capacity compared with test results.*

CHAPTER VI COMPARISON OF THEORY WITH TESTS

We have now derived the equations for the ultimate load-carrying capacity of shear walls, chapter III and chapter IV. In this chapter, 184 tests with shear wall specimens have been treated using the theory. The effectiveness factor ν is taken as (5.10) or (4.72) according to the different failure modes as explained before.

6 . 1 Determining the Shear Capacity by Optimization Routines

The equations derived in chapter 4 show that the design of shear walls using lower bound solutions is a rather simple task. To find the load-carrying capacity in shear of a prescribed shear wall is more complicated. The load-carrying capacity of a shear wall with specified geometry and reinforcement may be determined by standard computer optimization routines. The effectiveness factor ν is taken as (4.72).

Consider a shear wall composed of web and boundary elements. The vertical boundary elements are at both sides of the web as illustrated in Fig. 6.1. The transverse load P is transferred to the wall by means of a top beam or slab and the wall transfers the force to the bottom beam or slab. The top beam or slab might be subjected to normal stresses along the horizontal face, which are statically equivalent to a normal force N.

Generally, the reinforcement in boundary elements is assumed to be symmetrical and constant and the web reinforcement is uniform.

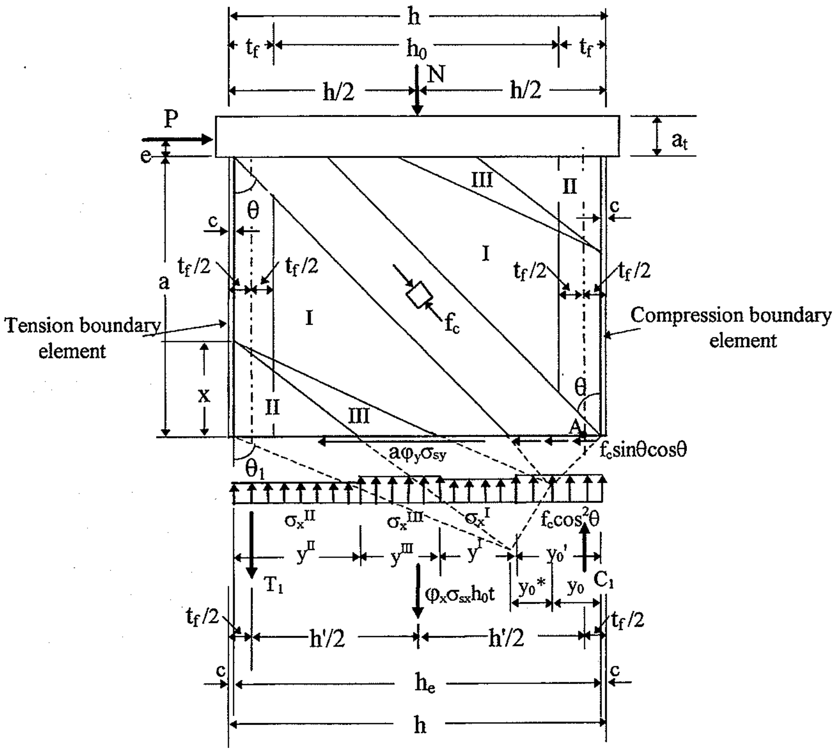

Fig. 6.1 *Stress distribution in the wall*

The stress distribution of the wall is shown in Fig. 6.1.

The optimization problem may be formulated in the following way:
Maximize:

$$\frac{\tau}{\upsilon f_c} = \frac{y_0'}{h}\cos\theta\sin\theta + \frac{\varphi_y\sigma_{sy}}{\upsilon f_c}\left(1-\frac{y_0'}{h}\right)\cot\theta \qquad \leq 0.5 \tag{6.1}$$

under the subsidiary conditions:

$$\Phi_l^* \frac{\sigma_{sl}}{f_{Yl}} + \frac{1}{2}\Phi_x^* \frac{\sigma_{sx}}{f_{Yx}}\frac{h_0}{h} + \frac{1}{2}n^* - \frac{1}{2hh'}\{ y_0^*(h_e + h' - 2y^{II} - y^{III})$$

$$-\psi \frac{\sigma_{sy}}{f_{Yy}}[\, y^{I}\cos^2\theta(y^{III} + y^{I}) - y^{II}\cos^2\theta_1(y^{III} + y^{II})\,] \tag{6.2}$$

$$- y_0(y_0' - h_e + h')\} - \frac{\tau}{\upsilon f_c}\frac{a+e}{hh'} = 0$$

$$\left.\begin{aligned} -f_{Yl} &\le \sigma_{sl} \le f_{Yl} \\ -f_{Yx} &\le \sigma_{sx} \le f_{Yx} \\ -f_{Yy} &\le \sigma_{sy} \le f_{Yy} \end{aligned}\right\} \tag{6.3}$$

$$0 \le \theta \le \frac{\pi}{2} \tag{6.4}$$

$$0 \le \sigma_c = \varphi_y \sigma_{sy}(1 + \cot^2\theta) \le \nu f_c \tag{6.5}$$

$$0 \le \frac{y_0'}{h} \le \frac{\Phi^*}{\cos^2\theta} \tag{6.6}$$

In the equation (6.1), τ on the left hand side is the average shear stress as defined in section 4.1; the first term on the right hand side is the contribution from the strut which is zero when $y_0' = 0$; the second term is the contribution from the triangular homogenous stress fields (see Fig 6.1).

The physical meaning of equation (6.2) is as same as (4.41).

By means of the equations derived in Chapter 4 and Fig. 6.1, all the parameters in the above equations are determined as follows:

$$y_0^* = (h_e - y_0) - \sqrt{\begin{aligned}&(h_e - y_0)^2 - \psi^* \frac{\sigma_{sy}}{f_{Yy}}(h_e - y_0')\cot^2\theta\Big[(h_e - y_0')\\ &+ 2y_0 \tan^2\theta + \psi^* \frac{\sigma_{sy}}{f_{Yy}}(h_e - y_0')\Big]\end{aligned}} \tag{6.7}$$

$$\tan\theta_1 = \frac{h_e - y_0 - y_0^*}{y_0 \tan\theta + \psi^* \dfrac{\sigma_{sy}}{f_{Yy}} \cot\theta} \tag{6.8}$$

$$x = \frac{(h_e - y_0')\psi^* \dfrac{\sigma_{sy}}{f_{Yy}} \cot^2\theta - y_0^*}{\psi^* \dfrac{\sigma_{sy}}{f_{Yy}}(\cot\theta - \cot\theta_1)} \tag{6.9}$$

$$\left.\begin{aligned}
y^{II} &= x \frac{h_e - y_0 - y_0^*}{x + y_0 \tan\theta + \psi^* \dfrac{\sigma_{sy}}{f_{Yy}} \cot^2\theta}\\
y^{III} &= \frac{x(h_e - y_0)}{x + y_0 \tan\theta} - y^{II}\\
y^{I} &= h_e - y_0' - y^{II} - y^{III}
\end{aligned}\right\} \tag{6.10}$$

In these equations :

$e = \dfrac{a_t}{2}$: the parameter determining the position of P on the top slab;

a_t : the thickness of the top slab;

c : the concrete cover measured to the center of the first row of reinforcement bars in the boundary element

h : the total width of the wall ;

$h_e = h - 2c$: the effective width of the wall ;

$h' = h - t_f$: the distance between the centers of two boundary elements ;

$h_0 = h - 2t_f$: the width of the web;

$$\Phi_l^* = \frac{\Phi_l}{\upsilon}; \qquad \Phi_x^* = \frac{\Phi_x}{\upsilon}; \qquad \psi^* = \frac{\psi}{\upsilon}; \qquad n^* = \frac{n}{\upsilon};$$

$$\Phi^* = \Phi_l^* + \frac{1}{2}(\Phi_l^* + n^*).$$

Notation otherwise as in Chapter IV.

The forces in the boundary elements are as shown in Fig. 6.2. By means of equation (4.43) and (4.63) the forces may be found as follows :

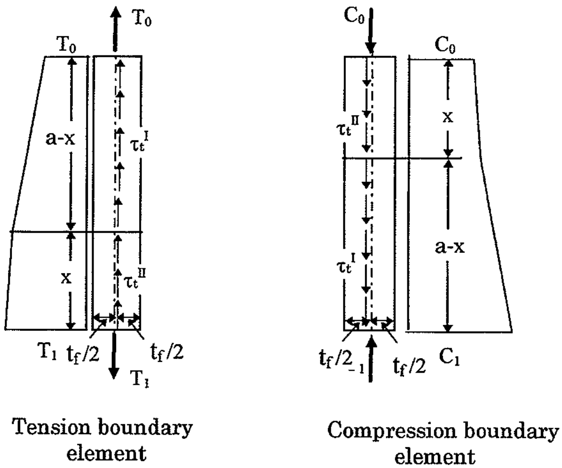

Fig. 6.2 *Forces in the boundary elements*

$$\left.\begin{aligned}
T_I &= A_{sI}\,\sigma_{sI} = \Phi_I^{*}\frac{\sigma_{sI}}{f_{YI}} f_c\, ht \\[2ex]
C_I &= T_I + \varphi_x\,\sigma_{sx}\,h_0\,t + N - (f_c y_0' \cos^2\theta + \sigma_x^{II}\,y^{II} + \sigma_x^{III}\,y^{III})\,t \\
&= \Big[\,\Phi_I^{*}\frac{\sigma_{sI}}{f_{YI}} + \Phi_x^{*}\frac{\sigma_{sx}}{f_{Yx}}\frac{h_0}{h} + \frac{N^{*}}{thf_c} - \frac{y_0^{*}}{h}\,\Big]\upsilon f_c\, ht \\[2ex]
T_0 &= T_I - \tau_t^{I}(a-x)t - \tau_t^{II}xt \\
&= \Big[\,\Phi_I^{*}\frac{\sigma_{sI}}{f_{YI}} - \psi^{*}\frac{\sigma_{sy}}{f_{Yy}}\cot\theta\Big(\frac{a}{h} - \cot\theta\Big) - \frac{y_0^{*}}{h}\,\Big]\upsilon f_c\, ht \\[2ex]
C_0 &= C_I - \tau_t^{I}(a-x)t - \tau_t^{II}xt \\
&= \Big\{\,\Phi_I^{*}\frac{\sigma_{sI}}{f_{YI}} + \Phi_x^{*}\frac{\sigma_{sx}}{f_{Yx}}\frac{h_0}{h} + \frac{N^{*}}{thf_c} - \Big[\,\frac{y_0}{h} + \psi^{*}\frac{\sigma_{sy}}{f_{Yy}}\cot\theta\Big(\frac{a}{h} - \cot\theta\Big) + \frac{2y_0^{*}}{h}\,\Big]\Big\}\upsilon f_c\, ht
\end{aligned}\right\}\quad(6.11)$$

For a shear wall without stirrups, we set the effective width h_e of the wall equal to the total width h, i.e

$$h_e = h$$

6.2 Comparison with Tests Results

In this section, seventeen groups of altogether 184 test specimens of reinforced concrete shear walls described in the literature are compared with the theoretical solutions. The specimens consist of 52 specimens with rectangular section and 92 specimens with column boundaries (barbell) and 40 specimens with flange boundaries.

For all specimens we set c = 25mm and $e = \frac{a_t}{2}$. Here a_t is the thickness of the top slab. In cases of a large difference between the yield strength and the ultimate strength of the reinforcement a mean value has been used.

The comparison correponding to different height-width ratios and different geometry of sections is shown in sections 6.2.1 and 6.2.2, respectively. The comparison reveals that for squat shear walls ($a/h<1$) as well as moderate walls ($1<a/h<2$) with strong flexible reinforcement the failure is mainly controlled by shear and for moderate walls with week flexible reinforcement as well as slender walls ($a/h>2$) the failure is mainly controlled by bending.

The comparison tables as well as figures for each group are shown in sections 6.2.3 through 6.2.14. The details of the test specimens and the calculation results are given in the appendix.

The data of all specimens are presented in table 6.1 and the comparison between test results and theory is shown in Fig 6.3. The comparison of the results of the theory and the tests demonstrates that the theoretical results coincide very well with the test results.

6.2.1 Comparison for Shear Walls Corresponding to Different Height-Width Ratios

Fig. 6.4 through Fig. 6.6 show the comparison between test results and theory corresponding to different height-width ratios, respectively.

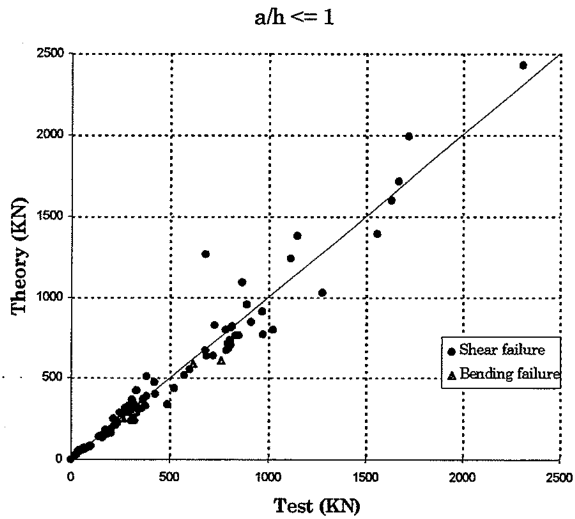

Fig. 6.4. *Comparison between test results and theory for low-rise shear walls (a/h<=1)*

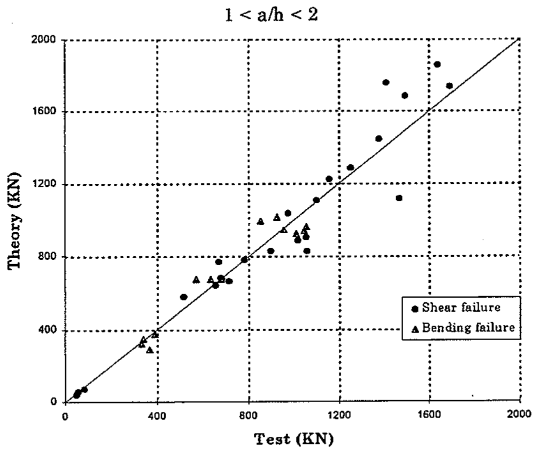

Fig. 6.5 *Comparison between test results and theory for shear walls (1< a/h < 2)*

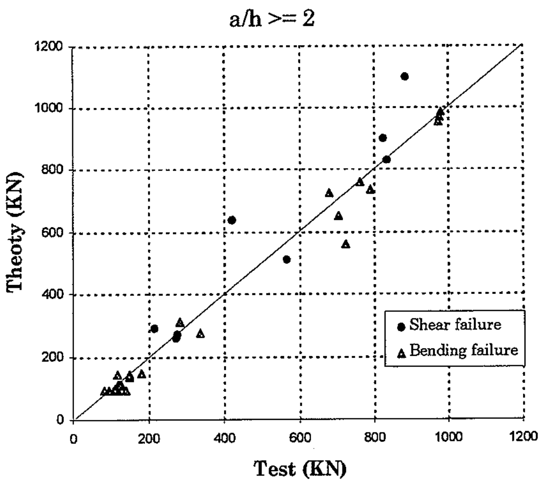

Fig. 6.6 *Comparison between test results and theory for slender shear walls (a/h >= 2)*

6.2.2 Comparison for Shear Walls Corresponding to Different Geometry of Sections

6.2.2.1 Comparison for Shear Walls with Rectangular Section

The range of the various parameters for shear walls with rectangular section is

$$0.31 < \frac{a}{h} < 2.4$$

$$13\ \text{MPa} < f_c < 66\ \text{MPa}$$

$$300\ \text{MPa} < f_{Yl} < 690\ \text{MPa}$$

$$300\ \text{MPa} < f_{Yx} < 670\ \text{MPa}$$

$$380\ \text{MPa} < f_{Yy} < 670\ \text{MPa}$$

$$0.08\ \% < \varphi_l < 1.16\ \%$$

$$0.22\ \% < \varphi_x < 2.9\%\ (\text{excluding } \varphi_x = 0)$$

$$0.25\ \% < \varphi_y < 1.6\%\ (\text{excluding } \varphi_y = 0)$$

$$0.0062 < \Phi_l = \frac{\varphi_l f_{Yl}}{f_c} < 0.375$$

$$0.058 < \Phi_x = \frac{\varphi_x f_{Yx}}{f_c} < 0.662$$

$$0.044 < \psi = \frac{\varphi_y f_{Yy}}{f_c} < 0.34$$

Fig 6.7 shows a comparison between test results and theory for shear walls with rectangular section.

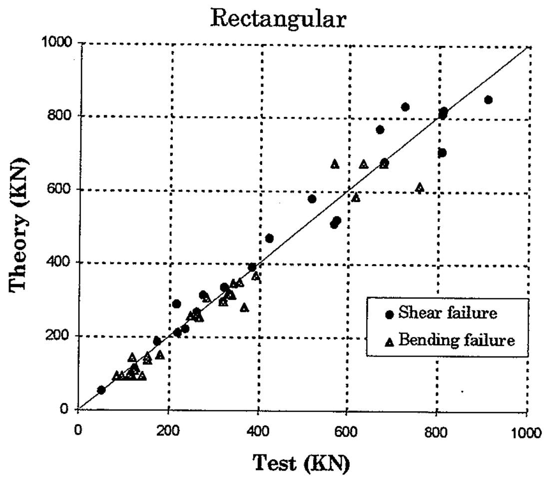

Fig. 6.7 *Comparison between test results and theory for shear walls with rectangular section*

6.2.2.2 Comparison for Shear Walls with Boundary Elements

Fig. 6.8 and 6.9 show the comparison between test results and theory for shear walls with column boundaries (barbell) and flange boundaries (flanged), respectively.

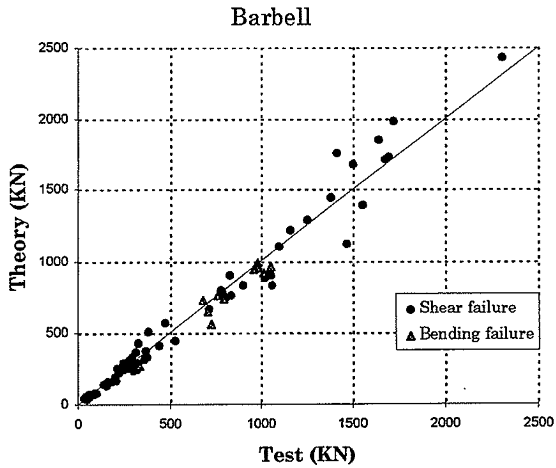

Fig. 6.8 *Comparison between test results and theory for shear walls with column boundaries (barbell)*

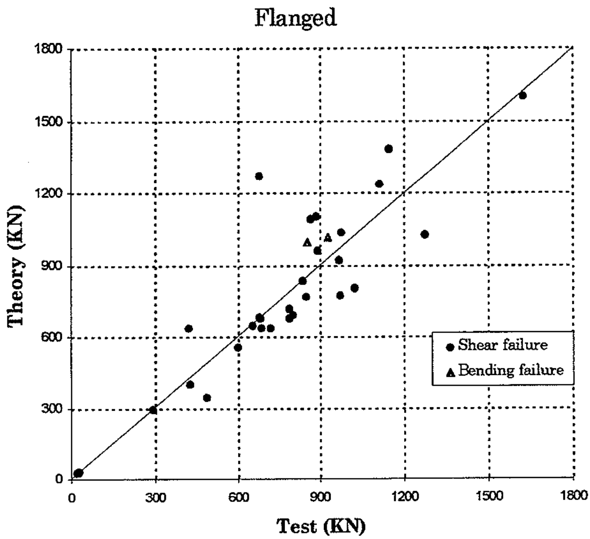

Fig. 6.9 *Comparison between test results and theory for shear walls with flange boundaries*

6.2.3 Reinforced Concrete Shear Walls Tested by Gupta and Rangan

In [93.4] and [94.2] eight high strength concrete shear walls were tested under inplane axial and transverse loads. All specimens had the same geometry and the same height/width ratio a/h = 1. The boundary elments of the walls are flanged. The full value of of the axial load was applied first and then the transverse load was applied in several increments until failure occured. These tests mainly gave rise to shear failures.

Table 6.2 Test specimens by Gupta and Rangan [93.4] [94.2]

Specimen No.	Concrete strength f_c (MPa)	Reinforcement degree		Normal force (KN)	Load capacity		Failure mode		Ratio (Theory/ Test)
		Φ	ψ		Test (KN)	Theory (KN)	Test	Theory	
S-F	60.5	0.204	0.095	310	487	343	B	S	0.7053
S-1	79.3	0.224	0.089	0	428	401	S	S	0.9367
S-2	65.1	0.416	0.089	610	720	637	S	S	0.8853
S-3	69.0	0.542	0.080	1230	851	765	S	S	0.8991
S-4	75.2	0.356	0.092	0	600	553	S	S	0.9223
S-5	73.1	0.507	0.085	610	790	714	S	S	0.9042
S-6	70.5	0.614	0.079	1230	970	769	S	S	0.7930
S-7	71.2	0.406	0.164	610	800	690	S	S	0.8623

Mean value $\bar{x}$ = 0.8635

B: Bending failure
S: Shear failure

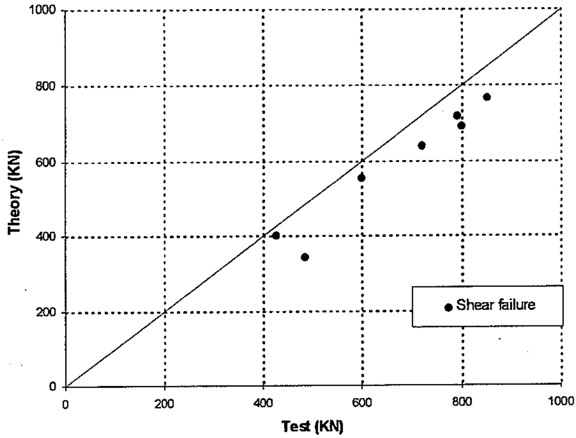

Fig. 6.10 *Comparison of theoretical load carrying capacity with test results by Gupta and Rangan [93.4] [94.2]*

6.2.4 Low-rise Shear Wall Tests by Felix Barda

In [76.2] eight low-rise shear walls with boundary elements were tested under inplane transverse load reversals. The section geometry of all specimens is flanged. These tests were governed by shear failures.

Table 6.3 Test specimens by Felix Barda [76.2]

Specimen	a/h	Reinforcement ratio (in web)(%)		Reinforcement degree		Normal force	Load capacity		Failure mode		Ratio (Theory/
No.		φ_x	φ_y	Φ	ψ	(KN)	Test (KN)	Theory (KN)	Test	Theory	Test)
B1-1	0.5	0.5	0.5	0.231	0.131	0	1276	1025	S	S	0.803
B2-1	0.5	0.5	0.5	0.967	0.213	0	969	917	S	S	0.946
B3-2	0.5	0.5	0.5	0.378	0.143	0	1113	1237	S	S	1.111
B4-3	0.5	0.5	0	0.616	0.000	0	1023	802	S	S	0.784
B5-4	0.5	0	0.5	0.365	0.131	0	680	1271	S	S	1.869
B6-4	0.5	0.5	0.5	0.513	0.168	0	867	1088	S	S	1.256
B7-5	0.25	0.5	0.5	0.487	0.145	0	1145	1383	S	S	1.208
B8-5	1	0.5	0.5	0.483	0.155	0	889	959	S	S	1.078

Mean value $\bar{x}$ = 1.132

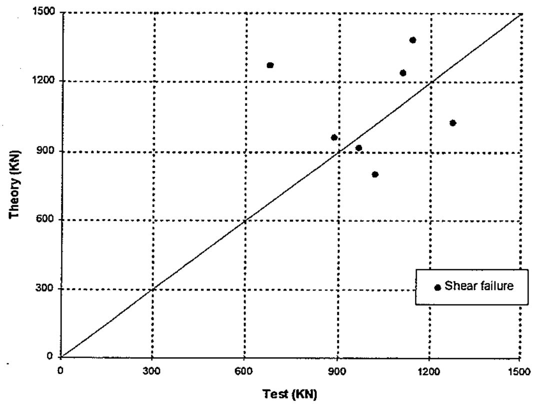

Fig. 6.11 *Comparison of theoretical load carrying capacity with test results by Felix Barda [76.2]*

6.2.5 Shear Wall Tests by Maier and Thurlimann

Nine shear wall tests were carried out by Maier and Thürlimann in Zürich [85.3]. The height/width ratio of all specimens was a/h = 1.02. The mean value of the yield strength and the ultimate strength of the reinforcement has been used.

Table 6.4 Test specimens by Maier and Thürlimann [85.3]

Specimen No.	Geometry	Reinforcement degree		Normal force (KN)	Load capacity		Loading method	Failure mode		Ratio (Theory/ Test)
		Φ	ψ		Test (KN)	Theory (KN)		Test	Theory	
S1	Flanged	0.341	0.281	433	680	681	Monotonic	Ductile	S	1.001
S2	Flanged	0.469	0.239	1653	928	1016	Monotonic	Brittle	B	1.094
S3	Flanged	0.611	0.283	424	977	1036	Monotonic	Brittle	S	1.060
S5	Flanged	0.337	0.280	416	683	676	Cyclic	Ductile	S	0.989
S6	Flanged	0.333	0.149	416	656	644	Monotonic	Ductile	S	0.982
S7	Flanged	0.474	0.239	1657	855	993	Cyclic	Brittle	B	1.161
S10	Rectangular	0.530	0.275	262	670	768	Monotonic	Ductile	S	1.146
S4	Rectangular	0.232	0.306	262	392	370	Monotonic	Ductile	B	0.944
S9	Rectangular	0.238	0.000	260	342	346	Monotonic	Ductile	B	1.012

Mean value $\bar{x}$ = 1.043

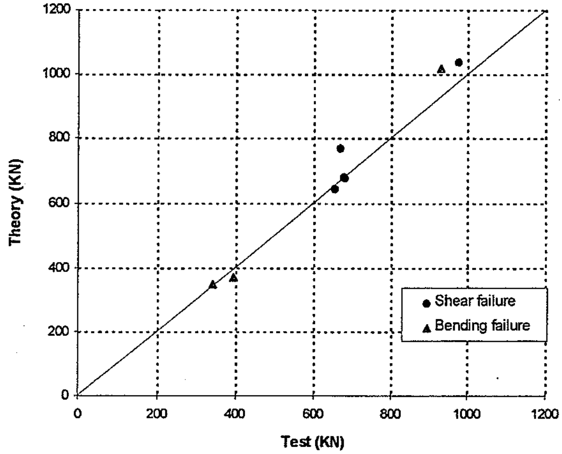

Fig. 6.12 *Comparison of theoretical load carrying capacity with test results by Maier and Thürlimann [85.3]*

6.2.6 Shear Walls Tests by Lefas, Micheal and Nicholas

Twenty large-scale wall models were tested by Lefas, Micheal and Nicholas [90.3] [90.4] under the combined action of a constant axial and a horizontal load monotonically increasing to failure. The section shape of all specimens is rectangular. For the longitudinal reinforcement the mean value of the yield strength and the ultimate strength has been used. These tests were governed by bending failures.

Table 6.5 Test specimens by Lefas [90.3] [90.4]

Specimen No.	a/h	Reinforcement degree Φ	Reinforcement degree ψ	Normal force (KN)	Load capacity Test (KN)	Load capacity Theory (KN)	Failure mode Test	Failure mode Theory	Ratio (Theory/ Test)
SW11	1	0.327	0.221	0	260	261	B	B	1.006
SW12	1	0.360	0.196	230	340	316	B	B	0.931
SW13	1	0.432	0.213	355	330	321	B	B	0.973
SW14	1	0.371	0.250	0	265	255	B	B	0.964
SW15	1	0.394	0.223	185	320	297	B	B	0.929
SW16	1	0.396	0.167	460	355	353	B	B	0.994
SW17	1	0.341	0.077	0	247	259	B	B	1.050
SW21	2	0.405	0.180	0	127	113	B	B	0.893
SW22	2	0.399	0.147	182	150	137	B	B	0.913
SW23	2	0.434	0.138	343	180	149	B	B	0.828
SW24	2	0.376	0.168	0	120	115	B	B	0.958
SW25	2	0.445	0.144	325	150	146	B	B	0.973
SW26	2	0.519	0.116	0	123	109	B	B	0.883
SW30	2	0.387	0.101	0	118	93	B	B	0.791
SW31	2	0.344	0.090	0	116	94	B	B	0.813
SW32	2	0.265	0.069	0	111	96	B	B	0.868
SW33	2	0.277	0.073	0	112	96	B	B	0.861
SW31R*	2	0.346	0.091	0	140	94	B	B	0.674
SW32R*	2	0.325	0.085	0	83	95	B	B	1.144
SW33R*	2	0.326	0.085	0	94	95	B	B	1.008

Mean value $\bar{x} =$ 0.923

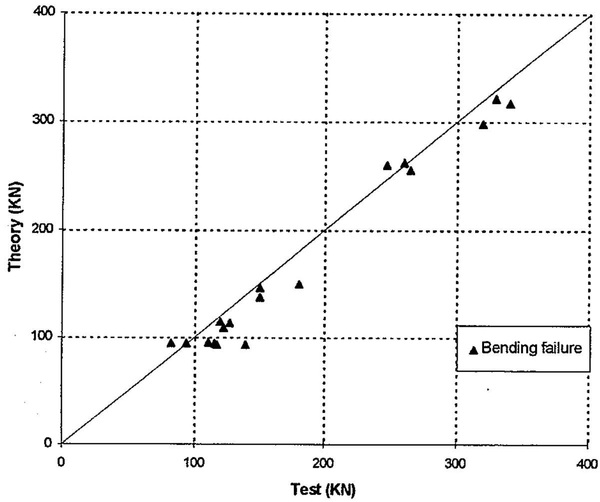

Fig.6.13 *Comparison of theoretical load carrying capacity with test results by Lefas [90.3] [90.4]*

6.2.7 Slender Shear Wall Tests by Oesterle

Twenty large-scale wall models were tested by Oesterle [84.3] under the combined action of a constant axial and a horizontal load monotonically increasing to failure. The section shape of all specimens was rectangular and the value of a/h is 2.4. . The mean value of the yield strength and the ultimate strength of the reinforcement has been used.

From the table 6.5 it can be seen that the theoretical load carrying capacities obtained from optimized lower bound solutions are almost as same as those obtained for bending solutions.

Table 6.6 Test specimens by Oesterle [84.3]

Specimen	Section geomety	Reinforcement degree		Normal force	Load capacity (KN)			Failure mode		Ratio (Theory/Test)
No.		Φ	ψ	(KN)	Test (KN)	Theory Bending	Theory Shear	Test	Theory	
R-1	Rec.	44.7	0.088	0.073	118	143	145	IB	Bending	1.209
R-2	Rec.	46.4	0.169	0.072	217	291	290	IC	Shear	1.340
R-3	Rec.	24.4	0.447	0.113	568	520	507	B	Shear	0.893
R-4	Rec.	22.7	0.289	0.094	282	308	310	B	Bending	1.093
F1	Flanged	38.4	0.496	0.187	836	874	830	WC	Shear	0.993
F2	Flanged	45.6	0.556	0.119	887	1195	1100	WC	Shear	1.240
F3	Flanged	27.9	0.463	0.098	421	681	636	WC	Shear	1.512
B1	Barbell	53.0	0.129	0.066	271	258	257	IB	Shear	0.947
B2	Barbell	53.6	0.371	0.137	680	724	736	WC&IB	Bending	1.065
B3	Barbell	47.3	0.144	0.066	276	270	270	IB	Shear	0.978
B4	Barbell	45.0	0.152	0.071	334	275	276	B	Bending	0.823
B5	Barbell	45.3	0.430	0.142	762	760	773	WC	Bending	0.998
B6	Barbell	21.8	0.787	0.218	825	904	898	WC	Shear	1.089
B7	Barbell	49.3	0.483	0.124	980	986	997	WC	Bending	1.005
B8	Barbell	42.0	0.521	0.304	978	970	987	WC	Bending	0.992
B9	Barbell	44.1	0.497	0.120	977	954	962	WC	Bending	0.976
B10	Barbell	45.6	0.329	0.121	707	649	663	B	Bending	0.917
B11	Barbell	53.8	0.283	0.113	726	558	566	WC	Bending	0.768
B12	Barbell	41.7	0.438	0.128	792	735	746	WC	Bending	0.928

Mean value $\bar{x} = 1.040$

IB : Bar fracture precipated by inelastic bar buckling
IC : Bar fracture precipated by instability of compression zone
F : Flexural bar fracture
WC : Web crushing
BC : Boundary region crushing
SC : Shear compression

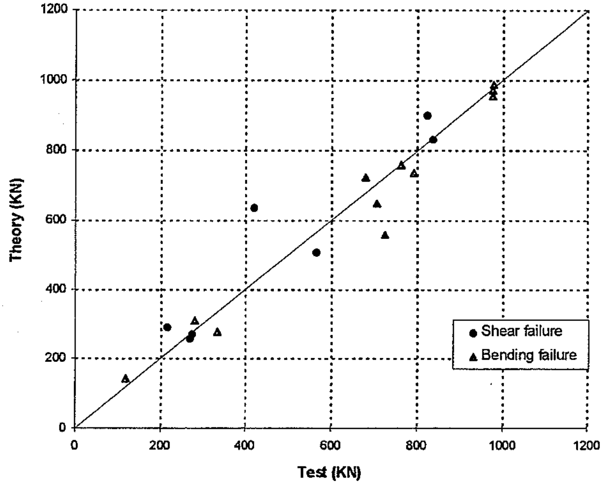

Fig. 6.14 *Comparison of theoretical load carrying capacity with test results by Oesterle [84.3]*

6.2.8 High Strenth Shear Wall Tests by Toshimi

Twentyone high strength reinforced concrete shear walls were tested by Toshimi and others in Japan from 1989 to 1992 [93.3]. The concrete strength of the specimens varied from 50MPa up to 140MPa and the main reinforcement yield strength was as high as 1400MPa. All the specimens had the same sectional geomety with boundary columns.

Table 6.7 Test specimens by Toshimi [93.3]

Specimen No.	a/h	Concrete strength f_c (MPa)	Reinforcement degree Φ	ψ	Normal force (KN)	Load capacity Test (KN)	Thoery (KN)	Failure mode Test	Theory	Ratio (Theory/ Test)
W08	0.59	103.3	0.301	0.107	1764	1670	1714	S	S	1.026
W12	0.59	137.5	0.281	0.088	2313	1719	1988	S	S	1.156
NW-1	1.76	87.6	0.328	0.109	1764	1062	826	B	S	0.778
NW-3	1.76	55.5	0.342	0.052	1372	714	662	S	S	0.927
NW-4	1.76	54.6	0.412	0.051	1568	784	778	S	S	0.993
NW-5	1.76	60.3	0.411	0.100	1372	900	828	S	S	0.920
NW-6	1.76	65.2	0.433	0.096	1568	1056	902	S	S	0.854
No.5	1.76	76.7	0.592	0.094	1568	1158	1218	S	S	1.052
NW-2	1.18	93.6	0.316	0.105	1764	1468	1116	S	S	0.760
No.1	1.18	65.1	0.599	0.038	1568	1100	1103	S	S	1.003
No.2	1.18	70.8	0.602	0.064	1568	1254	1284	S	S	1.024
No.3	1.18	71.8	0.614	0.098	1568	1378	1444	S	S	1.048
No.4	1.18	103.4	0.535	0.073	2617	1696	1735	S	S	1.023
No.6	1.18	74.1	0.662	0.212	1568	1411	1757	S	S	1.245
No.7	1.18	71.5	0.659	0.184	1568	1498	1681	S	S	1.122
No.8	1.18	76.1	0.677	0.259	1568	1639	1855	S	S	1.132
W35X	1.18	62.6	0.407	0.153	1764	1049	941	B	B	0.897
W35H	1.18	60.8	0.419	0.152	1921	1054	961	B	B	0.912
W30H	1.18	57.7	0.423	0.155	1862	958	945	B	B	0.987
P35H	1.18	62.2	0.391	0.158	1470	1020	883	B	S	0.866
NW35H	1.18	59.7	0.407	0.157	1666	1011	921	B	B	0.911

Mean value $\bar{x}$ = 0.983

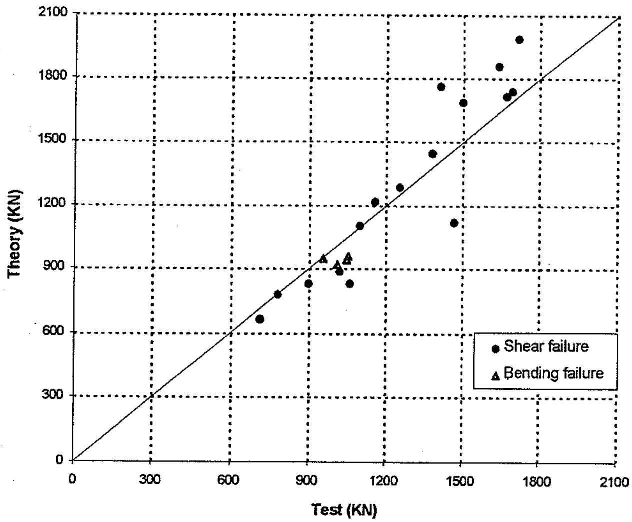

Fig. 6.15 *Comparison of theoretical load carrying capacity with test results by Toshimi [93.3]*

6.2.9 Shear Walls Tested by Hirosawa

The following twentyone shear wall tests were carried out by Hirosawa [75.1]. There was concentrated reinforcement in both sides of the specimens which had rectangular section.

Table 6.8 Test specimens by Hirosawa [75.1]

Specimen No.	a/h	Reinforcement degree Φ	Reinforcement degree ψ	Normal force (KN)	Load capacity Test (KN)	Load capacity Thoery (KN)	Loading method	Failure mode Test	Failure mode Theory	Ratio (Theory/ Test)
Barbell										
3-w7103	0.33	0.137	0.047	368	524	442	Reversal	S	S	0.842
5-w7105	0.33	0.306	0.254	368	783	798	Reversal	B	S	1.020
70-WA1	0.52	0.269	0.060	0	833	762	Monotonic	S	S	0.914
71-WA2	0.52	0.215	0.019	0	804	739	Monotonic	S	S	0.919
95-2	0.71	0.205	0.000	0	39	47	Monotonic	S	S	1.209
97-5	0.79	0.266	0.000	0	31	46	Monotonic	S	S	1.474
98-6	0.79	0.177	0.000	0	39	54	Monotonic	S	S	1.383
99-7	0.79	0.129	0.000	0	59	58	Monotonic	S	S	0.987
6-0w1-1	1.04	0.202	0.038	0	49	37	Reversal	B	S	0.762
9-40w1-1	1.04	0.335	0.031	125	86	67	Reversal	S	S	0.780
12-20w1-2	1.04	0.239	0.029	63	59	55	Reversal	B	S	0.942
Rectangular										
72-A103a	0.94	0.305	0.077	549	809	811	Reversal	B	S	1.002
73-A103B	0.94	0.260	0.069	533	725	831	Reversal	B	S	1.146
75-A106B	0.94	0.361	0.208	533	813	821	Reversal	B	S	1.009
77-A112B	0.94	0.287	0.164	533	911	852	Reversal	B	S	0.935
79-B106b	0.94	0.258	0.224	533	617	585	Reversal	B	B	0.947
81-B112b	0.94	0.205	0.176	533	760	611	Reversal	B	B	0.805
96-1	0.71	0.102	0.000	0	50	54	Monotonic	S	S	1.068
83-B206b	1.88	0.394	0.170	267	333	317	Reversal	B	B	0.953
85-B212b	1.88	0.313	0.282	267	368	284	Reversal	B	B	0.774

Mean value $\overline{x} =$ 0.994

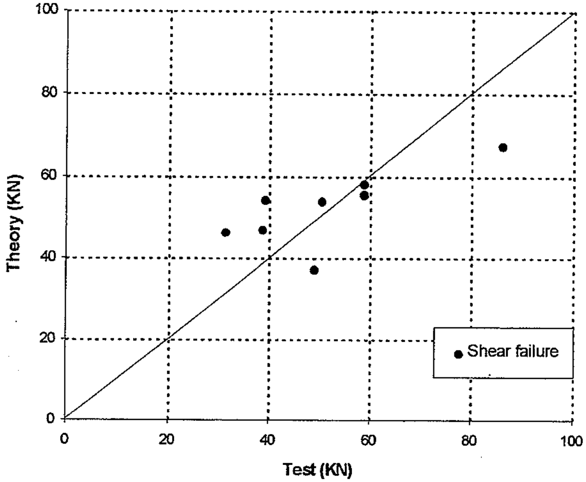

Fig. 6.16 *Comparison of theoretical load carrying capacity with test results by Hirosawa [75.1]*

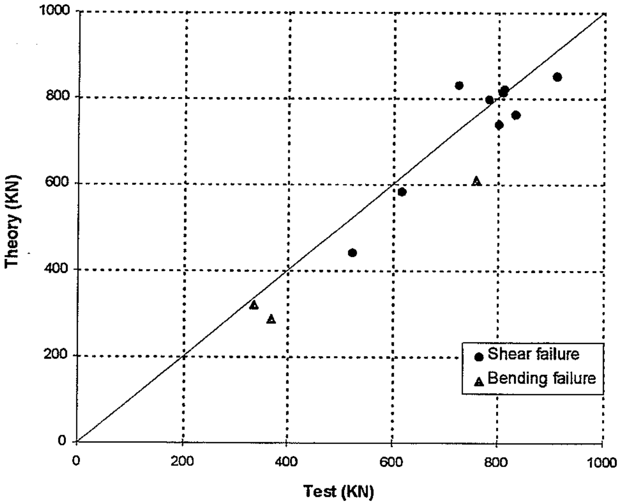

Fig. 6.16 *(Continued)*

6.2.10 Shear Wall Tests by Yoshzaki

Nine reinforced concrete shear walls tested by Yoshzaki [75.1] were selected in the calculation. All the specimens had rectangular section. The transverse load was alternating.

Table 6.9 Test specimens by Yoshzaki [75.1]

Specimen No.	a/h	Reinforcement de Φ	ψ	Normal force (KN)	Load capacity Test (KN)	Thoery (KN)	Failure mode Test	Theory	Ratio (Theory/ Test)
169-1-88-12	1.00	0.349	0.316	0	174	187	S	S	1.075
171-2/3-36-8	0.67	0.183	0.214	0	235	224	S	S	0.952
172-2/3-52-4	0.67	0.171	0.107	0	220	213	S	S	0.969
173-2/3-52-8	0.67	0.225	0.214	0	260	268	S	S	1.030
174-2/3-52-12	0.67	0.276	0.305	0	274	316	S	S	1.150
176-2/2-27-8	0.50	0.160	0.207	0	322	337	S	S	1.049
177-1/2-42-4	0.50	0.135	0.104	0	319	299	S	S	0.937
178-1/2-42-8	0.50	0.191	0.207	0	383	390	S	S	1.019
179-1/2-42-12	0.50	0.245	0.296	0	422	471	S	S	1.117

Mean value $\overline{X}$ = 1.033

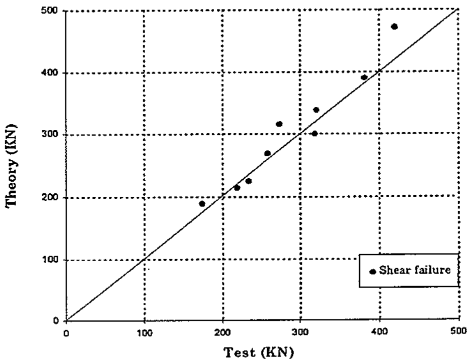

Fig. 6.17 *Comparison of theoretical load carrying capacity with test results by Yoshizaki [75.1]*

6.2.11 Shear Wall Tests by Tanabe

Sixteen reinforced concrete shear walls were tested by Tanabe [75.1]. All the specimens had column boundaries. The transverse load was monotonic.

Table 6.10 Test specimens by Tanabe [75.1]

Specimen No.	a/h	Reinforcement degree		Normal force (KN)	Load capacity		Failure mode		Ratio (Theory/ Test)
		Φ	ψ		Test (KN)	Thoery (KN)	Test	Theory	
101-9	0.79	0.373	0.241	0	63	72	S	S	1.142
102-10	0.79	0.412	0.266	0	75	70	S	S	0.936
112-42	0.79	0.280	0.214	0	68	67	S	S	0.979
113-44	0.79	0.260	0.199	0	71	68	S	S	0.960
104-12	0.79	0.243	0.157	0	94	78	S	S	0.829
105-13	0.79	0.249	0.161	0	90	78	S	S	0.867
106-14	0.79	0.251	0.168	0	86	78	S	S	0.903
114-4M	0.79	0.196	0.150	0	71	71	S	S	1.002
115-49	0.79	0.179	0.137	0	77	72	S	S	0.937
107-15	0.79	0.193	0.125	0	98	81	S	S	0.830
108-16	0.79	0.183	0.119	0	97	82	S	S	0.843
109-17	0.79	0.182	0.118	0	102	82	S	S	0.804
116-52	0.79	0.136	0.104	0	78	74	S	S	0.945
117-54	0.79	0.141	0.108	0	77	74	S	S	0.953
110-36	0.79	0.436	0.206	0	43	47	S	S	1.101
111-39	0.79	0.450	0.213	0	44	47	S	S	1.056

Mean value $\bar{x} =$ 0.943

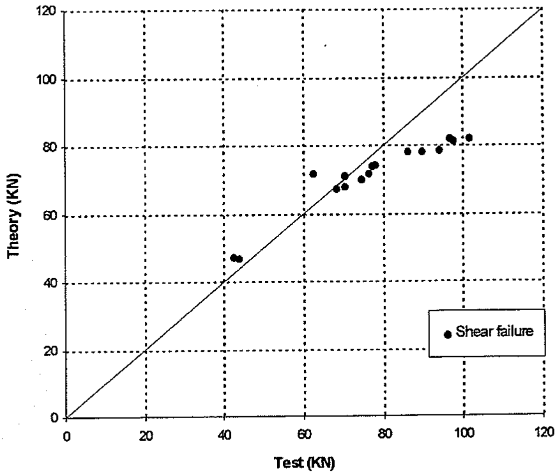

Fig.6.18 *Comparison of theoretical load carrying capacity with test results by Tanabe [75.1]*

<u>6.2.12 Shear Wall Tests by NUPEC, Cardenas, Kebeyasawa, Wiradinata, Aoyagi and Paulay</u>

The comparison between theoretical results and tests by NUPEC [94.3], Cardenas [80.2], Kebeyasawa [84.5] [85.4], Wiradinata [86.6], Aoyagi [90.1] and Paulay [80.1] is shown in table 6.10 and Fig. 6.12.

Table 6.11 Test specimens by NUPEC [94.3], Cardenas [80.2], Kebeyasawa [84.5] [85.4], Wiradinata [86.6], Aoyagi [90.1] and Paulay [80.1]

Specimen No.	Section geometry	a/h	Reinforcement degree Φ	Reinforcement degree ψ	Normal force (KN)	Load capacity Test (KN)	Load capacity Thoery (KN)	Loading method	Failure mode Test	Failure mode Theory	Ratio (Theory/ Test)
NUPEC	Flanged	0.65	0.383	0.264	1195.6	1627	1599	Dynamic	S	S	0.983
Cardenas											
SW-7	Rect.	1.05	0.225	0.044	12.5	519	577	Monotonic	S	S	1.113
SW-8	Rect.	1.05	0.281	0.050	12.3	570	672	Monotonic	S	B	1.180
SW-9	Rect.	1.05	0.279	0.164	12.5	679	673	Monotonic	S	B	0.991
SW-13	Rect.	1.05	0.277	0.179	12.6	632	674	Monotonic	S	B	1.067
Kabeyasawa											
K1	Barbell	0.75	0.163	0.070	396.5	439	372	Reversal	S	S	0.847
K2	Barbell	0.75	0.250	0.141	399.8	471	522	Reversal	S	S	1.108
K4	Barbell	0.75	0.177	0.125	398.4	508	592	Reversal	S	S	1.165
Wiradinata	Rect.	0.55	0.1116	0.0631	14.9	573.8	519.0	Alternating	S	S	0.904
Wiradinata	Rect.	0.31	0.122	0.070	8.8	680.5	675.8	Alternating	S	S	0.993
Aoyagi	Barbell	0.5147	0.1284	0.1094	0	1555	1394	Alternating	S	S	0.897
Aoyagi	Barbell	0.51	0.269	0.110	0	2309	2430	Alternating	S	S	1.052
Paulay	Rect.	0.5	0.093	0.339	0	810	707	Alternating	S	S	0.874
Paulay	Flanged	0.5	0.086	0.351	0	786	674	Alternating	S	S	0.857

Mean value $\overline{X} = 1.002$

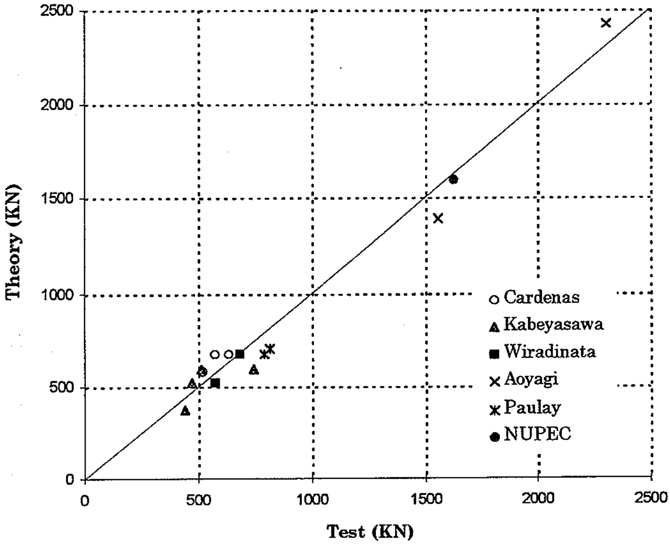

Fig. 6.19 *Comparison of theoretical load carrying capacity with test results by NUPEC [94.3], Cardenas [80.2], Kebeyasawa [84.5][85.4],Wiradinata[86.6], Aoyagi[90.5] and Paulay [80.1]*

6.2.13 Shear Walls Tests by Kokusho

Eleven reinforced concrete shear walls were tested by Kokusho [75.1]. All the specimens had flange boundaries and the transverse load was alternating .

Table 6.12 Test specimens by Kokusho [75.1]

Specimen No.	a/h	Reinforcement degree		Normal force (KN)	Load capacity		Failure mode		Ratio (Theory/ Test)
		Φ	ψ		Test (KN)	Thoery (KN)	Test	Theory	
S1	0.47	0.171	0.169	0	29.4	30.9	S	S	1.053
S2	0.47	0.174	0.172	0	27.6	30.8	S	S	1.116
S3	0.70	0.303	0.147	0.53	24.5	29.7	S	S	1.212
S4	0.70	0.324	0.134	0.50	23.6	27.3	S	S	1.159
S6	0.70	0.501	0.211	0.40	19.6	23.5	S	S	1.200
S7	0.70	0.317	0.183	0.30	24.9	31.1	S	S	1.249
S8	0.70	0.338	0.194	0.56	25.8	30.7	S	S	1.191
S9	0.70	0.206	0.089	0.42	26.7	30.4	S	S	1.141
S10	0.70	0.310	0.134	0.54	26.7	27.9	S	S	1.045
S11	0.70	0.310	0.134	0.54	25.8	27.9	S	S	1.081
S12	0.70	0.328	0.140	0.54	24.5	27.5	S	S	1.124

Mean value $\overline{X}$ = 1,143

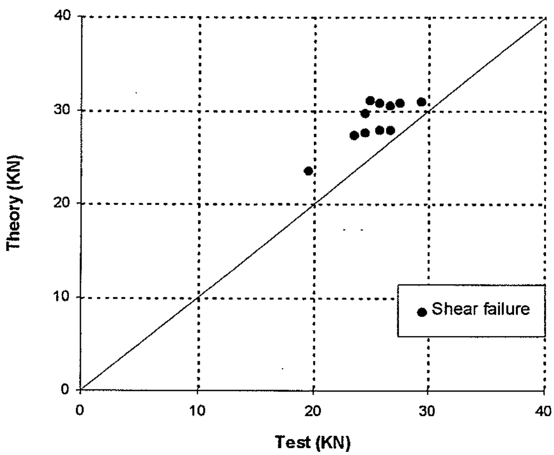

Fig.6.20 *Comparison of theoretical load carrying capacity with test results by Kokusho [75.1]*

6.2.14 Shear Walls Tests by Benjamin

Twenty-nine reinforced concrete shear walls were tested by Benjamin [53.1] [55.1] [56.1] [56.2] [57.1]. All the specimens had column boundaries and the transverse load was monotonic.

Table 6.13 Test specimens by Benjamin [53.1] [55.1] [56.1] [56.2] [57.1].

Specimen No.	a/h	Reinforcement degree Φ	ψ	Normal force (KN)	Load capacity Test (KN)	Thoery (KN)	Failure mode Test	Theory	Ratio (Theory/ Test)
4BII-1	0.98	0.266	0.122	0	89	75	S	S	0.848
4BII-2	0.61	0.187	0.115	0	155	134	S	S	0.864
4BII-3	0.44	0.169	0.126	0	201	192	S	S	0.954
4BII-4	0.29	0.104	0.097	0	294	334	S	S	1.137
1BII-1	0.53	0.159	0.061	0	249	248	S	S	0.994
3AII-1	0.66	0.246	0.102	0	205	162	S	S	0.793
3AII-2	0.60	0.273	0.063	0	138	140	S	S	1.014
NV-1	0.48	0.107	0.095	0	301	240	S	S	0.795
NV-11	0.96	0.307	0.102	0	222	214	S	S	0.963
NV-18	0.31	0.121	0.118	0	374	332	S	S	0.889
VR-3	0.55	0.179	0.115	0	302	288	S	S	0.953
R-1	0.55	0.161	0.062	0	316	257	S	S	0.813
A1-A	0.31	0.185	0.228	0	311	368	S	S	1.181
A1-B	0.31	0.179	0.220	0	367	373	S	S	1.016
A2-B	0.31	0.255	0.359	0	329	427	S	S	1.296
M-1	0.54	0.167	0.059	0	214	252	S	S	1.178
MR-1	0.40	0.167	0.055	0	317	283	S	S	0.892
MR-3	0.40	0.241	0.079	0	318	243	S	S	0.764
MR-2	0.30	0.196	0.064	0	245	287	S	S	1.173
MR-4	0.30	0.261	0.085	0	245	250	S	S	1.022
VRR-1	0.49	0.162	0.096	0	329	288	S	S	0.874
MS-1	0.47	0.220	0.049	0	274	306	S	S	1.114
MS-2	0.47	0.177	0.043	0	368	335	S	S	0.909
MS-2-2	0.47	0.202	0.049	0	359	319	S	S	0.889
MS-5	0.24	0.139	0.047	0	380	509	S	S	1.338
SD-1A	0.53	0.179	0.126	0	178	158	S	S	0.886
SD-1C	0.53	0.179	0.126	0	160	158	S	S	0.984
3BI-3	0.53	0.170	0.109	0	294	292	S	S	0.995
1BII-3	0.54	0.179	0.118	0	685	634	S	S	0.926

Mean value $\bar{x}$ = 0,981

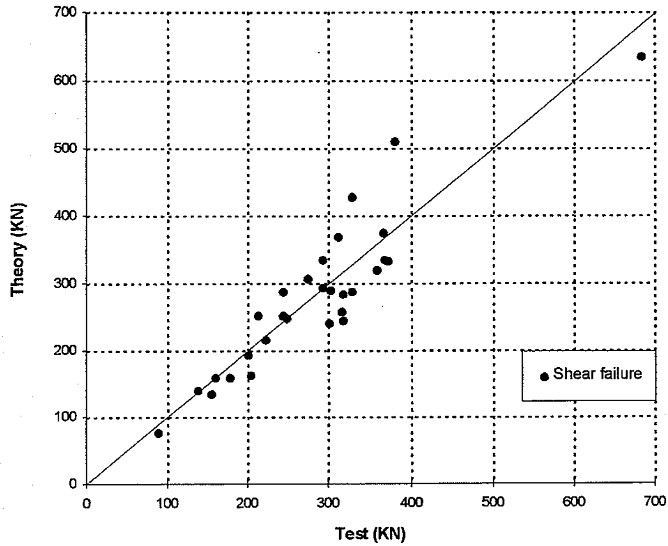

Fig.6.21 *Comparison of theoretical load carrying capacity with test results by Benjamin [53.1] [55.1] [56.1] [56.2] [57.1].*

CHAPTER VII CONCLUSION

In this report a theoretical model which is composed of a strut or a diagonal compression field combined with triangular homogenous stress fields has been developed for shear walls in shear. The solution satisfies the equilibrium conditions and statical boundary conditions and is based on a safe stress distribution. It is thus a lower bound solution. The theory is capable of predicting the load-carrying capacity of reinforced concrete structural walls as well as available for designing the walls.

Some of the capabilities of the theory are listed below :

1. The theory can be applied to shear walls with different height-width ratios (normally $a/h \leq 3$) and with rectangular, barbell and flanged cross sections.

2. The theory is applicable to shear walls subjected to a normal force as well as a concentrated transverse load which can be applied monotonicly or cyclicly.

3. The theory is applicable to shear walls with normal strength materials as well as ultra-high strength materials such as concrete strength up to about 140 MPa and steel yield stresses up to 1420 MPa.

4. By means of optimizing routines, by which the shear capacity of shear walls may be found easily, the theory predicts the balanced reinforcement ratios beyond which the steel will not yield at failure or the concrete will not reach its limit strength.

A large number of shear wall tests are available in the literature. A number of 184 typical test specimens have been treated using the theory proposed in this report. The agreement between theory and experiment is good.

CHAPTER VIII. REFERENCES

[21.1] Ingerslev.Å : Om en elementær beregningsmetode af krydsarmerede plader (on an elementary method of calculation for two-way slabs) : Ingeniøren , Vol. 30, No. 69, 1921, pp. 507-515.

[22.1] Mörsh, E. : Der Eisenbetonwehrung unter einem Winkel mit der Richtung der Normalkraft : Beton u. Eisen, Vol. 21, 1922, pp. 145-149.

[23.1] Ingerslev. Å. : The Strength of Rectangular Slabs : J. Inst. Struct. Eng. ,Vol. 1, No. 1, 1923 pp.3- 14.

[28.1] Johansen , K. W. : Om Virkningen af Bøjler og Skråjern i Jernbetonbjælker, Danmarks Naturvidenskabelige Samfund, A no. 17, København 1928.

[31.1] Johansen, K. W. : Beregning af Krydsarmerede Jernbetonpladers Brudmoment (Calculation of the rupture moment of two-way slabs) : Bygningsstat. Medd . ,Vol . 3 , No .1 , 1931 , pp. 1- 18.

[32.1] Johansen, K . W . : Bruchmomente der Kreuzweise bewehrten Platten : Mem. Ass. Int . Ponts Charp., Vol.1 ,1932, pp. 277-295

[38.1] Gvozdev, A . A . : Opredelenie velichiny razrushayushchei nagruzki dlya staticheski neopredelimykh sistem preterpevayushchikh plasticheskie deformatsii : Moscow/Leningrad, Akademia Nauk SSSR, 1938,pp.19-38. (English Translation: The Determination of the Value of the Collapse Load for Statically Indeterminate Systems Undergoing Plastic Deformation: Int. J. Mech. Sci., Vol. 1, 1960, pp. 322-333)

[43.1] Johansen , K. W. : Brudlinieteorier (Yield line theories) : Copenhagen, Gjellerup, 1943, 189 pp.

[51.1] Hill, R. : On the State of Stress in a Plastic-Rigid Body at the Yield Point : Phil. Mag. (7), Vol. 42, 1951, pp. 868-875.

[52.1] Drucker , D. C. , H. J. Greenberg , and W. Prager : Extended Limit Design Theorems for Continuous Media : Q . Appl. Math., Vol . 9, 1952, pp. 381-389.

[52.2] Prager, W. : The General Theory of Limit Design: Proc. 8th Int. Congr. Theor. Appl. Mech., Istanbul, 1952, Vol. II, pp. 65-72.

[52.3] Hill, R. : A Note on Estimating the Yield-Point Loads in a Plastic-Rigid Body : Phil. Mag.(7), Vol.43,1952, pp. 353-355.

[53.1] Benjamin, J. R., and Williams, H. A.,Investigation of Shear Walls, part 3–Experimental and Mathematical Studies of the Behavior of Plain and Reinforced Concrete Walled Bents Under Static Shear Loading, Technical Report No.1, part 3. Department of Civil Engineering, Stanford University, July 1,1953, 63 pp.

[55.1] Benjamin, J. R., and Williams, H. A.,Investigation of Shear Walls, part 9 – Continued Experimental and Mathematical Studies of the Behavior of Plain and Reinforced Concrete Walled Bents Under Static Shear Loading, Technical report No.7, Department of Civil Engineering , Stanford University, Sept. 1, 1955, 98 pp.

[56.1] Benjamin ,J. R.,Williams , H. A. ; and Erickson, J. A., Investigation of Shear - walls, part 11 – Continued Studies of Combined Normal and Shear Wall Bents and Resistance of Brick Filler Walls with Openings, Technical Report No . 9 , Department of Civil Engineering , Stanford University, Dec. 1956, 43 pp.

[56.2] Benjamin, J R., and Williams, H. A., Investigation of Shear Walls , part 12– Studies of Reinforced Concrete Shear Walls Assemblies, Technical Report No. 10, Department of Civil Engineering, Stanford University, Dec. 1956, 221 pp.

[57.1] Benjamin, J. R., and Williams, H. A.,The Behavior of One-Story Reinforced Concrete Shear Walls, Proc, ASCE, V. 83, ST3, May 1957, pp.1254-1–1254-49.

[61.1] Wood, R. H. : Plastic and Elastic Design of Slabs and Plates: London, Thames & Hudson ,1961.

[62.1] Johansen, K.W : Yield Line Theory : London, Cement and Concrete Association, 1962.

[62.2] Nielsen,M.P. :Plasticitetsteorien for Jernbetonplader (Theory of plasticity for reinforced concrete slabs) : Licentiatafhandling, Danmarks Tekniske Højskole, Copenhagen, 1962.

[63.1] Sawczuk , A., and T. Jaeger : Grenztragfähigkeitstheorie der Platten : Berlin, Springer, 1963.

[63.2] Massonnet , C. E. , and M. A. Save : Calcul Plastique des Constructions, Vol . II : Structure Spatiales : Brussels, Centre Belgo -Luxemburgeois d' Information de 1' Acier . 1963 (English edition : Plastic Analysis and Design of Plates , Shells and Disks: Amsterdam, North- Holland, 1972)

[63.3] Nielsen, M . P. : Yield Conditions for Reinforced Concrete Shells in the Membrane State : IASS Symp. Non-classical Shell Problems, Warsaw, 1963; Proc . , Amsterdam , North - Holland Publishing Company, 1964.

[64.1] Nielsen,M. P. :Limit Analysis of Reinforced Concrete Slabs: Copenhagen, Acta Polytech. Scand.,Civil Eng. Build. Constr. Ser. No. 26, 1964, 167 pp.

[68.1] Winokur, A and J.Gluck, Ultimate Strength Analysis of Coupled Shear Walls, ACI Journal, Proc, Vol. 65, No. 12, 1968, pp. 1029-1036.

[69.1] Nielsen , M . P . : Om Jernbetonskivers Styrke : Copenhagen , Polyteknisk Forlag , 1969 , 254 pp. (English edition: On the Strength of Reinforced Concrete Discs: Acta Polytech. Scand., Ci-70, Copenhagen, 1971, 261pp.)

[70.1] Paulay. T. : An Elasto-plastic Analysis of Coupled Shear Walls, ACI Journal, Proc., Vol .67 No.11,1970, pp. 915-922.

[73.1] Cardenas, A. E., J. M. Hanson, W. G. Corley and E. Hognestad, : Design Provisions for Shear Walls, ACI Journal, Proc., Vol. 70, No. 3, 1974, pp 221-230.

[74.1] Fintel, M. ; Ductile Shear Walls in Earthquake Resistant Multistory Buildings. ACI Journal, Proc. Vol. 71. No. 6. June, 1974, pp. 296-305.

[74.2] Mitchell, D. and M. P.Collins,: Diagonal Compression Field Theory – A Rational Model for Structural Concrete, ACI, Journal, Proc., Vol. 71, No. 8, 1974. pp. 396-408.

[75.1] Hirosawa, M. : Past Experimental Results on Reinforced Concrete Shear Walls and Analysis on Them, Kenchiku Kenkyu Shiryo, Building Research Institute, Ministry of Construction. (No. 6), March, 1975. 277 pp. (in Japanese)

[76.1] Paulay, T. A. and A. R. Santhakumar, : Ductile Behavior of Coupled Shear Walls, Journal of the Structural Division, ASCE, Vol. 102, No. ST1, Jan. 1976, pp. 93-108.

[76.2] Barda, F., Hanson, J. M. and Corley, W. G. : Shear Strength of Low - Rise Walls with Boundary Elements, ACI Symposium, " Reinforced Concrete Structures in Seismic Zones,"Detroit, Michigan,1976.

[77.1] Bræstrup, M. W., M. P. Nielsen, and F. Bach: Plastic Analysis of Shear in Concrete : Z. Angew. Math. Phys., Vol. 58, 1978, pp. 3-14. (also : Copenhagen, Technical University of Denmark, DCAMM Report No.120, May, 1977, 24 pp.).

[78.1] Nielsen, M. P., M. W. Bræstrup, B. C. Jensen, and F. Bach: Concrete Plasticity, Beam Shear–Shear in Joints–Punching Shear: Lyngby, Special Publication,

Danish Society for Structural Science and Engineering, Draft, 1976 (final edition: Lyngby, 1978, 129pp.).
[78.2] IABSE : Plasticity in Reinforced Concrete, Introductory Report : Zürich, International Association for Bridge and Structural Engineering, Reports of the Working Commissions, Vol. 28, Oct. 1978, 172 pp.
[78.3] Collins, M. P. : Towards a Rational Theory for RC Members in Shear, ASCE, Vol. 104 , No. ST4, Apr. 1978, pp. 649- 666.
[78.4] Wang, P. T. , S. P., Shan and A. E. Naaman : Stress-Strain Curves of Normal and Lightweight Concrete in Compression : ACI Journal, Proc., Vol. 75, No. 11, Nov. 1978, pp. 603-611.
[79.1] IABSE : Plasticity in Reinforced Concrete , Final Report : Zürich, International Association for Bridge and Structural Engineering, Reports of the Working Commissions, Vol. 29, Aug. 1979, 360 pp.
[79.2] Bræstrup, M. W. , : Effect of Main Steel Strength of the Shear Capacity of Reinforced Concrete Beams with Stirrups , Structural Research Laboratory, Technical University of Denmark, Report , No. 110, 1979, 49 pp.
[79.3] Exner, H. : On the Effectiveness Factor in Plastic Analysis of Concrete:IABSE colloquium,Copenhagen, 1979, Session I. Plasticity in Reinforced Concrete, Final Report, Vol. 29, Aug. 1979, pp. 35-42.
[80.1] Paulay, T. : Earthquake–Resisting Shear Walls–New Zealand Design Trends, ACI Journal, Proc., Vol. 77, No.3, 1980.
[80.2] Cardenas, A. E. , Russell H. G. ; and Corley W. G. : Strength of Low-Rise Structural Walls, Reinforced Concrete Structures Subjected to Wind and Earthquake Forces, Sp- 63, American Concrete Institute, Detroit 1980, pp. 221- 241.

[80.3] Collins, M. P. and Mitchell, D. , : Shear and Torsion Design of Prestressed and Non-prestressed Concrete Beams,Journal of the Prestressed Concrete Institute, Vol. 25, No.5, Sept.- Oct. , 1980, pp. 32-100

[81.1] Jensen, J. F. : Plasticitetsteoretiske Løsninger for Skiver og Bjælker af Jernbeton (plastic solutions for disks and beams of reinforced concrete): Copenhagen, Technical University of Denmark , Structural Research Laboratory, Ph. D. Thesis,Report No.R-141, 1981, 153pp.

[81.2] Vecchio , F. , and M . P . Collins , : Stress - Strain Characteristics of Reinforced Concrete in Pure Shear , Final Report , IABSE Colloquium on Advanced Mechanics of Reinforced Concrete (Delft, 1981) , International Association for Bridge and Structural Engineering, Zürich, pp. 211- 225.

[82.1] Chen, W. F. : Plasticity in Reinforced Concrete, McGraw-Hill Book Company, 1982.

[82.2] Vecchio, F. and M. P. Collins, : The Response of Reinforced Concrete to In-Plane Shear and Normal Stresses, Publication No. 82-03, Department of Civil Engineering, University of Toronto, Mar, 1982,17 pp.

[82.3] Paulay, T. , M . J . N . Priestley and A. J. Synge, : Ductility in Earthquake Resisting Squat Shearwalls, ACI Journal, Proc., Vol. 79, No.4, 1982, pp. 257-269.

[83.1] Allen, C. Micheal, : Discussion of "ACI Committee 318 Report , " Concrete International : Design & Construction, Vol. 5, No. 6, June 1983, p.62.

[83.2] Wyllie, Loriry A., Jr., : Discussion of "ACI Committee 318 Report , " Concrete International : Design & Construction, Vol. 5, No. 6, June 1983,p76.

[83.3] Kotsovos, M. D. : Mechanisms of ' Shear ' Failure, Magazine of Concrete Research, Vol. 35, No.123, 983. pp. 99- 106.

[84.1] Nielsen, M. P. : Limit Analysis and Concrete Plasticity, Prentice - Hall , Inc. , Englewood Cliffs , New Jersey, 1984.

[84.2] Kotsovos, M. D. : Concrete : A Brittle Fracturing Material , Materials and Structures, Research and Testing, RILEM, Paris, Vol. 17, No. 98, 1984. pp. 107-115.

[84.3] Oesterle, R. G. , J. D. Aristizabal - Ocha, J. D. , K. N. Shiu and W. G. Corley, : Web Crushing of Reinforced Concrete Structural Wall, ACI Journal, Proceedings, Vol. 81, No. 3, 1984, pp. 231-241

[84.4] Feddersen, B. and M. P. Nielsen,: Plastic Analysis of Reinforced Concrete Beams in Pure Bending or Pure Torsion, Bygningsstatiske Meddelelser, Vol. 55, No.2, 1984, pp. 37-61.

[84.5] Ogata, K., and T. Kabeyasawa, : Experimental Study on the Hysteretic Behavior of Reinforcement Concrete Shear Walls Under the Loading of Different Moment - to - Shear Ratios , Transactions , Japan Concrete Institute, Tokyo, V. 6, 1984, pp. 717-724

[85.1] Marti, P. : Basic Tools of Reinforced Concrete Beam Design, ACI Journal, Proc. Vol. 82, No.1, Jan–Feb. 1985, pp. 46-56.

[85.2] Hsu, T. T. C. and Y. L Mo, Softening of Concrete in Low-Rise Shearwalls, ACI Journal, Proc. Vol. 82, No.6, 1985, pp. 883-889.

[85.3] Maier , and Thürlimann , B . : Bruchversuche an Stahlbetonscheiben , Institut für Baustatik und Konstruktion ETH Zürich, 1985.

[85.4] Kabeyasawa, T. , and Somaki, T. , Reinforcement Details for Reinforced Concrete Shear Walls with Thick Panel, Transactions Japan Concrete Institute, Tokyo, V. 7, 1985, pp. 317-324

[86.1] Paulay, T. , Critique of the Special Provisions for Seismic Design of the Building Code Requirements for Reinforced Concrete (ACI 318-83), ACI Journal, Proc. Vol. 83, No.2, Mar-Apr.1986, pp.274-283.

[86.2] Vecchio, F. J. and M. P. Collins , : The Modified Compression – Field Theory for Reinforced Concrete Element Subjected to Shear, ACI Journal, Proc. Vol. 83, No.3, 1986, pp. 219-231.

[86.3] Mau, S. T. and T. T. C. Hsu, : Shear Design and Analysis of Low-Rise Structural Walls, ACI Journal, Proc. Vol. 83, No. 2, 1986. pp. 306-315.

[86.4] Wiradinate, S. ,and Saatcioglu , M., : Tests of Squat Shear Wall under Lateral Load Reversals, Proc. 3rd U. S. National Conference on Earthquake Engineering, Charleston, 1986, Vol. 2, pp.1395-1406.

[86.5] Aoyama, H. and H. Shiohara, : Plastic Analysis for Ultimate Strength of Reinforced Concrete Shear Walls, Proc. International Symposium on Fundamental Theory of Reinforced and Prestressed Concrete, Nanjing, China, 1986. pp 1406 -1413. Transactions of the Japan Concrete Institute. Vol.8,1986, pp.489-496.

[86.6] Wiradinata, S., and M. Saatcioglu, : Tests of Squat Shear Wall under Lateral Load Reversals, Proc. , 3rd U. S. National Conference on Earthquake Engineering, Charleston, 1986, V.2, pp. 1395-1406.

[87.1] Mau, S. T. and T. T. C. Hsu, : Shear Behavior of Reinforced Concrete Framed Wall Panels with Vertical Loads, ACI Structural Journal, Vol. 84, No. , 1987, pp. 228-234.

[88.1] Kotsovos, M. D. : Compressive Force Path Concrete: Basis for Reinforced Concrete Ultimate Limit State Design, ACI Structural Journal, Vol. 85, No. 1988, pp. 68-75.

[88.2] Lefas,I.D. : Behavior of RC Walls and Its Implication for Ultimate Limit State Design , Ph . D . Thesis, Imperial College, University of London, 1988. 330 pp.

[88.3] Chen, G. , : Plastic Analysis of Shear in Beams, Deep Beams and Corbels , Department of Structural Engineering, Technical University of Denmark, Ph. D. Report , No 237, 1988, 228 pp.

[90.1] Wood, S. L. : Shear Strength of Low- Rise Reinforced Concrete Walls, ACI Structural Journal, Vol. 87, Jan.-Feb. 1990. pp. 99-106.

[90.2] Schlaich, M. and G. Anagnoslou, : Stress Fields for Nodes of Strut- and- Tie Models, ASCE, Journal of Structural Engineering Vol. 116, No.1 Jan,1990. pp. 13-23.

[90.3] Lefas, I. D., M. D. Kostsovos, and N. N. Ambraseys, : Behavior of Reinforced Concrete Structural Walls: Strength, Deformation Characteristics, and Failure Mechanism, ACI Structural Journal, Vol. 87. No.1, 1990, pp. 23- 31.

[90.4] Lefas, I. D. and M. D. Kotsovos, : Strength and Deformation Characteristics of Reinforced Concrete Walls Under Load Reversals , ACI Structural Journal, Vol. 87, No.6, 1990. pp. 716-726.

[91.1] Takeda T. , T. Yamaguchi, K. Naganuma : Reports on Tests of Nuclear Prestressed Concrete Containment Vessels, Proc. Int . Workshop on Concrete Shear in Earthquake , University of Houston, Houston, Texas, U. S. A. Jan. 1991.

[92.1] Paulay T. and M. J. N. Priestley, : Seismic Design of Reinforced Concrete and Masonry Buildings, A Wiley Interscience Publication , John Willey & Sons, INC. , 1992

[93.1] Hsu, T. T. C. : Unified theory of Reinforced Concrete, CRC Press, Inc, 1993.

[93.2] Siao, W. B.: Strut- and- Tie Model for Shear Behavior in Deep Beams and Pile Caps Failing in Diagonal Splitting , ACI Structural Journal. Vol. 90,July- Aug. 1993. pp. 356- 363.

[93.3] Kubeyasawa T., H. Kuramoto, and K. Matsumoto, : Tests and Analyses of High Strength Shear Walls, Report on the First Meeting of the Multilateral Project on the Use of High Strength Concrete.

[93.4] Gupta , A. and B. V. Rangan , : High - Strength Concrete Structural Walls under Inplane Vertical and Horizontal Loads, Proc. of the Third International Conference on Utilization of High Strength Concrete, Lillehammer,Norway,June1993,pp177-183.

[94.1] Siao, W. B. : Shear Strength of Short Reinforced Concrete Walls,Corbels, and Deep Beams, ACI Structural Journal, Vol.91, March-April,1994. pp.123-132.

[94.2] Gupta, A. and Rangan, B. V. High-strength Concrete Shear Walls, Report presented at the Australian Structural Engineering Conference, Sydney, Sept., 1994.

[94.3] Proposal of Seismic Shear Wall ISP on NUPEC ' s Seismic Ultimate Response Test, Committee on the Safety of Nuclear Installations Energy Agency March, 1994.

[95.1] Gurfinkel, G. : Simple Design of Concrete Walls and Structural Members under Combined Tension and Moment , ACI , Structural Journal . Vol . 92, No. 5, 1995, pp. 574- 579.

APPENDIX A Test Data and Calculation Results of Shear Wall Tests by Gupta and Rangan [93.4] [94.2]

Table A

Specimen No.	S-F	S-1	S-2	S-3	S-4	S-5	S-6	S-7
a(mm)	1000	1000	1000	1000	1000	1000	1000	1000
h(mm)	1000	1000	1000	1000	1000	1000	1000	1000
a / h	1	1	1	1	1	1	1	1
a_t (mm)	200	200	200	200	200	200	200	200
t_f (mm)	100	100	100	100	100	100	100	100
b (mm)	375	375	375	375	375	375	375	375
t (mm)	75	75	75	75	75	75	75	75
h_0 (mm)	800	800	800	800	800	800	800	800
φ_l	0.002	0.008	0.013	0.017	0.013	0.017	0.020	0.013
φ_x	0.012	0.012	0.012	0.012	0.018	0.018	0.018	0.012
ψ	0.005	0.005	0.005	0.005	0.005	0.005	0.005	0.011
f_{Yl} (MPa)	578	529	531	531	531	531	531	531
f_{Yx} (MPa)	545	545	545	545	533	533	533	545
f_{Yy} (MPa)	578	578	578	578	578	578	578	545
f_c (MPa)	60.5	79.3	65.1	69.0	75.2	73.1	70.5	71.2
N (KN)	310	0	610	1230	0	610	1230	610
P (KN)	487	720	851	600	790	970	800	428
ν	0.525	0.430	0.525	0.551	0.437	0.486	0.541	0.492
Φ_l	0.107	0.072	0.147	0.164	0.106	0.144	0.183	0.150
Φ_x	0.076	0.067	0.130	0.148	0.098	0.130	0.145	0.129
Ψ	0.107	0.072	0.147	0.164	0.106	0.144	0.183	0.150
$\tau_{test} / \nu f_c$	0.107	0.072	0.147	0.164	0.106	0.144	0.183	0.150
$\tau_{theory} / \nu f_c$	0.076	0.067	0.130	0.148	0.098	0.130	0.145	0.129
$\tau_{theory} / \tau_{test}$	0.705	0.937	0.885	0.899	0.922	0.904	0.793	0.862
T_1 (KN)	91	333	522	689	522	689	696	522
C_1 (KN)	782	714	1512	2297	1091	1866	2466	1510
Failure mode	S	S	S	S	S	S	S	S
θ (rad)	0.705	0.681	0.527	0.406	0.585	0.450	0.380	0.640
θ_1 (rad)	1.398	1.377	1.163	0.957	1.244	1.035	0.889	1.196
y'_0 / h_e	0.104	0.146	0.388	0.548	0.303	0.491	0.580	0.216
σ_c^l / f_c	0.227	0.224	0.350	0.511	0.302	0.449	0.577	0.461
σ_{sl} / f_{Yl}	1	1	1	1	1	1	1	1
σ_{sx} / f_{Yx}	1	1	1	1	1	1	1	1
σ_{sy} / f_{Yy}	1	1	1	1	1	1	1	1
x / a*	0.481	0.480	0.460	0.427	0.469	0.441	0.411	0.449
a*/ a	1	1	1	1	1	1	1	1

APPENDIX B Test Data and Calculation Results of Shear Wall Tests by Felix Barda [76.2]

Table B

Specimen No.	B1-1	B2-1	B3-2	B4-3	B5-4	B6-4	B7-5	B8-5
a(mm)	953	953	953	953	953	953	476	1905
h(mm)	1905	1905	1905	1905	1905	1905	1905	1905
a / h	1	1	1	1	1	1	0	1
a_t (mm)	152	152	152	152	152	152	152	152
t_f (mm)	102	102	102	102	102	102	102	102
b (mm)	610	610	610	610	610	610	610	610
t (mm)	102	102	102	102	102	102	102	102
h_0 (mm)	1702	1702	1702	1702	1702	1702	1702	1702
φ_l	0.006	0.020	0.013	0.013	0.013	0.013	0.013	0.013
φ_x	0.005	0.005	0.005	0.005	0.000	0.003	0.005	0.005
ψ	0.005	0.005	0.005	0.000	0.005	0.005	0.005	0.005
f_{Yl} (MPa)	525	487	414	527	527	529	539	489
f_{Yx} (MPa)	543	552	545	535	0	496	531	527
f_{Yy} (MPa)	496	499	513	0	495	496	501	496
f_c (MPa)	29.0	16.3	27.0	19.0	28.9	21.2	25.7	23.4
N (KN)	0	0	0	0	0	0	0	0
P (KN)	1276	969	1113	1023	680	867	1145	889
ν	0.655	0.718	0.665	0.705	0.656	0.694	0.671	0.683
Φ_l	0.159	0.849	0.302	0.516	0.365	0.471	0.410	0.401
Φ_x	0.143	0.235	0.152	0.199	0	0.084	0.154	0.165
ψ	0.131	0.213	0.143	0	0.131	0.168	0.145	0.155
$\tau_{test} / \nu f_c$	0.347	0.427	0.320	0.394	0.185	0.304	0.342	0.287
$\tau_{theory} / \nu f_c$	0.279	0.404	0.356	0.309	0.347	0.382	0.414	0.309
$\tau_{theory} / \tau_{test}$	0.803	0.946	1.111	0.784	1.869	1.256	1.208	1.078
T_1 (KN)	586	959	1026	694	1274	1261	951	1241
C_1 (KN)	1054	1401	1486	1108	1272	1450	1357	1692
Failure mode	S	S	S	S	S	S	S	S
θ (rad)	0.828	0.548	0.658	0.554	0.670	0.548	0.673	0.563
θ_1 (rad)	1.208	0.686	0.984	1.017	1.013	0.772	0.839	1.060
y'_0 / h_e	0.441	0.686	0.603	0.691	0.594	0.686	0.795	0.352
σ_c^l / f_c	0.241	0.783	0.382	0	0.339	0.620	0.374	0.543
σ_{sl} / f_{Yl}	1	0	1	1	1	1	1	1
σ_{sx} / f_{Yx}	1	1	1	1	0	1	1	1
σ_{sy} / f_{Yy}	1	1	1	0	1	1	1	1
x / a*	0.486	0.404	0.469	0	0.473	0.433	0.480	0.431
a*/ a	1	1	1	1	1	1	1	1

APPENDIX C Test Data and Calculation Results of Shear Wall Tests by Maier and Thurlimann [85.3]

Table C

Specimen No.	S1	S2	S3	S5	S6	S7	S10	S4	S9
a(mm)	1200	1200	1200	1200	1200	1200	1200	1200	1200
h(mm)	1180	1180	1180	1180	1180	1180	1180	1180	1180
a / h	1	1	1	1	1	1	1	1	1
a_t (mm)	240	240	240	240	240	240	240	240	240
t_f (mm)	100	100	100	100	100	100	240	100	100
b (mm)	400	400	400	400	400	400	100	100	100
t (mm)	100	100	100	100	100	100	100	100	100
h_0 (mm)	980	980	980	980	980	980	700	980	980
φ_l	0.004	0.004	0.008	0.004	0.004	0.004	0.012	0.001	0
φ_x	0.012	0.012	0.025	0.012	0.013	0.011	0.010	0.011	0
φ_y	0.010	0.010	0.010	0.010	0.006	0.010	0.010	0.010	0
f_{Yl} (MPa)	669	669	634	669	622	669	629	669	661
f_{Yx} (MPa)	669	669	634	669	622	669	606	669	661
f_{Yy} (MPa)	669	669	669	669	641	669	606	669	0
f_c (MPa)	36.9	35.4	36.7	37.3	37.3	34.1	31.0	32.9	29
N (KN)	433	1653	424	416	416	1657	262	262	260
P (KN)	680	928	977	683	656	855	670	392	342
ν	0.663	0.813	0.664	0.659	0.659	0.827	0.697	0.684	0.709
Φ_l	0.107	0.091	0.217	0.107	0.097	0.091	0.338	0.026	0.027
Φ_x	0.317	0.269	0.641	0.316	0.329	0.268	0.281	0.312	0.316
ψ	0.281	0.239	0.283	0.280	0.149	0.239	0.275	0.306	0
$\tau_{test} / \nu f_c$	0.235	0.273	0.340	0.236	0.226	0.257	0.263	0.148	0.140
$\tau_{theory} / \nu f_c$	0.236	0.299	0.360	0.233	0.222	0.298	0.301	0.139	0.142
$\tau_{theory} / \tau_{test}$	1.001	1.094	1.060	0.989	0.982	1.161	1.146	0.944	1.012
T_l (KN)	310	310	624	310	281	302	862	70	65
C_l (KN)	1499	2475	2306	1482	1228	2448	1482	1019	398
Failure mode	S	B	S	S	S	B	S	B	B
θ (rad)	0.852		0.672	0.856	0.674		0.732		
θ_1 (rad)	1.289		1.012	1.293	1.282		1.167		
y'_0 / h_e	0.000		0.156	0.000	0.152		0.045		
σ_c^l / f_c	0.497		0.731	0	0.382		0.615		
σ_{sl} / f_{Yl}	1		1	1	1		1		
σ_{sx} / f_{Yx}	1		1	1	1		1		
σ_{sy} / f_{Yy}	1		1	1	1		1		
x / a*	0.460		0.400	0	0.462		0.430		
a*/ a	1		1	1	1		1		

APPENDIX D Test Data and Calculation Results of Shear Wall Tests by Lefas, Micheal and Nicholas [90.3] [90.4]

Table D

Specimen No.	SW11	SW12	SW13	SW14	SW15	SW16	SW17	SW21	SW22	SW23
a(mm)	750	750	750	750	750	750	750	1300	1300	1300
h(mm)	750	750	750	750	750	750	750	650	650	650
a/h	1	1	1	1	1	1	1	2	2	2
a_t (mm)	150	150	150	150	150	150	150	150	150	150
t_f (mm)	140	140	140	140	140	140	140	140	140	140
b (mm)	70	70	70	70	70	70	70	65	65	65
t (mm)	70	70	70	70	70	70	70	65	65	65
h_0 (mm)	470	470	470	470	470	470	470	370	370	370
φ_l	0.006	0.006	0.006	0.006	0.006	0.006	0.006	0.007	0.007	0.007
φ_x	0.024	0.024	0.024	0.024	0.024	0.024	0.024	0.025	0.025	0.025
φ_y	0.011	0.011	0.011	0.011	0.011	0.011	0.004	0.008	0.008	0.008
f_{yl} (MPa)	517	517	517	517	517	517	517	517	517	517
f_{yx} (MPa)	517	517	517	517	517	517	517	517	517	517
f_{yy} (MPa)	565	565	565	565	565	520	565	565	565	565
f_c (MPa)	52.3	53.6	40.6	42.1	43.3	52	48	43	51	48
N(KN)	0	230	355	0	185	460	0	0	182	343
P(KN)	260	340	330	265	320	355	247	127	150	180
ν	0.539	0.591	0.718	0.590	0.643	0.664	0.559	0.586	0.609	0.684
Φ_l	0.106	0.094	0.103	0.121	0.108	0.087	0.111	0.147	0.119	0.112
Φ_x	0.441	0.392	0.426	0.500	0.446	0.362	0.460	0.516	0.420	0.396
ψ	0.221	0.196	0.213	0.250	0.223	0.167	0.077	0.180	0.147	0.138
$\tau_{test}/\nu f_c$	0.176	0.204	0.216	0.208	0.219	0.197	0.174	0.120	0.115	0.130
$\tau_{theory}/\nu f_c$	0.177	0.190	0.210	0.196	0.203	0.196	0.183	0.107	0.105	0.108
$\tau_{theory}/\tau_{test}$	1.006	0.931	0.973	0.964	0.929	0.994	1.050	0.893	0.913	0.828
T_1 (KN)	157	157	157	157	157	157	157	155	155	155
C_1 (KN)	342	479	550	342	452	593	200	383	528	650
Failure mode	B	B	B	B	B	B	B	B	B	B

Table D (continued)

Specimen No.	SW24	SW25	SW26	SW30	SW31	SW32	SW33	SW31R	SW32R	SW33R
a(mm)	1300	1300	1300	1300	1300	1300	1300	1300	1300	1300
h(mm)	650	650	650	650	650	650	650	650	650	650
a/h	2	2	2	2	2	2	2	2	2	2
a_c (mm)	150	150	150	150	150	150	150	150	150	150
t_f (mm)	140	140	140	140	140	140	140	140	140	140
b (mm)	65	65	65	65	65	65	65	65	65	65
t (mm)	65	65	65	65	65	65	65	65	65	65
h_b (mm)	370	370	370	370	370	370	370	370	370	370
φ_l	0.007	0.007	0.007	0.007	0.007	0.007	0.007	0.007	0.007	0.007
φ_x	0.025	0.025	0.025	0.015	0.015	0.015	0.015	0.015	0.015	0.015
φ_y	0.008	0.008	0.004	0.004	0.004	0.004	0.004	0.004	0.004	0.004
f_{yl} (MPa)	517	517	517	517	517	517	517	517	517	517
f_{yx} (MPa)	517	517	517	517	517	517	517	517	517	517
f_{yy} (MPa)	565	565	565	565	565	565	565	565	565	565
f_c (MPa)	48	45	30	30	35	54	49	35	38	38
N(KN)	0	325	0	0	0	0	0	0	0	0
P(KN)	120	150	123	118	116	111	112	140	83	94
ν	0.559	0.699	0.650	0.650	0.624	0.532	0.554	0.626	0.609	0.610
Φ_l	0.136	0.117	0.188	0.188	0.167	0.129	0.135	0.168	0.158	0.158
Φ_x	0.480	0.411	0.662	0.397	0.353	0.272	0.285	0.356	0.334	0.334
ψ	0.168	0.144	0.116	0.101	0.090	0.069	0.073	0.091	0.085	0.085
$\tau_{test}/\nu f_c$	0.105	0.113	0.149	0.142	0.125	0.092	0.097	0.151	0.084	0.096
$\tau_{theory}/\nu f_c$	0.101	0.110	0.132	0.113	0.102	0.080	0.083	0.102	0.096	0.097
$\tau_{theory}/\tau_{test}$	0.958	0.973	0.883	0.791	0.813	0.868	0.861	0.674	1.144	1.008
T_i (KN)	155	155	155	155	155	155	155	155	155	155
C_i (KN)	381	636	307	241	242	243	242	242	242	242
Failure mode	B	B	B	B	B	B	B	B	B	B

APPENDIX E Test Data and Calculation Results of Shear Wall Tests by Oesterle [84.3]

Table E

Specimen No.	R-1	R-2	R-3	R-4	F1	F2	F3	B1	B2
a(mm)	4570	4570	4570	4570	4570	4570	4570	4570	4570
h(mm)	1910	1910	1910	1910	1910	1910	1910	1910	1910
a / h	2.393	2.393	2.393	2.393	2.393	2.393	2.393	2.393	2.393
a_t (mm)	203	203	203	203	203	203	203	203	203
t_f (mm)	305	305	305	305	102	102	102	305	305
b (mm)	102	102	102	102	910	910	910	305	305
t (mm)	102	102	102	102	102	102	102	102	102
h_0 (mm)	1300	1300	1300	1300	1706	1706	1706	1528	1528
φ_l	0.002	0.006	0.010	0.006	0.019	0.021	0.011	0.005	0.018
φ_x	0.003	0.003	0.002	0.003	0.003	0.003	0.003	0.003	0.003
φ_y	0.003	0.003	0.004	0.003	0.007	0.006	0.003	0.003	0.006
f_{Yl} (MPa)	639	579	690	597	576	576	630	579	553
f_{Yx} (MPa)	611	610	473	507	615	536	618	608	620
f_{Yy} (MPa)	611	610	473	507	615	536	618	608	620
f_c (MPa)	44.7	46.4	24.4	22.7	38.4	46	28	53	54
N (KN)	0	0	296	296	0	1190	546	0	0
P (KN)	118	217	568	282	836	887	421	271	680
ν	0.576	0.568	0.723	0.735	0.608	0.625	0.700	0.535	0.532
Φ_l	0.058	0.140	0.375	0.200	0.457	0.420	0.351	0.098	0.340
Φ_x	0.059	0.058	0.059	0.085	0.079	0.058	0.079	0.062	0.063
ψ	0.073	0.072	0.113	0.094	0.187	0.119	0.098	0.066	0.137
$\tau_{test} / \sqrt{f_c}$	0.024	0.042	0.165	0.087	0.184	0.160	0.111	0.049	0.122
$\tau_{theory} / \sqrt{f_c}$	0.028	0.056	0.148	0.095	0.182	0.198	0.167	0.047	0.130
$\tau_{theory} / \tau_{test}$	1.209	1.340	0.893	1.093	0.993	1.240	1.512	0.947	1.065
T_l (KN)	292	721	1288	650	2080	2327	1338	539	1887
C_l (KN)	208	919	1717	1132	2396	3795	2146	742	2162
Failure mode	B	S	S	B	S	S	S	S	B
θ (rad)		0.387	0.639		0.784	0.527	0.519	0.381	
θ_1 (rad)		1.508	1.400		1.361	1.315	1.364	1.520	
y'_0 / h_e		0	0		0	0	0	0.015	
σ_c^l / f_c		0.166	0.317		0.375	0.468	0.398	0.125	
σ_{sl} / f_{Yl}		1	1		1	1	1	1	
σ_{sx} / f_{Yx}		1	1		1	1	1	1	
σ_{sy} / f_{Yy}		0	1		1	1	1	0.261	
x / a*		0.480	0.468		0.469	0.438	0.450	0.485	
a*/ a		1.000	0.548		0.408	0.699	0.712	1.000	

Table E (continued)

Specimen No.	B3	B4	B5	B6	B7	B8	B9	B10	B11	B12
a(mm)	4570	4570	4570	4570	4570	4570	4570	4570	4570	4570
h(mm)	1910	1910	1910	1910	1910	1910	1910	1910	1910	1910
a / h	2.393	2.393	2.393	2.393	2.393	2.393	2.393	2.393	2.393	2.393
a_t (mm)	203	203	203	203	203	203	203	203	203	203
t_f (mm)	305	305	305	305	305	305	305	305	305	305
b (mm)	305	305	305	305	305	305	305	305	305	305
t (mm)	102	102	102	102	102	102	102	102	102	102
h_0 (mm)	1528	1528	1528	1528	1528	1528	1528	1528	1528	1528
φ_l	0.005	0.005	0.018	0.018	0.018	0.018	0.018	0.009	0.013	0.018
φ_x	0.003	0.003	0.003	0.003	0.003	0.003	0.003	0.003	0.003	0.003
φ_y	0.003	0.003	0.006	0.006	0.006	0.014	0.006	0.006	0.006	0.006
f_{Yl} (MPa)	567	579	589	587	604	597	582	597	575	574
f_{Yx} (MPa)	568	593	587	594	593	534	537	553	512	503
f_{Yy} (MPa)	568	593	587	594	593	605	537	553	512	503
f_c (MPa)	47	45	45	22	49	42	44	46	54	42
N (KN)	0	0	0	934	1197	1197	1197	1197	0	0
P (KN)	276	334.4896	762	825	980	978	977	707	726	792
ν	0.564	0.575	0.573	0.788	0.609	0.655	0.641	0.632	0.531	0.592
Φ_l	0.113	0.118	0.397	0.598	0.352	0.381	0.361	0.195	0.257	0.408
Φ_x	0.062	0.066	0.066	0.100	0.057	0.056	0.055	0.056	0.052	0.059
ψ	0.066	0.071	0.142	0.218	0.124	0.304	0.120	0.121	0.113	0.128
$\tau_{test} / \sqrt{f_c}$	0.053	0.066	0.151	0.246	0.168	0.183	0.177	0.126	0.131	0.165
$\tau_{theory} / \sqrt{f_c}$	0.052	0.055	0.150	0.268	0.169	0.181	0.173	0.116	0.100	0.153
$\tau_{theory} / \tau_{test}$	0.978	0.823	0.998	1.089	1.005	0.992	0.976	0.917	0.768	0.928
T_l (KN)	585	597	2010	2004	2062	2038	1987	1094	1428	1960
C_l (KN)	839	862	2270	3198	3519	3473	3419	2538	1656	2182
Failure mode	S	B	B	S	B	B	B	B	B	B
θ (rad)	0.391			0.669						
θ_1 (rad)	1.514			1.223						
y'_0 / h_o	0			0						
σ_c^l / f_c	0.152			0.566						
σ_{sl} / f_{Yl}	1			1						
σ_{sx} / f_{Yx}	1			1						
σ_{sy} / f_{Yy}	0.332			1						
x / a*	0.482			0.431						
a* / a	0.988			0.515						

APPENDIX F Test Data and Calculation Results of Shear Wall Tests by Toshimi [93.3]

Table F

Specimen No.	NW1	NW3	NW4	NW5	NW6	No.5	NW2	No.1	No.2	No.3	No.4
a(mm)	3000	3000	3000	3000	3000	3000	2000	2000	2000	2000	2000
h(mm)	1700	1700	1700	1700	1700	1700	1700	1700	1700	1700	1700
a/h	1.765	1.765	1.765	1.765	1.765	1.765	1.176	1.176	1.176	1.176	1.176
a_t (mm)	600	600	600	600	600	600	600	600	600	600	600
t_f (mm)	200	200	200	200	200	200	200	200	200	200	200
b (mm)	200	200	200	200	200	200	200	200	200	200	200
t (mm)	80	80	80	80	80	80	80	80	80	80	80
h_0 (mm)	1300	1300	1300	1300	1300	1300	1300	1300	1300	1300	1300
φ	0.007	0.007	0.009	0.009	0.012	0.016	0.007	0.016	0.016	0.016	0.016
φ_x	0.005	0.002	0.002	0.005	0.005	0.005	0.005	0.002	0.003	0.005	0.005
φ_y	0.005	0.002	0.002	0.005	0.005	0.005	0.005	0.002	0.003	0.005	0.005
f_{yl} (MPa)	776	840	840	840	726	1009	776	1009	1009	1009	1009
f_{yx} (MPa)	1001	753	753	753	753	792	1001	792	792	792	792
f_{yy} (MPa)	1001	753	753	753	753	792	1001	792	792	792	792
f_c (MPa)	87.6	55.5	54.6	60.3	65.2	77	94	65	71	72	103
N(KN)	1764	1372	1568	1372	1568	1568	1764	1568	1568	1568	2617
P(KN)	1062	714	784	900	1056	1158	1468	1100	1254	1378	1696
ν	0.495	0.620	0.640	0.588	0.569	0.515	0.480	0.569	0.534	0.530	0.492
Φ_l	0.124	0.169	0.222	0.219	0.229	0.399	0.120	0.425	0.417	0.414	0.310
Φ_x	0.109	0.052	0.051	0.100	0.096	0.094	0.105	0.038	0.064	0.098	0.073
ψ	0.109	0.052	0.051	0.100	0.096	0.094	0.105	0.038	0.064	0.098	0.073
$\tau_{test}/\nu f_c$	0.180	0.153	0.165	0.187	0.209	0.216	0.240	0.218	0.244	0.266	0.245
$\tau_{theory}/\nu f_c$	0.140	0.141	0.164	0.172	0.179	0.227	0.183	0.219	0.250	0.279	0.251
$\tau_{theory}/\tau_{test}$	0.778	0.927	0.993	0.920	0.854	1.052	0.760	1.003	1.024	1.048	1.023
T_l(KN)	731	792	1056	1056	1156	2143	731	1727	2143	2143	2143
C_l(KN)	2978	1846	1991	2785	2988	3384	2475	987	1552	2235	2630
Failure mode	S	S	S	S	S	S	S	S	S	S	S
θ (rad)	0.646	0.445	0.410	0.515	0.492	0.432	0.623	0.345	0	0.429	0.426
θ_1 (rad)	1.409	1.386	1.334	1.356	1.340	1.212	1.342	1.078	0.968	1.000	1.092
y_0/h_e	0	0.134	0.209	0.000	0.025	0.163	0.129	0.565	0.549	0.446	0.4500
σ_c^l/f_c	0.301	0.279	0.319	0.413	0.428	0.540	0.308	0.330	0.529	0.567	0.429
σ_l/f_{yl}	1	1	1	1	1	1	1	1	1	1	1
σ_{sx}/f_{yx}	1	1	1	1	1	1	1	1	1	1	1
σ_{sy}/f_{yy}	1	1	1	1	1	1	1	1	1	1	1
x/a*	0.470	0.466	0.459	0.448	0.444	0.418	0.469	0.456	0.419	0.415	0.442
a*/a	1	1	1	1	1	1	1	1	1	1	1

Table F (continued)

Specimen No.	No.6	No.7	No.8	W08	W12	W35X	W35H	W30H	P35H	NW35H
a(mm)	2000	2000	2000	1000	1000	2000	2000	2000	2000	2000
h(mm)	1700	1700	1700	1700	1700	1700	1700	1700	1700	1700
a/h	1.176	1.176	1.176	0.588	0.588	1.176	1.176	1.176	1	1
a_t (mm)	600	600	600	600	600	2000	2000	2000	2000	2000
t_f (mm)	200	200	200	200	200	200	200	200	200	200
b (mm)	200	200	200	200	200	200	200	200	200	200
t (mm)	80	80	80	80	80	80	80	80	80	80
h_0 (mm)	1300	1300	1300	1300	1300	1300	1300	1300	1300	1300
φ_l	0.016	0.016	0.016	0.007	0.007	0.007	0.007	0.007	0.007	0.007
φ_x	0.006	0.009	0.013	0.005	0.005	0.007	0.007	0.007	0.007	0.007
φ_y	0.006	0.009	0.013	0.005	0.005	0.007	0.007	0.007	0.007	0.007
f_{yl} (MPa)	1009	1009	1009	761	761	848	848	848	848	848
f_{yx} (MPa)	1420	792	792	1079	1079	810	810	810	810	810
f_{yy} (MPa)	1420	792	792	1079	1079	810	810	810	810	810
f_c (MPa)	74	72	76	103	138	63	61	58	62	60
N(KN)	1568	1568	1568	1764	2313	1764	1921	1862	1470	1666
P(KN)	1411	1498	1639	1670	1719	1049	1054	958	1020	1011
ν	0.523	0.531	0.517	0.460	0.423	0.598	0.620	0.639	0.582	0.611
Φ_l	0.407	0.415	0.401	0.111	0.091	0.157	0.156	0.159	0.162	0.161
Φ_x	0.212	0.184	0.259	0.107	0.088	0.153	0.152	0.155	0.158	0.157
ψ	0.212	0.184	0.259	0.107	0.088	0.153	0.152	0.155	0.158	0.157
$\tau_{test}/\nu f_c$	0.268	0.290	0.306	0.258	0.218	0.206	0.205	0.191	0.207	0.204
$\tau_{theory}/\nu f_c$	0.333	0.325	0.347	0.265	0.252	0.185	0.187	0.189	0.179	0.185
$\tau_{theory}/\tau_{test}$	1.245	1.122	1.132	1.026	1.156	0.897	0.912	0.987	0.866	0.911
T_l (KN)	2143	2143	2143	717	717	799	799	799	799	799
C_l (KN)	3892	3513	4447	1648	1924	3111	3227	3185	2857	3041
Failure mode	S	S	S	S	S	B	B	B	S	B
θ (rad)	0.591	0.554	0.644	0.766	0.770				0.708	
θ_l (rad)	1.037	1.021	1.046	1.216	1.238				1.361	
y_0/h_e	0.186	0.250	0.091	0.417	0.413				0	
σ_c^l/f_c	0.683	0.666	0.719	0.223	0.181				0.374	
σ_{sl}/f_{yl}	1	1	1	1	1				1	
σ_{sx}/f_{yx}	1	1	1	1	1				1	
σ_{sy}/f_{yy}	1	1	1	1	1				1	
x/a*	0.400	0.401	0.396	0.485	0.488				0.464	
a*/a	1	1	1	1	1				0.964	

APPENDIX G Test Data and Calculation Results of Shear Wall Tests by Hirosawa [75.1]

Table G

Specimen No.	3-w7103	5-w7105	6-0wl-1	9-40wl-1	12-20wl-2	70-WA1	71-WA2	72-A103a	73-A103B	75-A106B	77-A112B
a(mm)	750	750	625	625	625	1200	1200	1600	1600	1600	1600
h(mm)	2250	2250	600	600	600	2300	2300	1700	1700	1700	1700
a/h	0.333	0.333	1.042	1.042	1.042	0.522	0.522	0.941	0.941	0.941	0.941
a_t (mm)	2250	250	150	150	150	500	500	200	200	200	200
t_f (mm)	250	250	100	100	100	250	250	170	170	170	170
b (mm)	250	250	100	100	100	250	250	160	160	160	160
t (mm)	80	50	30	30	30	74	83	160	160	160	160
h_0 (mm)	1750	1750	400	400	400	1800	1800	1360	1360	1360	1360
φ_l	0.003	0.005	0.014	0.014	0.014	0.009	0.008	0.006	0.006	0.006	0.005
φ_x	0.002	0.008	0.002	0.002	0.002	0.002	0.001	0.005	0.005	0.005	0.005
φ_y	0.001	0.008	0.002	0.002	0.002	0.002	0.001	0.003	0.003	0.006	0.005
f_{Yl} (MPa)	359	359	209	209	209	418	418	376	376	376	376
f_{Yx} (MPa)	623	623	293	293	293	549	461	419	407	407	407
f_{Yy} (MPa)	623	623	293	293	293	549	461	407	419	419	415
f_c (MPa)	26.0	26.0	23.5	25.7	29.9	24	25	17	21	14	18
N(KN)	368	368	0	125	63	0	0	549	533	533	533.12
P(KN)	524	783	49	86	59	833	804	809	725	813	911.4
ν	0.709	0.718	0.682	0.782	0.698	0.679	0.674	0.799	0.765	0.835	0.786
Φ_l	0.055	0.087	0.181	0.145	0.140	0.238	0.205	0.155	0.135	0.187	0.149
Φ_x	0.054	0.264	0.042	0.034	0.032	0.060	0.019	0.152	0.128	0.178	0.141
ψ	0.047	0.254	0.038	0.031	0.029	0.060	0.019	0.077	0.069	0.208	0.164
$\tau_{test}/\nu f_c$	0.158	0.373	0.170	0.239	0.157	0.299	0.248	0.216	0.168	0.261	0.233
$\tau_{theory}/\nu f_c$	0.133	0.380	0.129	0.186	0.147	0.273	0.228	0.217	0.192	0.263	0.218
$\tau_{theory}/\tau_{test}$	0.842	1.020	0.762	0.780	0.942	0.914	0.919	1.002	1.146	1.009	0.935
T_1 (KN)	182	182	52	52	52	665	641	582	582	582	582
C_1 (KN)	498	435	23	78	53	84	8	819	818	1319	1279
Failure mode	S	S	S	S	S	S	S	S	S	S	S
θ (rad)	1.115	0.852	0.609	0.477	0.563	0.758	0.804	0.615	0.642	0.726	0.731
θ_1 (rad)	1.426	1.046	1.402	1.261	1.364	1.199	1.280	1.272	1.319	1.230	1.302
y_0/h_e	0.304	0.610	0.207	0.412	0.282	0.495	0.446	0.316	0.275	0.139	0.131
σ_c^l/f_c	0.059	0.448	0.117	0.145	0.103	0.128	0.037	0.231	0.191	0.473	0.369
σ_{sl}/f_{Yl}	1	1	1	1	1	1	1	1	1	1	1
σ_{sx}/f_{Yx}	1	1	1	1	1	1	1	1	1	1	1
σ_{sy}/f_{Yy}	1	1	1	1	1	1	1	1	1	1	1
x/a*	0.4986	0.4774	0.4895	0.4847	0.4903	0.4919	0.4980	0.4782	0.4830	0.4535	0.4669
a*/a	1	1	1	1	1	1	1	1	1	1	1

Table G (continued)

Specimen No.	79-B106b	81-B112b	83-B206b	85-B212b	71-WA2	95-2	97-5	98-6	99-7	96-1
a(mm)	1600	1600	1600	1600	1200	300	450	450	450	300
h(mm)	1700	1700	850	850	2300	420	570	570	570	420
a/h	0.941	0.941	1.882	1.882	0.522	0.714	0.789	0.789	0.789	0.714
a_s (mm)	200	200	200	200	500	60	60	60	60	60
t_f (mm)	170	170	85	85	250	60	60	60	60	42
b (mm)	160	160	160	160	250	40	60	60	60	40
t (mm)	160	160	160	160	83	20	20	30	40	40
h_0 (mm)	1360	1360	680	680	1800	300	450	450	450	336
φ_l	0.003	0.003	0.010	0.008	0.008	0.020	0.015	0.010	0.007	0.010
φ_x	0.005	0.005	0.004	0.004	0.001	0	0	0	0	0
φ_y	0.006	0.006	0.006	0.011	0.001	0	0	0	0	0
f_{yl} (MPa)	382	382	380	377	418	316	368	368	368	316
f_{yx} (MPa)	407	407	407	407	461	435	341	341	341	435
f_{yy} (MPa)	420	415	421	415	461	487	341	341	341	487
f_c (MPa)	14	18	18	21	25	65	32	32	33	65
N(KN)	533	533	267	267	0	0	0	0	0	0
P(KN)	617	760	333	368	804	39	31	39	59	50
v	0.835	0.786	0.790	0.765	0.674	0.474	0.640	0.639	0.633	0.474
Φ_l	0.084	0.067	0.267	0.201	0.205	0.205	0.266	0.177	0.129	0.102
Φ_x	0.178	0.141	0.115	0.102	0.019	0	0	0	0	0
ψ	0.224	0.176	0.170	0.282	0.019	0	0	0	0	0
τ_{test}/vf_c	0.198	0.194	0.174	0.170	0.248	0.149	0.134	0.112	0.122	0.097
τ_{theory}/vf_c	0.188	0.156	0.166	0.132	0.228	0.180	0.198	0.154	0.121	0.104
$\tau_{theory}/\tau_{test}$	0.947	0.805	0.953	0.774	0.919	1.209	1.474	1.383	0.987	1.068
T_1(KN)	261	261	512	433	641	53	57	61	62	53
C_1(KN)	1234	1234	955	876	8	1	-5	-1	2	5
Failure mode	B	B	B	B	S	S	S	S	S	S
θ(rad)					0.804	0.729	0.639	0.717	0.765	0.837
θ_1 (rad)					1.280					
y_0/h_e					0.446	0.362	0.413	0.312	0.241	0.208
σ_c^l/f_c					0.037	0	0	0	0	0
σ_{sl}/f_{yl}					1	1	1	1	1	1
σ_{sx}/f_{yx}					1	0	0	0	0	0
σ_{sy}/f_{yy}					1	0	0	0	0	0
x/a*					0.4980	0	0	0	0	0
a*/a					1	1	1	1	1	1

APPENDIX H Test Data and Calculation Results of Shear Wall Tests by Yoshzaki [75.1]

Table H

Specimen No.	169-1-88-12	171-2/3-36-8	172-2/3-52-4	173-2/3-52-8	174-2/3-52-12	176-2/2-27-8	177-1/2-42-4	178-1/2-42-8	179-1/2-42-12
a(mm)	800	800	800	800	800	800	800	800	800
h(mm)	800	1200	1200	1200	1200	1600	1600	1600	1600
a/h	1.00	0.67	0.67	0.67	0.67	0.50	0.50	0.50	0.50
a_c (mm)	120	120	120	120	120	120	120	120	120
t_f (mm)	80	120	120	120	120	160	160	160	160
b(mm)	60	60	60	60	60	60	60	60	60
t(mm)	60	60	60	60	60	60	60	60	60
h_e (mm)	640	960	960	960	960	1280	1280	1280	1280
φ_f	0.009	0.004	0.006	0.006	0.006	0.008	0.004	0.004	0.005
φ_x	0.012	0.008	0.004	0.008	0.012	0.008	0.004	0.008	0.012
φ_y	0.012	0.008	0.004	0.008	0.012	0.008	0.004	0.008	0.012
f_{yf} (MPa)	345	343	343	345	345	343	345	345	351
f_{yx} (MPa)	434	434	434	434	434	434	434	434	434
f_{yy} (MPa)	434	434	434	434	434	434	434	434	434
f_c (MPa)	24	25	25	25	25	26	26	26	26
N(KN)	0	0	0	0	0	0	0	0	0
P(KN)	174	235	220	280	274	322	319	383	422
ν	0.682	0.677	0.677	0.677	0.677	0.672	0.672	0.672	0.672
Φ	0.191	0.081	0.114	0.123	0.123	0.059	0.089	0.089	0.097
Φ_x	0.316	0.208	0.115	0.208	0.305	0.202	0.091	0.202	0.296
ψ	0.316	0.214	0.107	0.214	0.305	0.207	0.104	0.207	0.296
$\tau_{test}/\nu f_c$	0.226	0.197	0.184	0.217	0.229	0.195	0.194	0.232	0.256
$\tau_{theory}/\nu f_c$	0.243	0.187	0.178	0.224	0.264	0.205	0.181	0.237	0.286
$\tau_{theory}/\tau_{test}$	1.075	0.952	0.969	1.030	1.150	1.049	0.937	1.019	1.117
T_i (KN)	147	97	136	147	147	97	147	147	159
C_i (KN)	340	249	131	259	380	251	113	253	379
Failure mode	S	S	S	S	S	S	S	S	S
θ (rad)	0.884	0.915	0.840	0.872	0.897	0.983	0.947	0.943	0.936
θ_1 (rad)	1.274	1.355	1.358	1.301	1.249	1.335	1.361	1.289	1.221
y_0/h_e	0	0.096	0.224	0.172	0.129	0.226	0.282	0.289	0.299
σ_c^I/f_c	0.529	0.341	0.193	0.365	0.500	0.300	0.157	0.317	0.456
σ_{sf}/f_{yf}	1	1	1	1	1	1	1	1	1
σ_{sx}/f_{yx}	1	1	1	1	1	1	1	1	1
σ_{sy}/f_{yy}	1	1	1	1	1	1	1	1	1
x/a^*	0.4590	0.4797	0.4881	0.4760	0.4652	0.4864	0.4980	0.4842	0.4749
a^*/a	0.7693	1	1	1	1	1	1	1	1

APPENDIX I Test Data and Calculation Results of Shear Wall Tests by Tanabe [75.1]

Table I

Specimen No.	101-9	102-10	112-42	113-44	104-12	105-13	106-14	114-4M
a(mm)	450	450	450	450	450	450	450	450
h(mm)	570	570	570	570	570	570	570	570
a / h	0.79	0.79	0.79	0.79	0.79	0.79	0.79	0.79
a_t (mm)	60	60	60	60	60	60	60	60
t_f (mm)	60	60	60	60	60	60	60	60
b (mm)	60	60	60	60	60	60	60	60
t (mm)	20	20	20	20	30	30	30	30
h_0 (mm)	450	450	450	450	450	450	450	450
φ_l	0.015	0.015	0.015	0.015	0.010	0.010	0.010	0.010
φ_x	0.018	0.018	0.018	0.018	0.012	0.012	0.012	0.012
φ_y	0.018	0.018	0.018	0.018	0.012	0.012	0.012	0.012
f_{Yl} (MPa)	368	368	293	293	368	368	368	293
f_{Yx} (MPa)	284	284	294	294	284	284	284	294
f_{Yy} (MPa)	284	284	294	294	284	284	294	294
f_c (MPa)	34	30	43	49	36	34	34	40
N (KN)	0	0	0	0	0	0	0	0
P (KN)	63	75	68	71	94	90	86	71
ν	0.628	0.649	0.585	0.556	0.622	0.628	0.631	0.600
Φ_l	0.253	0.279	0.173	0.160	0.164	0.169	0.170	0.121
Φ_x	0.241	0.266	0.214	0.199	0.157	0.161	0.162	0.150
ψ	0.241	0.266	0.214	0.199	0.157	0.161	0.168	0.150
$\tau_{test} / \nu f_c$	0.255	0.335	0.239	0.229	0.249	0.244	0.236	0.172
$\tau_{theory} / \nu f_c$	0.291	0.314	0.234	0.220	0.207	0.211	0.213	0.173
$\tau_{theory} / \tau_{test}$	1.142	0.936	0.979	0.960	0.829	0.867	0.903	1.002
T_1 (KN)	62	62	50	50	62	62	62	50
C_1 (KN)	79	81	78	77	75	75	77	75
Failure mode	S	S	S	S	S	S	S	S
θ (rad)	0.732	0.728	0.781	0.784	0.757	0.755	0.760	0.794
θ_1 (rad)	1.146	1.100	1.261	1.283	1.298	1.291	1.289	1.354
y'_0 / h_e	0	0.229	0.142	0.138	0.182	0.185	0.177	0.119
σ_c^I / f_c	0.540	0.600	0.432	0.399	0.332	0.342	0.354	0.294
σ_{sl} / f_{Yl}	1	1	1	1	1	1	1	1
σ_{sx} / f_{Yx}	1	1	1	1	1	1	1	1
σ_{sy} / f_{Yy}	1	1	1	1	1	1	1	1
x / a*	0.4461	0.4365	0.4630	0.4669	0.4727	0.4716	0.4706	0.4778
a*/ a	1	1	1	1	1	1	1	1

Table I(continued)

Specimen No.	115-49	107-15	108-16	109-17	116-52	117-54	110-36	111-39
a(mm)	450	450	450	450	450	450	450	450
h(mm)	570	570	570	570	570	570	570	570
a / h	0.79	0.79	0.79	0.79	0.79	0.79	0.79	0.79
a_t (mm)	60	60	60	60	60	60	60	60
t_f (mm)	60	60	60	60	60	60	60	60
b (mm)	60	60	60	60	60	60	60	60
t (mm)	30	40	40	40	40	40	10	10
h_0 (mm)	450	450	450	450	450	450	450	450
φ_l	0.010	0.007	0.007	0.007	0.007	0.007	0.030	0.030
φ_x	0.012	0.009	0.009	0.009	0.009	0.009	0.018	0.018
φ_y	0.012	0.009	0.009	0.009	0.009	0.009	0.018	0.018
f_{Yl} (MPa)	293	368	368	368	293	293	293	293
f_{Yx} (MPa)	294	284	284	284	294	294	294	294
f_{Yy} (MPa)	294	284	284	284	294	294	294	294
f_c (MPa)	46	33	35	36	45	43	46	43
N (KN)	0	0	0	0	0	0	0	0
P (KN)	77	98	97	102	78	77	43	44
ν	0.569	0.636	0.623	0.621	0.573	0.587	0.571	0.583
Φ_l	0.110	0.130	0.124	0.123	0.084	0.087	0.333	0.344
Φ_x	0.137	0.125	0.119	0.118	0.104	0.108	0.206	0.213
Ψ	0.137	0.125	0.119	0.118	0.104	0.108	0.206	0.213
$\tau_{test} / \nu f_c$	0.170	0.205	0.193	0.201	0.132	0.136	0.287	0.305
$\tau_{theory} / \nu f_c$	0.160	0.170	0.163	0.162	0.125	0.129	0.315	0.322
$\tau_{theory} / \tau_{test}$	0.937	0.830	0.843	0.804	0.945	0.953	1.101	1.056
T_1 (KN)	50	62	62	62	50	50	50	50
C_1 (KN)	74	73	73	73	74	74	41	42
Failure mode	S	S	S	S	S	S	S	S
θ (rad)	0.798	0.772	0.775	0.776	0.809	0.807	0.645	0.642
θ_1 (rad)	1.373	1.355	1.366	1.368	1.421	1.415	1.047	1.028
y'_0 / h_e	0.113	0.157	0.152	0.151	0.094	0.096	0.348	0.353
σ_c^l / f_c	0.267	0.257	0.242	0.240	0.199	0.208	0.570	0.593
σ_{sl} / f_{Yl}	1	1	1	1	1	1	1	1
σ_{sx} / f_{Yx}	1	1	1	1	1	1	1	1
σ_{sy} / f_{Yy}	1	1	1	1	1	1	1	1
x / a*	0.4804	0.4805	0.4819	0.4821	0.4863	0.4856	0.4352	0.4309
a*/ a	1	1	1	1	1	1	1	1

APPENDIX J Test Data and Calculation Results of Shear Walls Tests by NUPEC[94.3], Cardenas [80.2], and Kebeyasawa [84.5][85.4]

Table J

		Cardenas				Kebeyasawa		
Specimen No.	NUPEC	SW-7	SW-8	SW-9	SW-13	K1	K2	K4
a(mm)	2020	2000	2000	2000	2000	1500	1500	1500
h(mm)	3100	1905	1905	1905	1905	2000	2000	2000
a/h	0.65	1.05	1.05	1.05	1.05	0.75	0.75	0.75
a_c (mm)	760	115	115	115	115	331	331	331
t_f (mm)	100	191	76	76	76	200	200	200
b (mm)	2980	76	76	76	76	200	200	200
t (mm)	75	76	76	76	76	80	80	80
h_0 (mm)	2900	1524	1753	1753	1753	1600	1600	1600
φ_l	0.006	0.008	0	0	0	0.002	0.004	0.004
φ_x	0.011	0.009	0.029	0.029	0.029	0.003	0.005	0.008
φ_y	0.012	0.003	0.003	0.010	0.010	0.003	0.005	0.008
f_{Yl} (MPa)	443	448	448	448	448	392	392	392
f_{Yx} (MPa)	443	448	448	448	448	395	395	395
f_{Yy} (MPa)	443	414	465	414	455	395	395	395
f_c (MPa)	29	43	42	43	43	20	19	21
N(KN)	1196	12	12	12	13	396	400	399
P(KN)	1627	519	570	679	632	439	471	508
ν	0.690	0.586	0.589	0.586	0.584	0.772	0.778	0.764
Φ_l	0.132	0.147	0.021	0.021	0.020	0.046	0.095	0.089
Φ_x	0.247	0.153	0.518	0.513	0.510	0.070	0.141	0.201
ψ	0.264	0.044	0.050	0.164	0.179	0.070	0.141	0.201
$\tau_{test}/\sqrt{f_c}$	0.347	0.142	0.157	0.185	0.172	0.181	0.199	0.201
$\tau_{theory}/\sqrt{f_c}$	0.341	0.158	0.185	0.184	0.183	0.153	0.220	0.235
$\tau_{theory}/\tau_{test}$	0.983	1.113	1.180	0.991	1.067	0.847	1.108	1.165
T_l (KN)	617	538	75	75	75	111	224	224
C_l (KN)	2086	416	1020	1664	1734	407	618	827
Failure mode	S	S	B	B	B	S	S	S
θ (rad)	0.732	0.728				0.755	0.760	0.794
θ_l (rad)	1.146	1.100				1.291	1.289	1.354
y_0/h_e	0	0.229				0.185	0.177	0.119
σ_c^{l}/f_c	0.540	0.600				0.342	0.354	0.294
σ_{sl}/f_{Yl}	1	1				1	1	1
σ_{sx}/f_{Yx}	1	1				1	1	1
σ_{sy}/f_{Yy}	1	1				1	1	1
x/a^*	0.4461	0.4365				0.4716	0.4706	0.4778
a^*/a	1	1				1	1	1

APPENDIX K Test Data and Calculation Results of Shear Wall Tests by Wiradinata [86.6], Aoyagi[90.5] and Pauley [80.1]

Table K

Specimen No.	Wiradinata	Wiradinata	Aoyagi	Aoyagi	Paulay	Paulay
a(mm)	1100	620	1400	1400	1500	1500
h(mm)	2000	2000	2720	2720	3000	3000
a / h	0.55	0.31	0.51	0.51	0.50	0.50
a_t (mm)	80	80	246	246	400	400
t_f (mm)	60	60	320	320	200	100
b (mm)	100	100	320	320	100	500
t (mm)	100	100	160	160	100	100
h_0 (mm)	1880	1880	2080	2080	2600	2800
φ_l	0	0	0.004	0.015	0.001	0.003
φ_x	0.008	0.008	0.006	0.006	0.008	0.004
φ_y	0.003	0.003	0.006	0.006	0.016	0.016
f_{Yl} (MPa)	434	434	363	272	308	308
f_{Yx} (MPa)	434	434	339	339	308	308
f_{Yy} (MPa)	425	425	339	339	380	380
f_c (MPa)	25	22	29	29	27	26
N (KN)	15	9	0	0	0	0
P (KN)	574	681	1555	2309	810	786
ν	0.678	0.691	0.653	0.654	0.664	0.670
Φ_l	0.006	0.007	0.077	0.217	0.024	0.051
Φ_x	0.206	0.228	0.102	0.103	0.138	0.069
ψ	0.063	0.070	0.109	0.110	0.339	0.351
$\tau_{test} / \sqrt{f_c}$	0.170	0.223	0.186	0.278	0.149	0.150
$\tau_{theory} / \sqrt{f_c}$	0.154	0.222	0.167	0.292	0.131	0.129
$\tau_{theory} / \tau_{test}$	0.904	0.993	0.897	1.052	0.874	0.857
T_1 (KN)	21	21	646	1807	130	266
C_1 (KN)	384	261	663	486	777	603
Failure mode	S	S	S	S	S	S
θ (rad)	0.798	0.772	0.775	0.776	0.809	0.807
θ_1 (rad)	1.373	1.355	1.366	1.368	1.421	1.415
y'_0 / h_e	0.113	0.157	0.152	0.151	0.094	0.096
σ_c^l / f_c	0.267	0.257	0.242	0.240	0.199	0.208
σ_{sl} / f_{Yl}	1	1	1	1	1	1
σ_{sx} / f_{Yx}	1	1	1	1	1	1
σ_{sy} / f_{Yy}	1	1	1	1	1	1
x / a*	0.4804	0.4805	0.4819	0.4821	0.4863	0.4856
a*/ a	1	1	1	1	1	1

APPENDIX L Test Data and Calculation Results of Shear Wall Tests by KoKusho [75.1]

Table L

Specimen No.	S1	S2	S3	S4	S6	S7	S8	S9	S10	S11
a(mm)	200	200	300	300	300	300	300	300	300	300
h(mm)	430	430	430	430	430	430	430	430	430	430
a/h	047	047	070	070	070	070	070	070	070	070
a (mm)	30	30	130	130	130	130	130	130	130	130
t_f (mm)	30	30	30	30	30	30	30	30	30	30
b(mm)	145	145	145	145	145	145	145	145	145	145
t (mm)	23	24	27	24	16	22	22	24	23	23
h_0 (mm)	370	370	370	370	370	370	370	370	370	370
φ_l	0003	0003	0006	0006	0010	0007	0007	0006	0007	0007
φ_x	0007	0007	0004	0005	0007	0007	0007	0005	0005	0005
φ_y	0007	0007	0004	0004	0007	0007	0007	0005	0005	0005
f_{yl} (MPa)	402	402	407	407	407	407	407	407	407	407
f_{yx} (MPa)	323	323	402	323	323	323	323	323	323	323
f_{yy} (MPa)	323	323	402	323	323	323	323	323	323	323
f'_c (MPa)	20	19	14	14	14	18	17	24	16	16
N(KN)	0	0	0531	0	0	0	0564	0	0541	0541
P(KN)	2936	2758	2446	2357	1957	2491	2580	2669	2669	2580
ν	0700	0707	0731	0730	0732	0711	0718	0681	0723	0723
Φ_l	0090	0091	0224	0252	0388	0223	0237	0160	0240	0240
Φ_x	0162	0165	0155	0140	0221	0165	0196	0089	0137	0137
ψ	0169	0172	0147	0134	0211	0183	0194	0089	0134	0134
$\tau_{test}/\sqrt{f'_c}$	0213	0203	0203	0220	0282	0207	0227	0159	0237	0230
$\tau_{theory}/\sqrt{f'_c}$	0224	0227	0246	0255	0338	0258	0270	0181	0248	0248
$\tau_{theory}/\tau_{test}$	1053	1116	1212	1159	1200	1249	1191	1141	1045	1081
T_l(KN)	1242	1242	2694	2694	2694	2694	2694	2694	2694	2694
C_l(KN)	1549	1552	2284	1812	2030	2821	2860	1840	1889	1889
Failure mode	S	S	S	S	S	S	S	S	S	S
θ(rad)	0899	0897	0704	0669	0597	0727	0719	0747	0683	0683
θ_l(rad)	1271	1267	1199	1167	0902	1186	1159	1322	1187	1187
y_0/h_e	0	0340	0329	0376	0464	0298	0309	0270	0358	0358
σ_c^l/f'_c	0276	0281	0351	0348	0670	0413	0446	0194	0336	0336
σ_{sl}/f_{yl}	1	1	1	1	1	1	1	1	1	1
σ_{sx}/f_{yx}	1	1	1	1	1	1	1	1	1	1
σ_{sy}/f_{yy}	1	1	1	1	1	1	1	1	1	1
x/a^*	04653	04849	04692	04681	04149	04633	04580	04856	04700	04700
a^*/a	1	1	1	1	1	1	1	1	1	1

APPENDIX M Test Data and Calculation Results of Shear Wall Tests by Benjamin [53.1] [55.1] [56.1] [56.2] [57.1]

Table M

Specimen No.	4BII-1	4BII-2	4BII-3	4BII-4	1BII-1	3AII-1	3AII-2	NV-1	NV-11	NV-18
a(mm)	600	560	540	520	920	600	550	800	1100	600
h(mm)	610	914	1219	1778	1727	914	914	1651	1143	1956
a/h	0.98	0.61	0.44	0.29	0.53	0.66	0.60	0.48	0.96	0.31
a_t (mm)	140	142	140	134	137	62	162	51	86	91
t_f (mm)	102	102	102	102	127	102	102	127	127	127
b (mm)	127	127	127	127	191	127	127	127	127	127
t (mm)	51	51	51	51	51	44	44	51	51	51
h_0 (mm)	406	711	1016	1575	1473	711	711	1397	889	1702
φ_l	0.009	0.006	0.005	0.003	0.006	0.011	0.011	0.003	0.014	0.003
φ_x	0.005	0.005	0.005	0.005	0.003	0.005	0.003	0.005	0.005	0.005
φ_y	0.005	0.005	0.005	0.005	0.003	0.005	0.003	0.005	0.005	0.005
f_{yl} (MPa)	312	312	312	312	312	312	312	312	312	312
f_{yx} (MPa)	341	341	341	341	341	341	341	341	341	341
f_{yy} (MPa)	341	341	341	341	341	341	341	341	341	341
f_c (MPa)	20.00	21.37	19.31	26.41	20.00	24.82	19.31	26.89	24.82	20.69
N(KN)	0	0	0	0	0	0	0	0	0	0
P(KN)	88.96	155	201	294	249	205	138	301	222	374
ν	0.700	0.693	0.703	0.668	0.700	0.676	0.703	0.666	0.676	0.697
Φ_l	0.205	0.129	0.106	0.056	0.129	0.196	0.242	0.059	0.257	0.062
Φ_x	0.122	0.115	0.126	0.097	0.061	0.102	0.063	0.095	0.102	0.118
ψ	0.122	0.115	0.126	0.097	0.061	0.102	0.063	0.095	0.102	0.118
$\tau_{test}/\sqrt{f_c}$	0.205	0.225	0.240	0.184	0.203	0.300	0.250	0.201	0.228	0.261
$\tau_{theory}/\sqrt{f_c}$	0.174	0.194	0.229	0.210	0.202	0.238	0.253	0.160	0.220	0.232
$\tau_{theory}/\tau_{test}$	0.848	0.864	0.954	1.137	0.994	0.793	1.014	0.795	0.963	0.889
T_1 (KN)	89.07	89.07	89.07	89.07	158	133	133	88.67	250	88.67
C_1 (KN)	95.04	75.24	68.92	68.61	45.19	59.34	19.36	95.35	162	71.98
Failure mode	S	S	S	S	S	S	S	S	S	S
θ (rad)	0.687	0.849	0.933	1.074	0.867	0.742	0.702	0.981	0.629	1.042
θ_1 (rad)	1.346	1.331	1.293	1.332	1.327	1.248	1.205	1.390	1.268	1.303
y_0'/h_e	0	0.264	0.377	0.445	0.353	0.363	0.462	0.253	0.268	0.461
σ_c'/f_c	0.303	0.204	0.195	0.125	0.105	0.223	0.151	0.138	0.294	0.159
σ_{sl}/f_{yl}	1	1	1	1	1	1	1	1	1	1
σ_{sx}/f_{yx}	1	1	1	1	1	1	1	1	1	1
σ_{sy}/f_{yy}	1	1	1	1	1	1	1	1	1	1
x/a^*	0.4721	0.4877	0.4912	0.4968	0.4945	0.4835	0.4889	0.4944	0.4713	0.4954
a^*/a	1	1	1	1	1	1	1	1	1	1

Table M (continued)

Specimen No.	VR-3	R-1	A1-A	A1-B	A2-B	M1	MR-1	MR-3	MR-2	MR-4
a(mm)	950	950	550	550	550	850	650	650	500	500
h(mm)	1727	1727	1778	1778	1778	1575	1645	1645	1645	1645
a/h	0.55	0.55	0.31	0.31	0.31	0.54	0.40	0.40	0.30	0.30
a_c (mm)	69	69	74	74	74	127	82	114	53	53
t_f (mm)	127	127	102	102	102	121	127	127	127	127
b (mm)	191	191	127	127	127	191	127	127	127	127
t (mm)	51	51	44	44	44	51	44	44	44	44
h_b (mm)	1473	1473	1575	1575	1575	1334	1391	1391	1391	1391
φ_l	0.006	0.006	0.004	0.004	0.004	0.006	0.007	0.007	0.007	0.007
φ_x	0.005	0.003	0.010	0.010	0.015	0.003	0.003	0.003	0.003	0.003
φ_y	0.005	0.003	0.010	0.010	0.015	0.003	0.003	0.003	0.003	0.003
f_{yl} (MPa)	312	324	296	296	296	324	324	324	324	324
f_{yx} (MPa)	341	359	341	341	341	359	359	359	359	359
f_{yy} (MPa)	341	359	341	341	341	359	359	359	359	359
f_c (MPa)	21.37	20.69	21.65	22.62	20.41	22.06	24.13	15.72	19.93	14.41
N(KN)	0	0	0	0	0	0	0	0	0	0
P(KN)	302	316	311	367	329	214	317	318	245	245
ν	0.693	0.697	0.692	0.687	0.698	0.690	0.679	0.721	0.700	0.728
Φ_l	0.121	0.130	0.071	0.069	0.075	0.138	0.140	0.202	0.164	0.218
Φ_x	0.115	0.062	0.228	0.220	0.359	0.059	0.055	0.079	0.064	0.085
ψ	0.115	0.062	0.228	0.220	0.359	0.059	0.055	0.079	0.064	0.085
$\tau_{test}/\nu f_c$	0.233	0.250	0.263	0.299	0.292	0.175	0.265	0.384	0.240	0.319
$\tau_{theory}/\nu f_c$	0.222	0.203	0.311	0.304	0.379	0.207	0.236	0.293	0.281	0.326
$\tau_{theory}/\tau_{test}$	0.953	0.813	1.181	1.016	1.296	1.178	0.892	0.764	1.173	1.022
T_1 (KN)	158	164	84.55	84.55	84.55	168	150	146	132	127
C_1 (KN)	110	44.05	129	129	216	41.26	9.80	6.04	-9.47	-14
Failure mode	S	S	S	S	S	S	S	S	S	S
θ (rad)	0.868	0.853	0.974	0.981	0.929	0.851	0.924	0.842	0.943	0.870
θ_1 (rad)	1.301	1.323	1.187	1.199	1.074	1.317	1.283	1.182	1.220	1.135
y_0/h_e	0.331	0.351	0.532	0.524	0.574	0.364	0.460	0.544	0.568	0.628
σ_c^l/f_c	0.198	0.110	0.333	0.318	0.560	0.104	0.086	0.142	0.098	0.146
σ_{sl}/f_{yl}	1	1	1	1	1	1	1	1	1	1
σ_{sx}/f_{yx}	1	1	1	1	1	1	1	1	1	1
σ_{sy}/f_{yy}	1	1	1	1	1	1	1	1	1	1
x/a^*	0.4890	0.4940	0.4878	0.4886	0.4754	0.4944	0.4964	0.4929	0.4965	0.4940
a^*/a	1	1	1	1	1	1	1	1	1	1

Table M (continued)

Specimen No.	VRR-1	MS-1	MS-2	MS-2-2	MS-5	SD-1A	SD-1C	3BI-3	1BII-3
a(mm)	850	760	760	760	550	650	650	920	1400
h(mm)	1727	1600	1600	1600	2337	1219	1219	1727	2591
a/h	0.49	0.47	0.47	0.47	0.24	0.53	0.53	0.53	0.54
a_t (mm)	131	80	80	80	68	90	90	137	154
t_f (mm)	127	127	127	127	127	102	102	127	191
b (mm)	178	127	127	127	127	102	102	305	286
t (mm)	51	51	51	51	51	51	51	51	76
h_o (mm)	1473	1346	1346	1346	2083	1016	1016	1473	2210
φ_l	0.006	0.010	0.010	0.010	0.007	0.005	0.005	0.006	0.006
φ_x	0.005	0.003	0.003	0.003	0.003	0.005	0.005	0.005	0.005
φ_y	0.005	0.003	0.003	0.003	0.003	0.005	0.005	0.005	0.005
f_{Yl} (MPa)	293	293	293	293	293	293	293	312	312
f_{Yx} (MPa)	293	293	293	293	293	293	293	341	341
f_{Yy} (MPa)	293	293	293	293	293	293	293	341	341
f_c' (MPa)	22.06	21.58	28.13	23.86	25.24	16.13	16.13	22.75	20.69
N(KN)	0	0	0	0	0	0	0	0	0
P (KN)	329	274	368	359	380	178	160	294	685
ν	0.690	0.692	0.659	0.681	0.674	0.719	0.719	0.686	0.697
Φ_l	0.113	0.193	0.155	0.178	0.116	0.116	0.116	0.116	0.120
Φ_x	0.096	0.053	0.043	0.049	0.047	0.126	0.126	0.109	0.118
ψ	0.096	0.049	0.043	0.049	0.047	0.126	0.126	0.109	0.118
$\tau_{test}/\sqrt{f_c}$	0.247	0.226	0.244	0.272	0.188	0.248	0.223	0.214	0.241
$\tau_{theory}/\sqrt{f_c}$	0.215	0.252	0.222	0.241	0.252	0.219	0.219	0.213	0.223
$\tau_{theory}/\tau_{test}$	0.874	1.114	0.909	0.889	1.338	0.886	0.984	0.995	0.926
T_l (KN)	152	206	213	210	176	83.18	83.18	158	340
C_l (KN)	84	0.57	8.26	4.87	-19.26	68.62	68.62	112	254
Failure mode	S	S	S	S	S	S	S	S	S
θ (rad)	0.904	0.821	0.867	0.840	1.056	0.883	0.883	0.888	0.882
θ_1 (rad)	1.312	1.243	1.295	1.263	1.278	1.302	1.302	1.314	1.304
y_o/h_e	0.356	0.473	0.422	0.453	0.575	0.323	0.323	0.326	0.330
σ_c'/f_c	0.156	0.092	0.073	0.088	0.061	0.211	0.211	0.182	0.199
σ_{sl}/f_{Yl}	1	1	1	1	1	1	1	1	1
σ_{sx}/f_{Yx}	1	1	1	1	1	1	1	1	1
σ_{sy}/f_{Yy}	1	1	1	1	1	1	1	1	1
x/a*	0.4924	0.4950	0.4964	0.4954	0.4986	0.4886	0.4886	0.4905	0.4893
a*/a	1	1	1	1	1	1	1	1	1

AFDELINGEN FOR BÆRENDE KONSTRUKTIONER
DANMARKS TEKNISKE UNIVERSITET

Department of Structural Engineering and Materials
Technical University of Denmark, DK–2800 Lyngby

SERIE R
(Tidligere: Rapporter)

R 10. HANSEN, THOMAS CORNELIUS: Fatigue in Welded Connections. A new approach to predict crack propagation behaviour. 1996.
R 11. HANSEN, THOMAS CORNELIUS, AND OLSEN, DAVID HOLKMANN: Fracture and crack growth in concrete. A new approach to predict crack propagation behaviour. 1996.
R 12. HOANG, LINH CAO AND NIELSEN, M.P.: Continuous Reinforced Concrete Beams – Stress and Stiffness Estimates in the Serviceability Limit State. 1996.
R 13. NIELSEN, LAUGE FUGLSANG: Composite Analysis of Concrete. Creep, Relaxation, and Eigenstrain/Stress. 1996.
R 14. PEDERSEN, CARSTEN: New Production Processes, Materials and Calculation Techniques for Fiber Reinforced Concrete Pipes. 1996.
R 15. NIELSEN, J.A., H. AGERSKOV AND T. VEJRUM: Fatigue in Steel Highway Bridges under Random Loading. 1997.
R 16. HOANG, LINH CAO: Shear Strength of Non–Shear Reinforced Concrete Elements. 1997
R 17. ZHANG, JIN–PING: Part 2. Micromechanical Modelling of Shear Failure in Cement Paste and in Concrete. 1997.
R 18. ZHANG, JIN–PING: Part 3. Load Carrying Capacity of Panels Subjected to In–plane Stresses. 1997.
R 19. VEJRUM, TINA: Bridges with Spatial Cable Systems. 1997.
R 20. WADSÖ, LARS: Sorption på lignocelluloser. 1997.
R 21. SCHAUMANN, JETTE: Karakterisering af lignocellulosers porestruktur. 1997.
R 22. CHRISTIANSEN, MORTEN BO, M.P. NIELSEN: Modelling Tension Stiffening in Reinforced Concrete Structurs – Rods, Beams and Disks. 1997.
R 23. CHRISTENSEN, CLAUS FRIDTJOF: Stochastic Oscillations induced by Vortex Shedding in Wind. 1997.
R 24. Resuméoversigt, BKM 1996 – Summaries of Papers, BKM 1996.
R 25. CHRISTOFFERSEN, JENS: Ultimate Capacity of Joints in Precast Large Panel Concrete Buildings. 1997.
R 26. NIELSEN, LAUGE FUGLSANG: On strength of porous material – simple systems and densified systems. 1997.
R 27. JOHANNESEN, JOHANNES M.: Model Correction Factor Method – Mechanically Based Response Surface Approach for Structural Reliabiligy Analysis. 1997.
R 28. RANDRUP–THOMSEN, SØREN: Analysis of the White Noise Exited Elasto–Plastic Oscillator of Several Degrees of Freedom. 1997.
R 29. HOANG, LINH CAO: Shear Strength of Non–Shear Reiforced Concrete Elements Part 2. T–Beams. 1997.
R 30. HOANG, LINH CAO: Shear Strength of Non–Shear Reinforced Concrete Elements Part 3. Prestressed Hollow–Coe Slabs. 1997.
R 31. JAGD, KRISTIAN JAGD: Non–linear FEM Analysis of 2D Concrete Structures. 1997.
R 32. LISE BRÄUNER, LISE POULSSON: Mechanical Properties of Sitka Spruce. 1997.
R 33. TORBEN VALDBJØRN RASMUSSEN: Time Dependent Interfacial Parameters in Cementitios Composite Materials. 1997.
R 34. KAREN GRØNDAHL LORENZEN, M.P. NIELSEN: Koncentreret last på beton. 1997.
R 35. ANDERS BOE HAUGGAARD–NIELSEN: Mathematical Modelling and Experimental Analysis of Early Age Concrete. 1997.

Abonnement 1.7.1997 – 30.6.1998 kr. 130,–
Subscription rate 1.7.1997 – 30.6.1998 D.Kr. 130.–.

Hvis De ikke allerede modtager Afdelingens resuméoversigt ved udgivelsen. kan Afdelingen tilbyde at tilsende næste års resuméoversigt, når den udgives. dersom De udfylder og returnerer nedenstående kupon:

Returneres til:

Institut for Bærende Konstruktioner og Materialer
Danmarks Tekniske Universitet
Bygning 118
2800 Lyngby

Fremtidig tilsendelse af resuméoversigter udbedes af
(bedes udfyldt med blokbogstaver):

Stilling og navn: ....

Adresse: ....

Postnr. og -distrikt: ....

*The Department has pleasure in offering to send you a next year's list of summaries, free of charge. If you do not already receive it upon publication, kindly complete and return the coupon below:

To be returned to:

Department of Structural Engineering and Materials
Technical University of Denmark
Building 118
DK-2800 Lyngby
Denmark

*The undersigned wishes to receive the Department's list of Summaries:
(Please complete in block letters):

Title and name: ....

Address: ....

Postal No. and district: ....

Country: ....